Detonation Theory of Liquid and Aluminized Liquid Explosives

by

Yumin Li

Department of Mechanical Engineering
McGill University
Montréal, Québec, Canada

A thesis submitted to the
Faculty of Graduate Studies and Research
in partial fulfillment of the requirements for the degree of
Doctor of Philosophy
in
Mechanical Engineering

May 2005

Your file Votre référence
ISBN: 978-0-494-21671-2
Our file Notre référence
ISBN: 978-0-494-21671-2

ABSTRACT

Non-ideal behavior of condensed explosives with metal particle additives has been observed experimentally. In general, adding metal particles to a homogeneous explosive leads to a reduction in the detonation velocity and pressure, depending on the charge diameter, the concentration of the additive, and the particle size. To investigate these phenomena, detonation propagation in liquid and aluminized liquid explosives has been studied theoretically by including source terms in the 1-D conservation equations for mass, momentum and energy. To predict the steady state detonation parameters and the detailed structure of the detonation, the generalized C-J condition has been used to obtain a unique solution from the spectrum of possible solutions to the differential equations.

The eigenvalue detonation solution is first determined for a weakly confined, cylindrical liquid explosive charge. The steady-state analysis assuming an Arrhenius reaction rate predicts the detonation failure diameter which depends on the curvature of the detonation wave, wall friction, and heat loss to the wall. The calculated detonation velocity deficit for liquid nitromethane (NM) is less than 2.1% near the failure diameter. The predicted failure diameter for liquid NM varies from 15–18 mm for activation energy E^*, ranging from 30–40 kcal/mol. These results agree well with the experimental data. A second form for the reaction rate law is also considered (i.e., the so-called "simple" law in which the reaction rate is not dependent on temperature). In this case, the detonation failure is not correctly predicted, and hence this rate law is not appropriate for liquid NM.

Detonation propagation in an aluminized liquid explosive involves complex exothermic and endothermic processes. A two-phase flow model is proposed to take into account the non-equilibrium processes which determine the differences in velocity and temperature between the liquid explosive detonation products and solid particles. The onset of reaction of the Al particles in the detonation zone is set based on a simple ignition criterion.

The calculations show that micron-sized Al particles are chemically inert whereas nanoscale particles may react within the detonation zone. For an explosive with

nanoscale additives, the reaction heat of the particles in the detonation zone, if any, contributes to an increase in the detonation temperature. The large detonation velocity deficit for an aluminized liquid explosive is primarily due to momentum losses to the particles, with heat losses playing a relatively minor role, unless the particles are very small. The calculations also reproduce the measured effects of particle size and concentration on detonation velocity. From Chariton's theory of failure diameter, the comparison of the measured failure diameter to the prediction of the detonation zone timescales by the two-phase model with an Arrhenius reaction rate law suggests that the addition of solid particles alters the chemical kinetics of the liquid explosive. A so-called "hot spot" reaction rate law is proposed. With this new reaction rate law, the model predicts the effects of particle size and concentration on the detonation velocity and the detonation zone timescale,, in general agreement with the experimental observations.

ABRÉGÉ

On a observé expérimentalement le comportement non-idéal des explosifs condensés auxquels des particules en métal ont été ajoutées. En général, l'ajout de particules métalliques à un explosif homogène mène à une réduction de la vitesse et de la pression de la détonation, selon le diamètre de la charge, de la concentration de l'additif, et de la dimension des particules. Pour étudier ces phénomènes, la propagation de détonations dans les explosifs liquides purs et avec de l'aluminium a été étudiée théoriquement en incluant des termes de source dans les équations de conservation 1-D de masse, de quantité de mouvement et d'énergie. Pour prédire les paramètres de détonation et la structure détaillée de la détonation, le critère généralisé de C-J a été employé pour obtenir une solution unique à l'éventail des solutions possibles aux équations.

La solution de détonation de valeur propre est d'abord déterminée pour une charge explosive liquide faiblement confinée et cylindrique. L'analyse temporellement invariante, supposant un taux de réaction Arrhenius prédit le diamètre auquel aucune solution n'existe (diamètre critique), qui dépend de la courbure de la détonation ainsi que de la friction et de la perte de chaleur au mur. Le déficit calculé de vitesse de détonation pour le nitrométhane liquide (NM) est moins de 2.1% près du diamètre critique. Ce diamètre varie de 15 à 18 millimètres pour les valeurs d'énergie d'activation, E^*, variant de 30 à 40 kcal/mol. Ces résultats sont en accord avec des données expérimentales. Une deuxième forme du taux de réaction est également considérée, la loi "simple," indépendante de la température. Dans ce cas-ci, le diamètre critique ne peut être correctement prédit, et par conséquent cette loi n'est pas appropriée pour le NM liquide.

La propagation d'une détonation dans un explosif liquide contenant des particules d'aluminium implique des processus exothermiques et endothermiques complexes. On propose un modèle à deux phases pour tenir compte des processus en déséquilibre mécanique et thermique, qui déterminent les différences de vitesses et de températures entre les produits de détonation et les particules solides. L'initiation de réaction des

particules d'aluminium dans la zone de détonation est fixé en se basant sur un critère simple d'ignition.

Les calculs démontrent que les particules micrométriques d'aluminium sont chimiquement inertes tandis que les particules nanométriques peuvent réagir dans la zone de détonation. Pour un explosif avec des additifs nanométriques, la chaleur de réaction des particules dans la zone de détonation contribue à une augmentation de la température de la détonation. Le déficit important de vitesse de la détonation pour un explosif liquide avec aluminium est principalement dû aux pertes de quantité de mouvement aux particules. Les pertes de chaleur jouent un rôle relativement mineur, à moins que les particules ne soient très petites. Les calculs reproduisent également les effets mesurés de la dimension des particules et de la concentration sur la vitesse de la détonation. En se basant sur la théorie de Chariton du diamètre critique, la comparaison entre le diamètre critique mesuré et la prédiction de la durée caractéristique de la zone de détonation par le modèle à deux phases avec taux de réaction d'Arrhenius, suggère que l'addition de particules solides change la cinétique chimique de l'explosif liquide. On propose une loi de taux de réaction "hot spot." Avec cette nouvelle loi de taux de réaction, le modèle prédit les effets de la dimension et de la concentration des particules sur la vitesse de la détonation et sur la heure de la zone de détonation, généralement en accord avec les observations expérimentales.

ACKNOWLEDGMENTS

I would like to express my sincere gratitude to my supervisor, Prof. David Frost, for his guidance, encouragement and support throughout the whole course of this work. He instilled in me his passion for scientific research and provided the motivation to always go further. I will never forget his invaluable advice and the countless discussions I have had with him on detonation science.

A special thanks to Prof. John Lee and Prof. Andrew Higgins from whom I have had very fruitful advice with this project. I wish to also express my gratitude to Dr. Samuel Goroshin, who was always willing to offer guidance and a helping hand in the pyrometer experiments.

The pleasant and friendly environment for studying and working created by the SWPG members and department staff along with their knowledge and skills are deeply appreciated. A very special thanks to Akio Yoshinaka, Massimiliano Romano and François Jettè for their dedicated assistance in pyrometer experiment, and Charles Kiyanda, Vincent Tanguay and Eddie Ng for translating my abstract into French.

I appreciate FCAR for providing me with financial support and making my life much easier.

Finally, I must also acknowledge my family and friends who have always supported me and encouraged me to achieve my goals. I am especially indebted to my wife Zhifang Ni and daughters Rui Li and Jessie Li. Their love, patience, understanding and ever-lasting support allowed me to confidently pursue my academic goals.

TABLE OF CONTENTS

LIST OF TABLES

LIST OF FIGURES

NOMENCLATURE

A	Fitted parameter of JWL EOS
a	Coefficient of curve fit
B	Fitted parameter of JWL EOS
b	Coefficient of curve fit
c	Local sound speed
c_0	Coefficient in shock Hugoniot
C_D	Drag coefficient
C_f	Coefficient of skin friction
C_p	Heat capacity at constant pressure
C_v	Heat Capacity at constant volume
D	Detonation velocity
d	Charge diameter or particle diameter
d_f	Failure diameter
e	Internal energy
e_h	Internal energy in the Mie-Gruneisen form
E	Sum of the internal and kinetic energies in shock frame
E'	Sum of the internal and kinetic energies in laboratory coordinate
E^*	Activation energy of chemical reaction
e_{MG}	Internal energy of the unreacted explosive in the Mie-Gruneisen form
e_{JWL}	Internal energy of detonation products in the JWL form
f	Source term in momentum conservation equation
H	A function of mass, momentum and heat source terms
H_1	A function of mass, momentum and heat source terms
H_2	A function of mass, momentum and heat source terms
H_f	Heat formation
h_c	Heat transfer coefficient

I	Variable
I_p	Energy in JWL EOS
J	Variable
k	Reaction rate constant
k_f	Friction factor
k_s	Equivalent sand roughness
K	Reaction rate constant
L	Detonation zone length
m	Source term in the mass conservation equation
M	Mach number
n	Numbers of aluminum particles per unit volume
N_u	Nusselt number
P	Pressure
P_h	Pressure in the Mie-Gruneisen form
P_s	Pressure in the JWL form
P_r	Prandlt number
q	Source term in the energy conservation equation
Q	Chemical energy
r	Radius of aluminum particle
R	Specific gas constant
R_1	Fitted parameter of JWL EOS
R_2	Fitted parameter of JWL EOS
R_c	Radius of detonation front curvature
R_e	Reynold number
S	Variable
s_0	Slope of shock Hugoniot
t	Time
t_r	Chemical reaction time
T	Temperature

T_w	Wall temperature
T^*	Stagnation temperature
U	Particle velocity in laboratory coordinate
u	Particle velocity relative to shock wave
u_p	Particle velocity in shock Hugoniot
v	Specific volume
x	Distance
Z	Pre-exponent of Arrhenius reaction rate law
Z_s	Pre-exponent of simple reaction rate law

Greek Symbols

ρ	Density
λ	Degree of reaction
λ_f	Thermal conductivity of fluid phase
ψ	Numerator of the *du/dx* equation or thermicity
η	Denominator of the *du/dx* equation or sonic condition
Γ	Gruneisen gamma
Ω	Fitted parameter of JWL EOS
ω_r	Radial flow divergent on central stream tube
μ	Viscosity
μ_c	Compaction viscosity
Φ	Volume fraction
τ	Rate of compaction
α	Ratio of particle velocities
β	Intragranular stress or configuration pressure
ζ	Effect coefficient of aluminum reaction heat release for each phase

Subscripts

ch	Chemical form
hs	Hot spot
ign	Ignition
JWL	JWL form
MG	Mie-Gruneisen form
NM	Parameter of liquid nitromethane
p	Constant pressure
v	Constant specific volume
λ	Constant degree of reaction
0	Initial state
1	Fluid phase
2	Solid phase

CHAPTER 1 INTRODUCTION

1.1 Background

A large amount of effort is expended throughout the world each year within the energetic materials community to develop new explosives and propellants with improved performance as well as decreased sensitivity (for safer handling). Even a small increase in the energy density or improvement in the dynamic performance of the material is considered to be significant. New explosives are typically constructed by either i) developing new chemical formulations, or ii) adding energetic additives to existing explosives.

A common technique in the explosives industry is to add reactive metal particles to an explosive. A common additive is aluminum (Al) powder, which then produces a so-called aluminized explosive. Since the energy release for the complete oxidation of aluminum is about 30 MJ/kg, in comparison with the typical energy release of an explosive of 5–6 MJ/kg, even a modest addition of aluminum leads to a significant increase in the energy density. However, it has been shown that although the potential for improved performance exists, predicting the effectiveness of aluminized explosives in various applications is complicated by the lack of knowledge of the chemical kinetic mechanisms during the extreme conditions that occur when these heterogeneous explosives are detonated.

Past experimental work on aluminized solid and liquid explosives will first be described, including the recent work with adding nanoscale aluminum powder to explosives. This is then followed by a review of models for detonation in homogeneous and heterogeneous explosives.

1.2 Review of Experimental Work with Aluminized Explosives

1.2.1 Aluminized Solid Explosives. Finger et al. (1970) were some of the first researchers to look at the effectiveness of adding aluminum to explosives. They measured the detonation velocity in composites consisting of HMX (cyclotetramethylene tetranitramine, $C_4H_8N_8O_8$) with combinations of AP (ammonium perchlorate, NH_4CLO_4), Al (aluminum) and Viton (vinylidine fluoride-hexafluoropropylene copolymer) using a conventional cylinder test. The overall results indicate that although the experimental detonation velocity decreases with the addition of aluminum particles, the ballistic performance of the explosive (i.e., the ability of the expanding combustion products to accelerate metal) actually improves.

Another study performed on the effects of adding aluminum to explosives was done by McGuire and Finger (1985). They measured the detonation parameters using a cylinder test for composite explosives containing HMX, TATB (1,3,5-triamino-2,4,6-trinitrobenzene, $C_6H_6N_6O_6$), BTF (1,2,5-oxadiazole-1-oxide, $C_6N_6O_6$) and Al. They found that by adding both BTF and Al, the ballistic performance of the explosive was improved. From experiments, they concluded that increasing the detonation temperature plays a key role in increasing the explosive energy delivered at low expansion volumes and that fine particle sizes (~1 μm) for the aluminum additives lead to an improved performance.

Grishkin et al. (1993) performed experiments to determine the effects of various forms (i.e., spherical or flaked powders) of aluminum additives on the detonation properties for desensitized RDX (cyclotrimenthylene trinitramine; $C_3H_6N_6O_6$) and HMX. The results of the experiments indicate that the detonation velocity for mixtures of HMX or RDX with aluminum particles decreases with increasing aluminum content. The measurements of radial and frontal acceleration indicate an increase in the performance of the explosives with a maximum occurring between 7 and 14% aluminum content.

Ishida et al. (1991) measured the detonation pressure and velocity of HMX with aluminum or lithium fluoride (LiF) additives using a shock-induced polarization method. LiF was added for comparison due to the fact that it is inert and has the same density and shock properties as aluminum. Several key results were reported by these authors. First, the LiF additive does not affect the extent of the reaction of the primary explosive, although there was a reduction in the detonation velocity and pressure. In addition, the reaction zone lengths for the organic explosive and composite explosive containing inert particles were more than 1 mm. For the aluminized explosives, the detonation zone length was determined to be more than twice this value. The measured particle velocity in PMMA (polymethacrylate)-cased samples for aluminized explosives exhibited a non-linear behaviour with aluminum mass content while the particle velocity for the explosive with LiF added decreased linearly with increasing LiF mass content. This suggests that there is some combustion of the aluminum particles which affects the detonation pressure even though the detonation velocity is similar for both LiF and aluminum loaded samples. The authors suggest that there are competitive energy balances that will affect these values. First, there is an endothermic behavior due to the heating and melting of the aluminum particles. Alternatively there is an exothermic behavior due to the aluminum reaction with the detonation product gases. These competing forces must be studied to further understand their effects on the detonation wave structure.

Arkhipov et al. (2000) studied the characteristics of explosions of HMX mixtures with aluminum particles 0.5, 20, 50, and 150 μm in size at Al weight concentrations of 5, 15, and 25%. They measured the detonation velocity, the velocity of copper cylinder expansion, the velocity of a steel plate accelerated by the explosion and the heat of detonation. The experimental results show that the addition of the aluminum particles reduces the detonation velocity of the explosive. The smaller the aluminum particles, the greater the detonation velocity deficit. In spite of a decrease in detonation velocity, aluminum additives significantly increase the total explosion

energy. The energy released by the aluminum oxidation in the expanding explosion products increases the velocity of accelerated metal plates.

1.2.2 Heterogeneous Liquid Explosives. The effect of particle additives on the failure diameter of a liquid explosive was illustrated in the pioneering work of Engelke (1983). He investigated the effect of the number density of heterogeneities on the failure diameter of liquid NM (with the addition of 1.25% by weight of guar gum to increase the viscosity of the NM). Small amounts of glass beads with sizes of 1-4, 35-45, and 105-125 μm were dispersed in the NM/guar explosive mixture. His experimental results showed that addition of the 35-45 and 105-125 μm diameter heterogeneities in amounts up to 9.0 wt. % produced no failure diameter reduction. However, addition of 1-4 μm diameter beads, in amounts as small as 0.5 wt. % produced a failure diameter reduction. The effect was enhanced as more 1-4 μm diameter heterogeneities were added up to, at least, 9.0 wt. %. A failure diameter reduction of about 40% at both the 3.0 and 9.0 wt. % levels was observed.

Kato et al. (1981, 1983, 1984, and 1985) conducted a series of experiments to determine the detonation characteristics of an aluminized liquid explosive consisting of aluminum particles with a 10 μm mean diameter suspended in a mixture of 97% NM with 3% PMMA added as a gelling agent. They investigated the detonation velocity as a function of charge diameter, the effect of aluminum addition on the detonation sensitivity, and on the brightness temperature of the detonation products. Some interesting results were obtained. First, the addition of aluminum particles decreases the detonation velocity relative to pure NM. Due to the narrow reaction zone in NM (Sheffield, 1999) the amount of heat transfer to the aluminum particles within the reaction zone is insignificant. Hence the Al particles are effectively chemically inert within the detonation zone. Secondly, the brightness temperature measurements showed that aluminum particles react, after a delay, with the gaseous products produced by the detonation of the liquid explosive. They estimated that the ignition delay is less than 100 ns and the duration of the aluminum reaction exceeds 2

μs for aluminum particles of mean diameter 10 μm. The time evolution of the measured brightness temperature of the detonation products containing aluminized compounds depends strongly on the aluminum concentration in the mixture. The brightness temperature at time zero (i.e., the C-J temperature) decreases with increasing aluminum concentration. This indicates that aluminum is chemically inert within the detonation zone, and the heat transfer to the aluminum particles is not sufficient to initiate chemical reaction of the aluminum in the detonation zone of the explosive component. The maximum brightness temperature occurred from 1 - 1.5 μs for all the NM-PMMA/Al mixtures studied, and increased with the aluminum concentration. This indicates that there are exothermic reactions between the aluminum particles and the detonation products of the NM after the detonation zone. Finally, they observed that an increase in Al concentration sensitized the explosive mixtures.

Lee et al. (1995) investigated the detonation of a heterogeneous mixture consisting of *sensitized* liquid nitromethane in a packed bed of inert spherical glass beads. The average propagation velocity of a detonation wave through this heterogeneous mixture is less than the detonation velocity of the liquid explosive itself but significantly in excess (~50%) of the ideal equilibrium C-J predictions based on full thermal, mechanical as well as chemical equilibrium. They found that for a packed bed of inert monodisperse spherical beads saturated with sensitized NM, two distinct propagation mechanisms can occur, depending on the bead diameter. The heterogeneous explosive is most insensitive (i.e., the failure diameter reaches a maximum) when the bead diameter is a critical value, which is on the order of the failure diameter for the pure liquid explosive. For larger beads, detonation wavelets can successfully propagate in the liquid explosive between the beads. The global detonation front thus consists of a series of wavelets that propagate in winding paths through the geometric irregularities of the pores. In this "large-bead" regime, as the bead size increases, diffraction effects become less severe and hence the failure diameter of the mixture decreases. For bead diameters less than the critical value, the

detonation fails to propagate around the beads, but instead the shock propagation through the beads is sufficient to initiate the explosion of the liquid in the interstitial pores. In turn, the explosions in the liquid explosive generate more shocks in the neighboring inert beads ahead. This results in sustained "sympathetic" detonation propagation through the heterogeneous explosive medium. In this "small-bead" regime, as the bead size decreases, the density of artificial hot-spots associated with the beads increases and failure diameter decreases. The average detonation velocity in the large bead regime is typically larger than that for the small-bead regime.

Haskins et al. (1998) reported experimental results on the detonation characteristics of neat nitromethane containing high volume percentages of small spherical glass beads and aluminum particles. These mixes were found to detonate at diameters less than that of the pure liquid explosive partly due to the hot-spot sensitization effect of solid particles. The detonation velocity of such mixtures again was less than that of NM alone but higher than would be expected if the particles and detonation products were always in equilibrium in detonation process. The authors suggested that the shock velocity within the solid particles also plays a role in determining the detonation velocity.

In general for the particle sizes that were typically used (10–100 μm) in the above experiments, the timescale of the ignition and combustion of the Al particles was much longer than that of the explosive itself (Kato & Brochet, 1984). Therefore, within the detonation zone of the explosive, the transfer of heat and momentum to the particles actually serves to reduce the detonation velocity and pressure. However, the later burning of the particles in the expanding detonation products increases the temperature of the product gases and the energy available to do expansion work, which is important for applications such as the commercial blasting of rock and underwater explosions (Persson et al., 1994).

1.2.3 Nanoscale Aluminum Additives. As the size of an Al particle is reduced, the surface area to volume ratio of the particle increases and the characteristic times for particle heating and combustion both decrease (Baudin, 1998). For submicron-sized (or nanoscale) particles, for some explosives, the particle ignition delay time can be smaller than the explosive detonation time, and therefore the energy release from the particles may augment the detonation pressure and velocity (Miller, 1998). Recent developments in materials technology have allowed the fabrication and processing of chemically stable ultra-fine reactive metal particles with particle sizes on the order of 50–100 nm. The most widely tested product is the ultrafine aluminum powder denoted "Alex©" which is comprised of spherical particles having a diameter of 100-200 nm (Argonide Corporation, FL). The potential for producing a new class of explosives with improved performance by mixing nanoscale powders with conventional explosives has received considerable interest recently.

Baudin et al. (1998) assessed the effect of the aluminum particle size in explosives. Liquid (NM + 3 wt. % PMMA) and solid (TNT) explosives with micrometric (5 μm) or nanocrystalline (100 nm) aluminum powder additives were compared using the conventional 1 inch cylinder test. Initially, the addition of nanoscale aluminum powder was expected to enhance the ballistic capability of the explosive. However, the cylinder test results obtained for 60-40 and 80-20 wt.% NM-Al gelled explosives, and 80-20 wt. % TNT-Al solid explosives showed similar efficiencies for both 5 μm and nanoscale Al particles. Moreover, the reduction in aluminum particle size led to a *decrease* in the detonation velocity. The authors speculated that a possible reason for the decrease in detonation velocity was the faster heat transfer between the cold nanoscale Al particles and the detonation products due to the larger specific surface area of the smaller particles. However, the fluxmeter records indicated that the temperature obtained with nanoscale Al particles was higher than that obtained with 5 μm Al particles during the first 200 ns of the interaction of the detonation products with the glass window. The authors speculated that a faster oxidization of the nanoscale particles in the detonation products had

moved the Al energy release closer to the detonation front. Other experiments done by these authors on high explosives containing RDX, AP, Al and wax binder with 5 μm and 100 nm aluminum particles resulted in the same detonation characteristics as that of the aluminized NM explosive, i.e., the detonation velocity decreased with decreasing particle size. They also observed a higher detonation products temperature, underwater impulse and bubble effect for nanoscale aluminum.

Brousseau et al. (2002) also studied the effect of adding nanometric aluminum particles to explosives. Various plastic-bonded explosives (PBXs) and TNT-based formulations were developed to compare the effect of adding ultra-fine "Alex" powder with conventional micron-sized (2 μm, 12 μm and 21 μm) aluminum powders. Explosive performance was determined by detonation velocity measurements and plate dent depth tests. The study was also complemented by air-blast tests to evaluate the difference in energy release in the far-field. The experimental results showed that the detonation velocity of PBXs based on an energetic binder is decreased when Alex replaces micrometric aluminum. In composition B and ANFO, at 10% Al, adding Alex powder also reduced the detonation velocity, but increased the heat of detonation. In TNT/Al mixtures, Alex increases the heat of detonation and the detonation velocity, presumably due to reaction of Alex in the detonation zone. No increase of pressure was found in aquarium tests with nanometric Al formulations. However, the expansion of the gas appears faster for Tritonal-type formulations containing nanometric aluminum. Alex was shown to significantly decrease the critical diameter of Tritonal-type mixes. They showed that there was no increase in air-blast performance with nanometric aluminum. In fact, for PBXs and melt-cast explosives, there seemed to be a reduction of air-blast pressure.

Miller et al. (1998) examined the effect of Al particle size (50 nm to 20 μm) on the detonation characteristics (detonation velocity and plate-push velocity) of ammonium dinitramide (ADN). The addition of about 25% Al with particle sizes of 3 and 20 μm gave detonation velocities of slightly less than, but nearly 4.0 mm/μs of

neat ADN (~ 4.0 mm/μs), while the addition of 150 nm and 50nm sized Al produced detonation velocities of 25 and 50% greater than of neat ADN, respectively. Likewise, the results from the terminal velocity plate-push tests revealed that the large 20 μm Al decreased the observed velocity from that of neat ADN, while the 3μm, 50nm and 150nm Al all increased the observed velocity in a similar manner. These results clearly demonstrate that varying the metal reaction kinetics can strongly affect the performance characteristics of the metalized explosives. In this case, AND has a relatively long reaction zone, so metal reaction within the reaction zone actually leads to augmentation of the detonation velocity.

Gogulya et al. (1998, 2002) studied the detonation performance of BTNEN (bis (2,2,2,-trinitro-ethyl) nitramine, $C_4H_4N_8O_{14}$) and HMX with added Al. BTNEN has a positive oxygen balance while HMX is a negative oxygen balance explosive. They measured the detonation velocity using contact gauges, the temperature profile using an optical pyrometer, the velocities of expansion of a copper cylinder wall using a cylinder test, the velocities of a steel plate accelerated by the detonation products using a standard technique and also the heat release using a calorimeter. In general, detonation velocities for both mixtures were smaller than those of pure high explosives. The smaller the Al particles, the larger was the detonation velocity deficit. Their investigation into the detonation performance of aluminized compositions based on high explosives of different classes has shown that the Al influence depends both on the nature of the high explosive and the Al particle size. The benefits of using nanoscale Al are obvious only when the characteristic time of the Al interaction with the detonation products is rather small, and the specific surface area plays a leading role. However, when this characteristic time is larger, the acceleration ability was found to be largest for particles with a size of about several micrometers. The authors explained this by the fact that the decrease of Al particle size from sub-micron to nanometric size is accompanied with an increase of the mass fraction of Al oxide, and hence with a drop in the initial aluminum content of the powder.

It appears that the reaction mechanism of nanoscale aluminum particles in explosives is still unclear. Many researchers have reported on a large number of different compositions with mixed results. Figs. 1 and 2 summarize some experimental results for the effect of aluminum mass fraction and aluminum particle size on the detonation velocity in aluminized high explosives. From these experiments, two distinct detonation characteristics of the aluminized high explosives can be seen. First, the detonation velocity of the explosives decreases as the Al concentration increases. Secondly, the Al particle size affects the detonation velocity. For conventional micron-sized aluminum particles, the addition of aluminum generally decreases the detonation velocity of high explosive mixtures. The smaller the aluminum particles are, the larger the detonation velocity deficit. For nano-sized particles, the detonation velocity can increase or decrease depending on the reaction mechanism of the aluminum particles within the detonation zone.

1.3. Review of Detonation Models

1.3.1 Equilibrium Chapman-Jouguet Model. To predict the detonation performance of an explosive material, various theories have been developed. At the end of the 19^{th} century, based on the experimental observation that detonation waves, once initiated, propagate with a well-defined constant velocity in a given explosive mixture. Chapman (1899), in his original paper, suggested that the only unique solution to the conservation laws is the one that corresponded to the minimum detonation velocity when the Rayleigh line is tangent to the Hugoniot curve. He adopted this as the criterion for selecting the steady detonation solution. Later, Jouguet (1906) demonstrated that this tangency solution also corresponds to one where the detonation products flow at a sonic velocity relative to the shock front. Thus, one can alternatively use the sonic condition as a criterion to determine a steady detonation solution. Following Chapman and Jouguet, the ideal steady detonation solution based on the minimum velocity (the tangency solution) or the sonic condition

is now referred to as the Chapman-Jouguet (C-J) solution. This ideal C-J solution can be obtained on the basis of the conservation laws and equilibrium thermodynamics without considering the details of the non–equilibrium detonation structure. Hence, the C-J detonation solution is independent of any chemical kinetics rate information. The C-J theory also predicts a detonation velocity independent of the initial and boundary conditions since it is based solely on the conservation laws for steady state, planar, one-dimension flow and the thermodynamic properties of the reactant and product species (e.g., heat of formation, heat capacity) across the wave front. Complete thermal and chemical equilibrium are assumed to occur at the C-J plane.

The C-J theory can be considered to be very successful since, in general, it predicts a detonation velocity within a few percent of the experimental value in homogenous explosives when the boundary condition (e.g., charge diameter) is far from the limiting values. However, in many situations, the measured experimental detonation velocities can be considerably lower than the equilibrium C-J values and in some chemical systems, the experimental values can even exceed the C-J values significantly. In the present investigation, detonation calculations for NM/Al mixtures have been carried out using the Cheetah equilibrium code (Fried et al., 1998) which is based on C-J theory. Detonation velocities calculated with the assumption that the aluminum particles are either fully reactive or inert are both lower than experimental values from Kato (1983), Baudin (1998), and Frost (2005) as shown in Fig. 1.3. Moreover, due to the assumptions inherent in the equilibrium calculations, the effect of varying the aluminum particle size on the detonation velocity cannot be determined. The departure of the ideal C-J predictions from the experimental results suggests that some of the assumptions inherent in the ideal theory (such as equilibrium at the downstream plane) are not valid.

As an aluminized explosive is a typical example of a heterogeneous explosive, the poor performance of thermo-chemical equilibrium codes when applied to these explosives is usually attributed to the relatively long reaction times of the metal additives (which may be an order of milliseconds) as compared to most homogeneous

condensed explosives (e.g., the detonation zone in pure NM has a timescale ~20 ns). In this case the C-J assumption of thermodynamic equilibrium at the CJ plane breaks down. For heterogeneous explosives, it is therefore necessary to consider the role of chemical kinetics to more accurately model the detonation propagation.

1.3.2 ZND Model. Zel'dovich (1940), Von Neumann (1942) and Döring (1943) independently arrived at the so-called "ZND" theory of detonation by considering a particular model for the structure of a detonation wave. ZND theory assumes a steady structure for a detonation wave which links the initial state to the equilibrium end state. A ZND detonation is described by an inert shock wave propagating into a reactive material. The passage of the shock wave leaves the material in a locally subsonic, high temperature state. The high temperature initiates an exothermic chemical reaction. Energy released by this chemical reaction then is coupled with the leading shock driving the detonation wave complex forward. For wave speeds greater than the C-J speed, the solution terminates at the so-called strong solution family, a subsonic state which requires piston support to remain steady. For a C-J wave, the solution terminates at a sonic point and thus is able to propagate without piston support. This classical ZND theory predicts the existence of a high pressure transient preceding the CJ state. The plane wave nature of the system considered, however, guarantees that the C-J state is always reached. Another consequence is that the detonation velocity in the classical ZND theory is always the same as that of C-J theory.

1.3.3 Detonation Front Curvature. It is found experimentally, however, that the detonation velocity for heterogeneous explosives varies distinctly from the CJ value. Moreover, the detonation velocity in heterogeneous explosives is observed to be a strong function of charge diameter (Engelke et al., 1979). Wood and Kirkwood (WK, 1954) proposed a two dimensional steady state kinetic detonation theory that avoids many of the limitations of the classical ZND theory. WK considered a cylindrical

charge of infinite length. They solved the hydrodynamic Euler equations in the steady state limit along the central streamline of the cylinder. Radial expansion was treated as a source term in the one-dimensional flow along the streamline. The WK equations have been extensively analyzed by Erpenbeck and co-workers (1962). It is found that the detonation velocity depends on the interplay between chemical kinetics and radial expansion. In the limit of no radial expansion, the ZND plane wave result is obtained. When radial expansion is allowed, the detonation velocity can vary from the C-J prediction. In the limit of strong radial expansion (or a severe curvature of the detonation front), the detonation wave fails. Bdzil (1981) and Steward (1998) have generalized the WK theory to off-axis flow and developed the so-called detonation shock dynamic (DSD) model. By appropriately modeling the detonation front curvature, they are able to reproduce qualitatively the so-called "diameter effect" (i.e., the dependence of detonation velocity on detonation front curvature) in PBX explosives, and thus provide a physical explanation for the existence of a failure diameter. Frost et al. (1999) used the DSD theory to track the detonation propagation in a heterogeneous explosive consisting of an array of inert cylindrical obstacles with a liquid explosive in the interstitial space. Using a simple Huygens construction, the average detonation velocity through the explosive is less than that for the liquid explosive alone, due to the increased detonation path length. With the use of the DSD model, which accounts for the dependence of velocity on the front curvature, the detonation velocity is reduced further. The detonation velocity deficits obtained in the computations are of the same order as those observed experimentally for a heterogeneous explosive consisting of a packed bed of spherical inert beads saturated with sensitized nitromethane in the so-called "large bead" regime.

1.3.4 Generalized C-J Criterion. It has long been known that flow impediments (wall roughness, obstacles, porous beds) may have a profound effect on the propagation of a gaseous detonation and can markedly reduce its propagation velocity compared to the corresponding C-J value. Moreover, the impediments can induce

striking jump-wise transitions from a high-velocity sub-CJ detonation (or quasi-detonation) to a low-velocity detonation. Previous researchers, (e.g., Zel'dovich, 1986; Dionne, 2000; Brailovsky, 2002) have successfully predicted the effects of momentum and heat losses to the flow impediments, on the multiplicity of detonation regimes, by adding appropriate source terms in the conservation equations. Due to the presence of the source terms in the conservation equations, the flow may become sonic prior to complete equilibrium of the flow properties. Hence, the ideal C-J criterion is no longer valid. An alternative criterion that relaxes the equilibrium requirement of the ideal C-J theory has to be used. Fickett and Davis (1979) describe how ZND theory can be placed in the context of the general theory of systems of ordinary differential equations. Details of this theory can be found in standard texts (Fickett and Davis, 1979). The theory describes how, given a set of ordinary differential equations, solutions link an initial state to a particular final state. In a steady-state detonation, these final states are defined at the points where the forcing functions for each differential equation are simultaneously zero. This is equivalent to stating that the numerator and the denominator of the differential equation (e.g., for the particle velocity) must vanish simultaneously for a regular solution. This is now referred to as the "generalized C-J criterion". Whether or not a final state is reached depends on the particular form of the differential equations. A solution which does not reach the defined point is rejected as a steady solution. Although the work of Zel'dovich (1986), Dionne (2000), and Brailovsky (2002) mainly focused on the phenomena of gaseous detonations, the procedure of including the source terms to represent the effects of mass, momentum and heat exchange is relevant for modeling the non-ideal detonations in heterogeneous explosives. Here, a "non-ideal detonation" is defined as a detonation that is not governed by the classical C-J theory.

1.3.5 Multiphase Models. Similar methods have been extensively used in the study of the detonation structure in heterogeneous media consisting of a gaseous component with solid particles. Two-phase media are treated separately and interaction terms are

introduced in the conservation equations to take into account the exchange of mass, momentum, and energy between the particles and gas. For example, Veyssiere et al. (1983, 1986, 1991) have systematically investigated the detonation of a gaseous explosive mixture with aluminum particles in suspension by considering a one-dimensional, two-phase flow with different velocities and temperatures for the particles and gas. The existence of a steady propagation regime for non-ideal detonations in such a hybrid two-phase mixture was studied numerically for different values of the mean solid particle size and shock tube diameter. Three steady regimes were identified in mixtures of aluminum particles with detonable gases, denoted as a pseudo gas (i.e., effectively a gas) detonation, a double–front detonation and a single-front detonation. In the pseudo gas detonation (PGD), the aluminum particles are not ignited upstream of the CJ plane. A single-front detonation (SFD) is supported by heat release from both gaseous reactions and solid particle-gas reactions. In the double-front detonation (DFD), a secondary detonation wave (supported by the reaction between the particles and the gas) propagates with a constant time delay, τ downstream of the leading detonation wave (supported by heat release from the gaseous reactions). In some particle concentration ranges, both a PGD and SFD may propagate but the velocity of a SFD is higher than that of a PGD. When the particle size decreases or the tube diameter increases, the domain of the SFD increases, whereas for coarse particles or small shock tube diameters, the PGD is the dominant detonation regime. For a given composition of the gas mixture, there are optimal values of the particle size and shock tube diameter for which the domain of the DFD is the largest. An increase in the particle size (or reduction of the tube diameter) increases the delay τ between the two fronts of a DFD which eventually disappears, being replaced by a PGD. With a decrease of the particle size (or increase of the tube diameter) a SFD propagation becomes more and more likely. Fedorov and Khmel (1999, 2002) also studied the steady-state detonation regimes on the basis of the non-equilibrium model of detonation of aluminum particles in oxygen taking into account differences in velocities and temperatures of the mixture components. The final

steady state was analyzed by determining the types of final singularities as a function of the relaxation parameters (the ratios of the characteristic times of thermal and velocity relaxation and combustion). The regions of existence of steady-state regimes were found numerically, depending on the detonation velocity and relaxation parameters. A similar two-phase model has also been widely used to study the problem of deflagration-to-detonation transition in granulated solid explosives by Krier, et al. (1978), Baer and Nunziato (1986), and Powers (1988), among others.

Although the above models deal with different systems, their common characteristic is the introduction of source terms in the conservation equations to account for non-equilibrium effects. Area change (i.e., expansion of the products) and/or mass transfer between the phases require the addition of a source term in the conservation of mass, friction and drag require a source term in the momentum equation, and heat transfers are taken into account by a source term in the conservation of energy equation. The conservation equations with source terms can then be integrated to obtain the detonation structure of the non-ideal detonation.

Orth (1999) presented an unsteady, one–dimensional model to simulate the buildup toward steady detonation in the condensed explosive HMX containing dispersed aluminum particles. She considered the heat transfer from the detonation products to the aluminum particles and mass transfer due to the formation of aluminum oxide particles. Heat liberated by secondary oxidation reactions of Al with the products of the initial decomposition of the explosive was also modeled, and parametric studies were presented in which the ignition delay time and the rate of the aluminum reactions were varied. Her results indicated that the induction delay for the aluminum particle ignition, combined with endothermic processes, alter the structure of the reaction zone, and produce a secondary shock wave which never reaches the detonation wave front. Under certain combinations of heat transfer rate and chemical release rate, the observed behaviour that detonation velocity and pressure decrease with the addition of micron-sized aluminum particles can be reproduced with the generalized model. However, the effects of aluminum particle size on the detonation

properties cannot be simulated. This work does not include momentum transfer effects which can play an important role in the detonation properties of two-phase mixtures.

Gonor et al. (2002) developed a more comprehensive, 1-D model of the steady-state detonation in a heterogeneous charge with metallic reactive particles. The model accounts for carrier, particle and oxide phases, velocities and temperatures of carrier and particle phases, their densities, pressure, etc. Sub-models were included for the vaporisation of the metallic particles at high pressure, the vapour-phase and heterogeneous combustion of the particles and the particle interaction with the leading shock wave. The calculations using the model show that a heterogeneous mixture of RDX with 100 nm aluminum particles leads to a reduction in detonation velocity compared to its corresponding value for pure RDX or a mixture with inert particles. Nanoscale particles burn completely in the RDX reaction zone for detonation with a particle mass fraction less than 20%. While 5 μm aluminum particles do not burn in the reaction zone. Analysis of the model results indicates that the detonation velocity of the heterogeneous mixture decreases as the intensity of the heterogeneous and vapour-phase combustion of the particles is increased. An important factor affecting the decrease in detonation velocity is the reduction in mass fraction of the gaseous component of the detonation products. However, with the many physical submodels included in this model (with the associated uncertainties), it is very difficult to determine the relative importance of the various physical parameters used in validating this model, e.g., the uncertain mechanisms on mass transfer and particle combustion.

Hawken et al (2002) developed a multiphase model within their IFSAS 2 code to simulate the detonation development in nitromethane mixed with metallic particles. The fluid and particles are treated as separate continua and their interactions are once again described using source terms of mass, momentum, and energy. The calculation is sensitive to the exponential pre-factor used in the Arrhenius law for gas reaction. The detonation decays unless the pre-exponential factor is above a certain value.

Above this value, the detonation is sustained but is initially slower than without the presence of particles. After a certain amount of time the detonation starts to accelerate and the velocity exceeds the velocity without particles. Although this transient analysis simulates the effect of mass, momentum and energy transfer from the gas to the particles, it is not very successful in predicting the detonation parameters of the nitromethane-particle system.

An aluminized explosive is a complex reactive system. Addition of aluminum particles will affect the detonation properties and structure, and may alter the chemical kinetics of the explosive due to the well known "hot-spot" effect of the particles under shock diffraction. Under shock loading, the multiphase system consisting of detonation products and aluminum particles can result in significant momentum transfer between the explosive products and the particles. This has been verified by the experiments in gas-particle systems (Boiko et al., 1983; Frost et al., 2001). In addition, the chemical reaction of organic explosives occurs very rapidly (e.g., on a ns timescale for NM). The metal particles are rapidly heated, removing energy from the detonation products. Following that, the particles undergo a slow reaction which can occur within the detonation zone or in the Taylor expansion zone, depending on the particle size. Therefore, heat transfers both to and from the particles to the detonation product gases are important in the detonation process. An understanding of how the rates of energy release from the metal particles, the ignition delays due to metal heating, and the thermicity effects (due to mass, momentum and heat transfer between the organic explosive, the metal particles and boundaries) affect the detonation parameters is critical to determine the performance of the aluminized explosives and to develop modeling capabilities. This research entailed the development of a hydrodynamic code to study the effects of the chemical rates, ignition delays and thermicity processes on the detonation wave structure, especially for a heterogeneous explosive of NM containing aluminum particles. The goal of the work was to determine the relative contribution of the various source terms to the

divergence of the properties of the heterogeneous explosive from that of a homogeneous explosive.

1.4 Outline of Thesis

The analysis of detonation propagation in homogenous liquid explosive is first considered in chapter 2. In particular, a model and implementation procedure are presented which give the detonation properties and detonation velocity-diameter effect of liquid explosives by solving the quasi-one-dimension conservation equations with source terms for mass, momentum and energy transfer. This analysis is then applied to the case of liquid nitromethane as a test bed to simulate the eigenvalue detonation of nitromethane and its failure. This is essential to verify an appropriate equation of state and choose suitable parameters for the reaction rate law of NM. Chapter 3 presents the 1-D two-phase fluid flow model for the aluminized liquid explosive detonation based on the characteristic analysis of the drag and heat transfer between the unreacted aluminum particles and liquid NM behind the leading shock wave. In this hydrodynamic model, the unreacted liquid explosive and its detonation products are taken as the fluid phase, with aluminum particles as the solid phase. Following the continuum theory of mixtures, the two phases are assumed to coexist at each spatial location, and are assigned individual state variables such as density, velocity, specific internal energy, etc. Each phase obeys the balance laws of mass, momentum and energy similar to those for a single continuum, except that the exchange of these quantities across the phase boundaries is represented by interaction source terms in the balance equations. With this set of equations, the detonation solution of the explosive system is determined by applying the generalized C-J criterion. A ZND detonation structure of the aluminized liquid explosive consisting of a steady flow from the Von Neumann state down to the sonic point is exhibited. For this non-ideal detonation, the flow is in a non-equilibrium state at the sonic plane. As a result, chemical reactions and other types of mass, momentum and energy transfer

are still occurring downstream of the sonic plane, while the flow proceeds towards complete equilibrium in a non-steady manner. These non-steady events behind the sonic plane can not have any influence on the propagation of the detonation wave since the sonic plane acts as a physical barrier, isolating the detonation zone from the transient flow in the products. The application of the 1-D two-phase fluid flow model to the non-ideal detonation of aluminized nitromethane is presented in chapter 4. Thermogravimetric (TGA) experimental results relevant to modeling the onset of particle oxidation are discussed. Compared with existing experimental results, this hydrodynamic code predicts well the detonation structure of aluminized NM and the effect of different sized aluminum particles in the detonation zone. Finally, the hydrodynamic code is modified to include a hot-spot reaction law and compared with experimental results. A summary of the work along with recommendations for further work is presented in Chapter 5.

Chapter 2 Eigenvalue Detonation of Nitromethane and Its Failure

2.1 Introduction

A detonation in a chemical explosive consists of a shock wave followed by a region of chemical reaction. The passage of the shock wave initiates the reaction and, in turn, the chemical heat release sustains the shock wave. A detonation is steady if the flow in the reaction zone, as seen by an observer riding on the shock wave, is not time dependent. Due to the extreme conditions generated by condensed material detonations, it is difficult to determine experimentally even simple reaction zone properties in such materials, e.g., the dependence of the chemical heat release rate on the thermodynamic state. Hence it is appropriate to seek theoretical models for the reaction zone properties. As noted in the last chapter, a one-dimensional steady-state model (ZND model) for the structure of detonation waves was first introduced in the 1940's. This model consists of an inert shock wave (normal shock moving at the detonation velocity) following by a reaction zone. The passage of the shock wave heats the reactants, which initiates the chemical reaction (an irreversible reaction is assumed). The reaction proceeds to completion, i.e., $\lambda = 1$, and the final C-J solution is reached (here λ is the degree of reaction: $\lambda = 0$ refers to no reaction and $\lambda = 1$ refers to complete reaction). As the reaction progresses towards completion, the pressure P and density ρ of the detonation products decrease as shown in figure 2.1 while the temperature T and relative particle velocity u behind the detonation wave increase. In a one-dimensional detonation, none of the chemical heat release causes lateral material motion. The planar nature of the system considered guarantees that the C-J state is always reached. Another consequence is that the detonation velocity in this classical ZND theory is always the same as that of C-J theory, i.e. the CJ plane detonation has a sonic state $c = u$ at the end of its reaction zone, $\lambda = 1$. Here c refers to the local sound speed. The simple argument made is that the weak disturbance

behind the detonation reaction zone can neither disturb nor catch up to the leading shock wave by passing through the reaction zone region from the detonation shock to the sonic locus. This planar, steady structure can be modified by wave shape changes or other losses in the reaction zone, which then alter the simple description and lead naturally to the concept of an eigenvalue detonation. Ficket & Davis (1979) attribute the earliest example of an eigenvalue detonation to Von Neumann's discussion of pathological detonation structure due to a mole decrement in the reaction zone. The state at the sonic locus is no longer a complete reaction state and independent of the detonation speed but instead depends on a special eigenvalue detonation speed that is determined as a consequence of constructing the solution in the reaction zone.

The eigenvalue detonation that we are concerned with here is associated with detonation shock curvature and wall losses. One of its first manifestations occurred during World War II with the observation of the diameter effect. At infinite diameter, the plane CJ detonation is obtained since the chemical-heat release does not cause any lateral material motion. In contrast to this, a detonation traveling in a charge of finite lateral extent uses some of its chemical heat to produce lateral material motion. There are three important consequences of this: (1) the shock pressure decreases as one moves along the shock from the charge center to its edge, (2) the shock velocity is reduced, and (3) a critical value of the lateral dimension exists, called the "failure diameter," below which a steady wave will not propagate.

It is known from previous work (Engelke, 1979; Dremin, 1999) that diameter-effect curves of high-density explosives appear to fall into two classes. High-density solid explosives at less than theoretical maximum density have diameter-effect curves which show a strong downward concavity and velocity decrements of approximately 10% between the infinite–medium detonation velocity and that at the failure diameter. The second class of diameter-effect curves is for (homogeneous) liquid explosives. The diameter-effect curves for the liquid forms of the explosives such as nitromethane and trinitrotoluene (TNT) are nearly linear and show very small velocity decrements at failure (< 2%). One can pose the question: what causes the

differences between the diameter effect curves for solid (at less than theoretical maximum density) and liquid explosives? Bdzil (1981) postulated that the difference

> *"is due to there being two mechanisms supporting wave propagation in heterogeneous solids; i.e., hot spots and homogenous burn, while in homogenous explosives only homogenous burn is present. Thus, one can speculate that in heterogeneous explosives at large diameters both mechanisms contribute to driving the wave while at diameters near failure only the hot-spot mechanism sustains wave motion. The lack of a region of sharp drop in the liquid curves is due then to absence of the hot-spot mechanism."*

Thus, the response of a detonation (i.e., the shape and velocity of the shock) to a change in the diameter of the charge is determined by the interaction between the fluid mechanics and the heat-release rate law in the reaction zone. In order to infer the thermodynamic-state dependence of the reaction rate from experimental measurements and predict the detonation properties of finite charge explosives, various theories of steady state detonation have been developed (Chan, 1983; Engelke, 1983; Zel'dovich, 1986; Stewart, 1998; Dionne, 2000) to predict the velocity-diameter effect. Among them is the quasi-one-dimensional steady ZND model with losses (e.g., Dionne, 2000). In the framework of this model, endothermic reactions, area divergence, momentum and heat losses are all of the same nature and can be treated as "negative" source terms in the one-dimensional Euler equations. The detonation propagation in the presence of these source terms possesses the common phenomenon that a wave velocity deficit with respect to the C-J value occurs. In the case of finite diameter charge detonation, a competition between the chemical energy release of the explosive (i.e., the "positive" source term) and the "negative" source terms such as detonation front curvature, momentum and heat losses to the charge wall, results in a deficit in the energy supporting the wave propagation and hence causes the wave velocity deficit. To simulate this so-called eigenvalue detonation in condensed explosives, most work in the past assumed the gaseous products obeyed the perfect gas law and detonation front curvature was considered only. In fact, to

predict the diameter effect of condensed explosives well, more realistic equations of state and wall effects besides the detonation front curvature should be taken into account. Here we report a solution of these problems for a detonation in liquid NM based on the Euler equations with source terms together with non-ideal equations of state and an appropriate reaction rate law. Our objectives are to determine whether the chosen equation of state and reaction rate law can reproduce the diameter effect of this explosive, to determine the most appropriate reaction rate law from the point of view of detonation failure and to investigate how and to what degree the detonation front curvature or charge diameter affects the detonation parameters in the reaction zone. In fact, the determination of an appropriate equation of state and reaction rate law for pure liquid explosives is required prior to simulating the non-ideal detonation of an aluminized liquid explosive with the two-phase flow model.

2.2 Governing Equations and Generalized C-J Condition

The one-dimensional steady Euler equations with source terms of mass, momentum and energy can be written as follows in the shock-attached frame (details are given in Appendix 1)

$$\frac{d(\rho u)}{dx} = m \tag{2.1}$$

$$\frac{d(\rho u^2 + P)}{dx} = um + f \tag{2.2}$$

$$\frac{d[\rho u(e + \frac{u^2}{2} + \frac{P}{\rho})]}{dx} = m(e + \frac{u^2}{2} + \frac{P}{\rho}) + uf - q \tag{2.3}$$

Here the variables D, ρ, P, u and e denote the detonation velocity, density, pressure, relative particle velocity and the internal energy, respectively; the source terms m, f, q are the rate of mass, momentum and energy losses, respectively. To further simplify equations (2.1)-(2.3), we consider internal energy e to be a function of P, ρ

(or specific volume v) and degree of reaction λ, i.e., $e = e(P, v, \lambda)$. Hence, the local sound speed c of flow can be written as

$$c^2 = \frac{v^2[P + (\frac{\partial e}{\partial v})_{p,\lambda}]}{(\frac{\partial e}{\partial P})_{v,\lambda}} \tag{2.4}$$

By using equation (2.4) and rearranging (2.1)-(2.3), the governing equations for a 1-D steady state detonation can be written explicitly as (see equations (27), (30), (31), (32) in Appendix 1)

$$\frac{du}{dx} = \frac{\psi}{\eta} \tag{2.5}$$

$$\frac{d\rho}{dx} = \frac{m}{u} - \rho\frac{du}{dx} \tag{2.6}$$

$$\frac{dP}{dx} = f - \rho u\frac{du}{dx} \tag{2.7}$$

$$\frac{de}{dx} = \frac{P}{\rho^2}\frac{d\rho}{dx} - \frac{q}{\rho u} \tag{2.8}$$

Here ψ is the thermicity and η is the sonic condition:

$$\psi = u(\frac{\partial P}{\partial \lambda})_{v,e}\frac{d\lambda}{dx} - [uf - mc^2 + \frac{q}{\rho}(\frac{\partial P}{\partial e})_{v,\lambda}] \tag{2.9}$$

$$\eta = \rho(c^2 - u^2) \tag{2.10}$$

In the right hand side of equation (2.9), the first term represents the heat release of detonation, the second term represents the heat losses due to the curvature of detonation wave, the wall friction and the heat transfer to the wall. It is just the competition between the exothermic and the endothermic that determines the eigenvalue detonation.

With the presence of source terms in equation (2.5), the classical C-J criterion can no longer be used to select the unique detonation solution. Chapman's minimum velocity solution does not apply, since the integral curve is no longer a straight line (Rayleigh line) to permit a solution tangent to the equilibrium Hugoniot to be found

directly. Jouguet's criterion is also invalid, since the detonation products are no longer in equilibrium within the reaction zone when the sonic plane is reached. Hence, an alternative criterion has to be defined to seek a unique solution to the conservation equations for the detonation structure. When the particle velocity u becomes sonic (i.e., Mach number $M = u/c = 1$) in equation (2.5) the denominator η vanishes. Hence, the governing equation (2.5) will be singular if η passes through zero unless ψ becomes zero at that point as well. If η goes through zero when ψ is not zero, steady-state shock propagation at the specified shock velocity is not possible. It is also possible that η never goes through zero. These solutions are overdriven. Self-supported detonation occurs at the boundary between the over-driven and non-propagating solutions. Hence η must go through zero exactly when $\psi = 0$. This results in an indeterminate value for the derivative du/dx and permits a smooth transition through the sonic point. The condition of requiring that the numerator vanishes when the sonic condition $c = u$ is reached is often referred to as the generalized C-J condition in the literature, even though both of the classical criteria of Chapman and Jouguet do not involve the analysis of a non-equilibrium detonation structure. This criterion provides a means of seeking a particular integral curve to the conservation laws for the detonation structure. By solving the equations (2.5)-(2.8) with this generalized C-J condition, we can determine the eigenvalue detonation parameters and the detonation structure. The initial conditions for solving equations (2.5)-(2.8) are the chemical concentrations and the initial pressure and particle velocity at the shock front. For a very thin shock front, it is usually assumed that no reaction takes place, i.e., $\lambda = 0$ across the shock front. In the calculation procedure, a shock velocity D is first specified, then a series of (P,v) states with different chemical concentrations are determined until the final condition $\psi = 0$, $\eta = 0$ is satisfied.

2.3 Equations of State and Reaction Rate Laws

In order to solve equations (2.5)-(2.8), several elements are needed: reaction product components and reaction heat release, the specification of the kinetic law $\frac{d\lambda}{dt}$, and the calibrated parameters of the equations of state of the detonation products and reactants.

2.3.1 Equations of State (EOS). The calculation of the detonation properties of an explosive requires the equation of state to define the P-v-T behavior of the detonation products. The inaccuracy of these equations of state can be a source of deviation between the theoretical detonation velocity and experimental observations. The perfect gas EOS used for low-pressure gaseous explosive detonation products is very simple and easy to incorporate into the detonation calculation. However, when dealing with condensed explosives, the detonation pressure is so high that the perfect gas and even real gas EOS are not valid. At these extremely high pressures (on the order of 10 GPa), the gases are very dense and we shall refer to them as fluids. They deviate significantly from ideal gas behavior. For instance, the compressibility factor can reach values as high as 8 compared to 1 for the ideal case. It has been verified that the ideal gas EOS is not adequate to make quantitative predictions for condensed explosives (Steward, 1998) and hence a more realistic EOS must be selected. Indeed, for condensed explosives, the equations of state become a major source of difficulties, due to their limited accuracy, as well as their complicated functional forms required to fit the experimental data. So far, the quest for accurate and realistic equations of state for very high pressure detonation calculations is an on-going process. However, there exists a number of EOS's applicable in condensed explosives, such as the BKW, the JCZ and the JWL. These equations of state are based on empirical observations. They contain arbitrary constants determined by fitting to experiments. The Jones-Wilkins-Lee (JWL) is an example of these equations of state. The JWL

EOS consists of additive corrections to a perfect gas EOS. Parameters may be found by fitting to a relatively narrow range of states, e.g., the region of a single expansion adiabatic in a cylinder test. Tables of the constants for the JWL equation of state, calibrated for many explosives are available in Dobratz and Crawford (1985). Although the physical validity is limited to the range of the data to which it is fitted, the JWL EOS is computationally efficient and is the most convenient EOS due to the fact that it relates the pressure to the density and specific internal energy. The JWL equation of state has proven to be very useful by Steward (1998) for calculating the normal detonation shock velocity-curvature of the PBX9502 explosive and has been widely used for engineering calculations. Here, we also assume the JWL EOS for detonation products and the Mie-Gruneisen EOS for the unreacted explosive in this study.

Considering a "u_p, D" shock Hugoniot for the unreacted material, the measured shock velocity D in response to a piston impact with speed u_p, is assumed to obey the standard form

$$D = c_0 + s_0 u_p \tag{2.11}$$

Where c_0 is the ambient sound speed in the unreacted explosive, and s_0 is a slope determined experimentally from piston impact experiments. A Mie-Gruneisen EOS form (Steward, 1998) for the unreacted explosive that is consistent with the equation (2.11) is

$$e_{MG} = e_h + \frac{v_0}{\Gamma}(P - P_h) \tag{2.12}$$

Where

$$e_h = \frac{1}{2}\left[\frac{c_0(v_0 - v)}{v_0 - s_0(v_0 - v)}\right]^2 \tag{2.13}$$

$$P_h = (v_0 - v)\left[\frac{c_0}{v_0 - s_0(v_0 - v)}\right]^2 \tag{2.14}$$

and Γ is Gruneisen gamma, v is specific volume, subscript "0" denotes initial state.

The JWL EOS of the detonation products is assumed to be of the form (Stewart, 1998)

$$e_{JWL} = I_p + \frac{v}{\Omega}(P - P_s) \tag{2.15}$$

Here

$$I_p = v_0\left(\frac{A}{R_1}e^{-\frac{R_1 v}{v_0}} + \frac{B}{R_2}e^{-\frac{R_2 v}{v_0}}\right) \tag{2.16}$$

$$P_s = Ae^{-(R_1 v)/v_0} + Be^{-(R_2 v)/v_0} \tag{2.17}$$

and A, B, R_1, R_2, Ω are the fitted parameters of the JWL EOS.

In the detonation zone, the detonation products and unreacted explosive consist of a mixture of gas, liquid and solid components. Often we need a mixing rule for this mixture when no experimental equation of state is available. Some approaches have been given by Kennedy (1993) and Davis (2000). A common treatment is to assume that the mixture is a continuum and the detailed micro-structure is not considered. A consequence of the continuum assumption is that the different material components are assumed to be moving together; that is, there is just one particle velocity, and it is the same for all the materials of the mixture. No relative flow is taken into account, and treatment is one dimensional, so no transverse motion is allowed. Another consequence is that all the materials are at the same pressure. For simplicity, following Kennedy (1993), we also assume that the unreacted explosive and detonation products have the same density or specific volume. The energy of the mixture is the sum of the energies of the components, so the internal energy (including specific internal energy and chemical energy) can be written as

$$e = (1-\lambda)e_{MG} + \lambda e_{JWL} - \lambda Q \tag{2.18}$$

i.e.,

$$
\begin{aligned}
e &= (1-\lambda)\left[e_h + \frac{v_0}{\Gamma}(P-P_h)\right] + \lambda\left[I_p + \frac{v}{\Omega}(P-P_s) - Q\right] \\
&= (1-\lambda)\left[e_h - \frac{v_0}{\Gamma}P_h\right] + \lambda\left[I_p - \frac{v}{\Omega}P_s - Q\right] + P\left[(1-\lambda)\frac{v_0}{\Gamma} + \lambda\frac{v}{\Omega}\right]
\end{aligned}
\tag{2.19}
$$

Where Q is heat of detonation, which can be determined as long as the detonation product species are known.

The products formed during the detonation of explosives can be estimated by applying the simple product hierarchy for CHNO explosives (and propellants) which states the following "rules of thumb" (Cooper, 1996)

1. First all the nitrogen forms N_2.
2. Then all the hydrogen is burned to H_2O.
3. Any oxygen left after H_2O formation burns carbon to CO.
4. Any oxygen left after CO formation burns CO to CO_2.
5. Any oxygen left after CO_2 formation forms O_2.
6. Traces of NO_x (mixed oxides of nitrogen) are always formed.

As long as the components of detonation products are known, the heat of detonation of the explosive can be determined by

$$
Q = \sum \Delta H_f^0 (detonation \quad products) - \Delta H_f^0 (explosive) \tag{2.20}
$$

where ΔH_f^0 is the heat of formation (Cooper, 1996).

From equation (2.19), we can derive the explicit expression for pressure and its derivative with respect to the reaction variable

$$
P = \frac{e + (1-\lambda)\left[\frac{v_0}{\Gamma}P_h - e_h\right] + \lambda\left[\frac{v}{\Omega}P_s - I_p + Q\right]}{(1-\lambda)\frac{v_0}{\Gamma} + \lambda\frac{v}{\Omega}} \tag{2.21}
$$

$$(\frac{\partial P}{\partial \lambda})_{e,v} = \frac{e_h - \frac{v_0}{\Gamma}P_h + \frac{v}{\Omega}P_s - I_p + Q}{(1-\lambda)\frac{v_0}{\Gamma} + \lambda\frac{v}{\Omega}}$$

$$+ \frac{e + (1-\lambda)(\frac{v_0}{\Gamma}P_h - e_h) + \lambda(\frac{v}{\Omega}P_s - I_p + Q)}{\left[(1-\lambda)\frac{v_0}{\Gamma} + \lambda\frac{v}{\Omega}\right]^2}(\frac{v_0}{\Gamma} - \frac{v}{\Omega})$$

$$= \frac{J(v)}{S(v,\lambda)} + \frac{P}{S(v,\lambda)}(\frac{v_0}{\Gamma} - \frac{v}{\Omega}) \tag{2.22}$$

Where

$$J(v) = e_h - \frac{v_0}{\Gamma}P_h + \frac{v}{\Omega}P_s - I_p + Q \tag{2.23}$$

$$S(v,\lambda) = (1-\lambda)\frac{v_0}{\Gamma} + \lambda\frac{v}{\Omega} \tag{2.24}$$

Differentiating (2.19), we also obtain the derivatives of energy

$$(\frac{\partial e}{\partial v})_{p,\lambda} = (1-\lambda)\left[\frac{\partial e_h}{\partial v} - \frac{v_0}{\Gamma}\frac{\partial P_h}{\partial v}\right] + \lambda\left[\frac{\partial I_p}{\partial v} - \frac{P_s}{\Omega} - \frac{v}{\Omega}\frac{\partial P_s}{\partial v}\right] + \lambda\frac{P}{\Omega}$$

$$= (1-\lambda)\left[\frac{v_0}{\Gamma}\frac{{c_0}^2\{v_0 + s_0(v_0 - v)\}}{\{v_0 - s_0(v_0 - v)\}^3} - \frac{{c_0}^2 v_0(v_0 - v)}{\{v_0 - s_0(v_0 - v)\}^3}\right]$$

$$+ \lambda\left[e^{-\frac{R_1 v}{v_0}}(\frac{AR_1 v}{v_0\Omega} - A - \frac{A}{\Omega}) + e^{-\frac{R_2 v}{v_0}}(\frac{BR_2 v}{v_0\Omega} - B - \frac{B}{\Omega})\right] + \lambda\frac{P}{\Omega} \tag{2.25}$$

$$(\frac{\partial e}{\partial P})_{v,\lambda} = (1-\lambda)\frac{v_0}{\Gamma} + \lambda\frac{v}{\Omega} \tag{2.26}$$

By substituting (2.25), (2.26) into (2.4), the sound speed of the mixture in the detonation zone can be calculated.

As for the temperature of the mixture, we assume it to be of the following form

$$T = (1-\lambda)T_{MG} + \lambda T_{JWL} \tag{2.27}$$

Where $T_{MG} = \frac{e_{MG}}{C_{VMG}}$, is the temperature of unreacted explosive; $T_{JWL} = \frac{e_{JEWL}}{C_V}$, is the temperature of detonation products; C_{VMG}, the specific heat capacity of the unreacted explosives; and C_v is the specific heat capacity of the detonation products.

2.3.2 Reaction Rate Laws. In general the reaction of an explosive is given schematically by

$$\mathrm{A} \xrightarrow{k} \mathrm{B} \tag{2.28}$$

Where species A is the liquid explosive and species B is the detonation products, and k is the reaction rate constant. The reaction rate law can be expressed by

$$\frac{d\lambda}{dt} = k\ (1-\lambda) \tag{2.29}$$

In the shock frame, for steady state, equation (2.29) becomes

$$\frac{d\lambda}{dx} = k\ (1-\lambda)/u \tag{2.30}$$

Several expressions for the reaction rate constant have been considered in the past, including a simple constant, temperature and pressure dependent forms, and hot-spot models (Fried, 1998). Here we assume that the reaction rate of NM obeys one of the following laws

Simple law
$$\frac{d\lambda}{dt} = Z_s(1-\lambda) \tag{2.31}$$

Arrhenius law
$$\frac{d\lambda}{dt} = Z(1-\lambda)e^{\frac{E^*}{RT}} \tag{2.32}$$

Here Z_s and Z are the reaction rate constants; E^* is the activation energy; R is the specific gas constant; and T is the temperature.

2.4 Detonation of Infinite Diameter Nitromethane

Nitromethane (NM) is perhaps the most widely studied explosive of all time. The advantage of using NM as a test bed is the large amount of data available on its detonation properties, which are useful for validating the quasi-1-D model, the generalized CJ condition and the chosen EOS. In addition, the baseline parameters for this explosive, such as the ignition delay and reaction rate, are adjusted to be in agreement with measurement of the total reaction time and reaction zone length in NM.

In the case of infinite diameter NM, the source terms $m = f = q = 0$. The governing equations (2.5) - (2.8) are then reduced to

$$\frac{du}{dx} = \frac{\psi}{\eta} \tag{2.33}$$

$$\frac{d\rho}{dx} = -\frac{\rho}{u}\frac{du}{dx} \tag{2.34}$$

$$\frac{dP}{dx} = -\rho u \frac{du}{dx} \tag{2.35}$$

$$\frac{de}{dx} = \frac{P}{\rho^2}\frac{d\rho}{dx} \tag{2.36}$$

Where

$$\psi = u(\frac{\partial P}{\partial \lambda})_{v,e}\frac{d\lambda}{dx}, \text{ and } \eta = \rho(c^2 - u^2) \tag{2.37}$$

In order to solve equations (2.33)-(2.36), we need first to determine the heat of NM detonation, and the parameters (or constants) in the reaction rate law and EOS.

By applying the above "rules of thumb" of detonation product formation (Cooper, 1996), the overall reaction equation of NM is

$$CH_3NO_2 \xrightarrow{K} 1.5H_2O + 0.5CO + 0.5C + 0.5N_2 \tag{2.38}$$

The heat of detonation of NM explosive can be determined as

$$Q_{NM} = \sum \Delta H_f^0 (detonation \quad products) - \Delta H_f^0 (explosive)$$

$$= 1.5 \times (57.8 \text{ kcal/mol}) + 0.5 \times (26.4157 \text{ kcal/mol}) - 1 \times (27 \text{ kcal/mol})$$

$$= 72.9 \text{ kcal/mol} \approx 5 \times 10^6 \text{ J/kg}$$

This calculation is identical with the experimental result of $Q_{NM} = 5 \times 10^6$ J/kg (Cooper, 1996)

For NM, various values for the activation energy, i.e., E^*=30, 40, 53.6 kcal/mol, can be found in the literature (Engelke, 1983; Presles, 1995; Mader, 1998). Since the reaction time of NM is on the order of $t = 7 - 50$ ns (Sheffield, 1999, 2002), the pre-exponent factors Z_s, Z of the reaction rate law can be selected to match this time. Taking $t = 20$ ns as the reaction time scale of NM, we can determine the reaction rate constants $Z_s = 4.5 \times 10^8$ and $Z = 1.45 \times 10^{10}$, 2.2×10^{12} and 9.5×10^{13} for E^* =30, 40, 53.6 kcal/mol, respectively.

As for an equation of state for NM, Dunnett (1998) gives empirical JWL parameters which are optimized to reproduce cylinder expansion data. These parameters are A=209.2 GPa, B=5.689 GPa, R_1=4.4, R_2 =1.20, Ω =0.30. In the unreacted explosive, the Gruneisen gamma Γ and NM's shock Hugoniot coefficients c_0, s_0 are determined from Sheffield (1999, 2002) which are Γ=2.1, c_0=1760 m/s, s_0 =1.56. Winey (2000) has modeled the specific heat capacity C_{vMG} of unreacted but shocked liquid nitromethane as functions of temperature and volume using the existing experimental data and gives the final expression for $C_{vMG}(T,v)$ in units of J/kg

$$C_v(T,v) = 1.146 + \frac{1.714 x^2 e^x}{(e^x - 1)^2} \tag{2.39}$$

where $x = \dfrac{2326 + 102.2\mu}{T}$ and $\mu = \dfrac{v_0}{v} - 1$.

There are two ways to determine the specific heat capacity C_{vJWL} of the detonation products. The first method is that we just simply assume C_{vJWL} =constant. Its value is calibrated by using the existing temperature data. The fact that numerous experiments show that the CJ temperature of NM is in the range of 3400 – 3800 K

(Gibson, 1958; Burton 1982; Kato, 1985; He, 1985; Leal, 1998), leads us to determine that C_v = 1800 J/kg-K is a good estimation of the specific heat capacity. The advantage of the assumption $C_{vJWL} = constant$ is that it simplifies the calculation of the governing differential equations and saves considerable computational time. Of course, in reality, C_{vJWL} is a function of temperature, especially in the case of high temperature and pressure detonation products. Hence, a second method is to make a regression of C_{vJWL} as a function of temperature from existing data in the literature (Cooper, 1996). Fortunately, plots of specific heat capacity of gases versus absolute temperature are very smooth and fit the form of a simple quadratic equation over the temperature range of 300 – 5000 K, i.e.,

$$C_{vJWL} = a + bT + cT^2 , \tag{2.40}$$

Where the constants a, b, and c vary with each particular gas. Table 2.1 gives the values for several gases. The specific heat capacity of solid product carbon is a constant that equals to 11.7152 $\frac{J}{K \cdot mol}$. The specific heat capacity value of detonation product mixture is equal to the sum of the products of the mole fraction of each component times its heat capacity

$$C_{vJWL} = \sum n_i C_{vi} = 1.5C_{vH_2O} + 0.5C_{vCO} + 0.5C_{vN_2} + 0.5C_{vC}$$

$$= 62.3361 + 12.3535\times10^{-3}\,T - 1.03546\times10^{-6}\,T^2 \quad \frac{J}{K \cdot mol}$$

$$\approx 1021.9 + 0.2\,T - 1.697\times10^{-5}\,T^2 \quad \frac{J}{K \cdot kg}$$

The initial conditions for solving equations (2.33)-(2.36) are the chemical concentrations and the initial pressure and particle velocity at the shock front. Since the shock front is very thin, it is usually assumed that no reaction takes, i.e., $\lambda = 0$, across the shock front. The initial state variables are found by finding the intersection of the Rayleigh line

$$P = \rho D u \tag{2.41}$$

with the unreacted shock Hugoniot

$$D = c_0 + s_0 u \tag{2.42}$$

if the shock velocity D is specified. From this point on, the calculation procedure visits a series of (P,v) states with different chemical concentrations.

The governing equations (2.33)-(2.36) will be singular if η passes through zero unless ψ becomes zero at that point as well. If η goes through zero when ψ is not zero, steady-state shock propagation at the specified shock velocity is not possible. It is also possible that η never goes through zero. These solutions are overdriven. Self-supported detonation occurs at the boundary between over-driven and non-propagating solution. η must go through zero exactly when $\psi = 0$. It is often referred as the generalized C-J. As a matter of fact, from equation (2.33) and the reaction rate equations (2.31) and (2.32), the generalized CJ condition $\eta = 0, \psi = 0$ leads to

$$c = u, \quad \lambda = 1 \tag{2.43}$$

This is also the classical C-J condition. Therefore, for the detonation of an infinite diameter homogeneous explosive, the generalized CJ condition is identical to the classical CJ condition.

With the above-specified conditions, the solution of equations (2.33)-(2.36) can be found by using the 4th order of Runge-Kutta method. Table 2.2 summarizes the results of this model together with Cheetah code calculations and some typical experimental results in NM.

The experimental detonation velocity and CJ pressure for NM with an initial density of 1.13 g/cm^3 are given by Blais (1997) as 6300 m/s and 13 GPa, respectively. This model predicts a detonation velocity of 6316.7 m/s and a CJ pressure of 12.85 GPa. The match between the model predictions and the experimental values for detonation velocity and pressure is good. In comparison, using the Cheetah code with the BKWC EOS, gives good agreement for the predicted CJ temperature, but predicts rather low values for the detonation velocity and pressure. This illustrates that the selected equations of state play an important role in the accuracy of the theoretical model.

The profiles of detonation temperature, pressure, density, reaction progress and Mach number within the detonation zone of NM are shown in Fig 2.2, corresponding to the different reaction rate laws. It is clear from this plot that although the initial and final states of the detonation are the same, the variation of the parameters within the reaction zone is strongly dependent on the reaction rate law. This indicates that an indirect method for determining the appropriate reaction rate law for an explosive is through measuring the profiles within the detonation zone, e.g., of the particle velocity and detonation pressure. At the present stage, due to the difficulty of measuring these profiles experimentally in the extremely short reaction zone of a liquid explosive, it is not clear which reaction rate law is the best choice. Therefore, both the simple and Arrhenius laws will be alternatively used in later calculations to further explore their validity.

2.5 Detonation of Finite Diameter NM Charges

2.5.1 Consideration of Front Curvature. In the case of an unconfined charge, the detonation front curvature plays a key role in the detonation-diameter effect. As in the WK theory (Wood and Kirkwood, 1954), if we examine only the relation between the axial detonation velocity of a rate stick and the curvature of the detonation shock on the central stream tube, the two-dimensional problem will be reduced to a quasi one-dimensional problem since the lateral velocity on the central streamline is zero. Therefore, the curvature effect of the two-dimensional problem is analogous to the standard equations for reactive flow in a nozzle, under the usual assumption of quasi-one-dimensional flow, i.e., one-dimensional Euler equations with mass source term only. Equations (2.1)-(2.4) can therefore be reduced to

$$\frac{d(\rho u)}{dx} = m \tag{2.44}$$

$$\frac{d(\rho u^2 + P)}{dx} = um \tag{2.45}$$

$$\frac{d[\rho u(e+\frac{u^2}{2}+\frac{P}{\rho})]}{dx} = m(e+\frac{u^2}{2}+\frac{P}{\rho}) \tag{2.46}$$

Or

$$\rho\frac{du}{dx}+u\frac{d\rho}{dx} = m \tag{2.47}$$

$$\rho u\frac{du}{dx}+\frac{dP}{dx} = 0 \tag{2.48}$$

$$\frac{de}{dx}+P\frac{dv}{dx} = 0 \tag{2.49}$$

Equations (2.47)-(2.49) are identical with the WK equations (Wood and Kirkwood, 1954) if the form of the source term is taken as

$$m = -2\rho\omega_r \quad , \tag{2.50}$$

Where ω_r is the radial flow divergence on the central stream tube. An ad-hoc estimation was made for the flow divergence by relating it to the radius of curvature of the detonation shock as in the WK model (Wood and Kirkwood, 1954), i.e.,

$$\omega_r = \frac{D-u}{R_c} \quad , \tag{2.51}$$

Where R_c is the radius of curvature of the detonation front. With this additional assumption, we obtain the governing equations for solving the dependence of the axial detonation velocity D on curvature, which are the reduced forms of equations (2.47)-(2.49) in pure NM:

$$\frac{du}{dx} = \frac{\psi}{\eta} \tag{2.52}$$

$$\frac{d\rho}{dx} = \frac{1}{u}(m-\rho\frac{du}{dx}) \tag{2.53}$$

$$\frac{dP}{dx} = -\rho u\ \frac{du}{dx} \tag{2.54}$$

$$\frac{de}{dx} = \frac{P}{\rho^2}\frac{d\rho}{dx} \tag{2.55}$$

Here

$$\psi = u\left(\frac{\partial P}{\partial \lambda}\right)_{v,e}\frac{d\lambda}{dx} + mc^2 \quad \text{, and}$$

$$\eta = \rho(c^2 - u^2). \tag{2.56}$$

These equations differ from those for plane one-dimensional flow in two ways: (1) the relation between ρ and u now depends on m, and (2) the term $m = -2\rho\omega_r$ is added to ψ. It is noted that this divergence term in ψ has, for positive ω_r, the same sign as for an endothermic reaction. With the addition of m these equations form a determinate set, and they have a critical point where ψ and η vanish simultaneously. The vanishing of ψ means that, roughly speaking, the release of energy by the chemical reaction is balanced by the expansion due to the radial flow; this point is reached before the attainment of chemical equilibrium. Usually $\psi = 0$ refers to the thermicity condition and $\eta = 0$ refers to the sonic condition in the literature (Fickett and Davis, 1979). To solve the eigenvalue detonation problem for a finite diameter explosive with curvature is equivalent to saying that these two conditions are satisfied simultaneously.

With the same equations of state and reaction rate laws as used in the detonation of infinite diameter NM, iterations are made to determine the eigenvalues of the detonation with different curvature values. The results are presented in Figs. 2.3 and 2.4. Figure 2.4 is a plot of non-dimensional detonation velocity vs. detonation front curvature in NM. For both the Arrhenius law and simple law, the predicted detonation velocities vary little with curvature. A decrease in the detonation velocity of less than 1.6% before detonation failure, is consistent with the experimental finding that detonation failure occurs with less then 2% velocity deficit. With the Arrhenius rate law, the phenomena of critical curvature and detonation failure are also captured in this calculation as shown in Fig.2.4. On the other hand, the simple law fails to predict

the existence of a critical curvature. We conclude that the Arrhenius rate law is more appropriate than the simple law in the simulation of the diameter effect for liquid NM. Figure 2.3 shows the change of the detonation zone time, and detonation temperature and pressure at the sonic point due to the detonation front curvature. Here the detonation zone time is the time from detonation wave front to the sonic point. With the Arrhenius rate law, with increasing detonation front curvature, the temperature and pressure at the sonic point decrease resulting in an increase in the reaction zone length. These results are reasonable in terms of the fact that curvature causes radial energy dissipation and hence less energy is available (relative to a C-J detonation) to support the detonation propagation. We note that near the detonation failure, the temperature at the sonic point decreases from 3676.5 K for a C-J detonation to non-ideal values of 3189 K and 3489.48 K for E^* =30 and 53.6 kcal/mol, respectively. The temperature deficit corresponds to 13% and 5% for E^* = 30 and 53.6 kcal/mol, respectively. Similarly, an increase in the reaction zone length occurs near detonation failure (up to a factor of 2 increase for E^* =30 kcal/mol). These plots illustrate that the detonation temperature and the reaction zone length are relatively sensitive parameters for the curvature. On the other hand, near detonation failure, the decrease in pressure at the sonic point is relatively small. The fact that the maximum deficit in the pressure at the sonic point is only 4% for E^* =30 kcal/mole demonstrates that the detonation pressure is a less sensitive parameter for non-ideal detonation behavior. From Fig. 2.4, we also note that far from the critical curvature or detonation failure point, the detonation deficits are quite small due to the detonation front curvature. Therefore, in dealing with the complex problem of non-ideal detonation propagation in an aluminized liquid explosive with a large charge diameter, the effects of the global curvature of the front can be neglected to a good approximation. In other words, for non-ideal detonation of aluminized explosives with large charge diameters, the deficits in detonation velocity, pressure and temperature may be due to other factors rather than the global curvature of the detonation front.

Figure 2.3 also shows the calculation results using the simple reaction rate law. Although the detonation temperature and pressure at the sonic point both decrease, the result that the detonation zone time also decreases with increasing curvature is not physically reasonable. Therefore we conclude again that the Arrhenius law is a better choice than the simple law in the simulation of eigenvalue detonation of NM.

In reality, detonation velocity deficits are often given in terms of the inverse charge diameter. To relate the charge diameter with the detonation front curvature, Leiper, et al., (1994) suggested the following empirical relation

$$\frac{d}{R_c} = 0.165 + 0.692\frac{d_f}{d} \tag{2.57}$$

Where d is the charge diameter and d_f is the failure diameter. From the critical radius of curvature calculated, the failure diameter d_f can be evaluated by equation (2.57), i.e.:

$$d_f = (0.165 + 0.692)R_c = 0.857R_c$$

The calculated values of the critical diameter are shown in Table 2.3. Compared with the experimental data, the calculated failure diameter of NM due to curvature only is quite reasonable but a little smaller than that of experiments. This can be improved by considering wall effects.

2.5.2 Detonation of a Finite Diameter NM Charge with Weak Confinement. In reality, the confinement of a cylindrical explosive charge depends on the material (and thickness) of the charge casing. In this section, we will focus on the detonation of charges weakly confined by tubes comprised of paper or plastic. With strong confinement such as that provided by a thick steel tube, due to its large strength and impedance mismatch between the explosive and the tube, the tube may act as a reflecting wall for the detonation wave. The role of confinement in reflecting transverse shock waves on the surface of a *gaseous* detonation wave is well known. Dremin (1999) has described the role of confinement and the generation of hot-spots

from shock collisions in the context of the propagation of detonation in condensed explosives. In general, increasing the confinement of the explosive reduces the failure diameter due to the interaction of a detonation wave with the confining material. In the present analysis, we will consider the weak confinement case, in which a reaction-quenching expansion wave moves from the charge surface to the charge axis leading to detonation failure. To estimate the detonation failure in this case, we consider not only the detonation wave curvature due to the lateral expansion, but also losses of momentum and heat from the wall. Frictional losses at the tube wall are modeled by introducing a source term f in the momentum equation. For example, Zel'dovich et al. (1986) suggested the following form:

$$f = k_f \rho U |U| \tag{2.58}$$

where U is the particle velocity in the laboratory frame, and k_f is a friction factor given by Schlichting's formula, i.e.:

$$k_f = 2\left[2\log\left(\frac{d}{2k_s}\right) + 1.74\right]^{-2} \quad , \tag{2.59}$$

where k_s is the equivalent sand roughness and R is the tube radius. This friction factor is valid for flow regimes with full exposure of roughness, and for Reynolds numbers based on the height of the roughness elements above 530. The absolute value in equation (2.58) accounts for the fact that friction always tends to oppose the motion of the flow. Zhang and Lee (1994) used a very similar function where they included the effect of the tube diameter independently from k_f, i.e.:

$$f = \left(\frac{2}{d}\right) k_f \rho U |U| \tag{2.60}$$

where k_f is assumed to obey the Blasius formula, i.e.:

$$k_f = \frac{0.3164}{R_e^{0.25}} \tag{2.61}$$

In the present study, we will use equation (2.60) to account for frictional losses at the tube wall. The Reynolds number is given by the following relation

$$R_e = \frac{\rho U d}{\mu} \quad , \tag{2.62}$$

where μ is the viscosity of the detonation products.

External heat losses are modeled by introducing a source term q in the conservation of energy equation. For example, Zel'dovich et al. (1986) used the following form to account for heat losses to the tube walls, i.e.,

$$q = \gamma h_c \rho u C_p \left(T^* - T_w\right) \quad , \tag{2.63}$$

Where h_c is the coefficient of heat transfer for a smooth tube, C_p is the heat capacity at constant pressure, γ is the adiabatic exponent, u is the particle velocity relative to the shock, T^* is the stagnation temperature and T_w is the wall temperature. An alternative approach to model heat losses in tubes with friction is to use Reynolds analogy. This analogy relates the heat losses to the frictional losses:

$$\frac{h_c}{\rho u C_p} = \frac{C_f}{2} = \frac{f}{\rho u^2} \tag{2.64}$$

Where h_c is the heat transfer coefficient, C_f is coefficient of skin friction, and f is the source term for friction, as given in equation (2.60), for example. This relation is then used to obtain a functional form for the source term q, i.e.:

$$q = C_p \frac{f}{u}\left(T - T_w\right) \quad , \tag{2.65}$$

Where T is the local temperature of the detonation products. In the present study, equation (2.65) will be used to account for heat losses. The advantage of using this formulation is that no additional coefficient is necessary to account for heat losses.

If we assume the same curvature-diameter relation as given in equation (2.57), with the equations (2.60) and (2.65), the source terms f and q can be easily determined for the given charge diameter d. The determination of the source term m involves the critical curvature and hence failure diameter. They cannot be determined *a priori* until the eigenvalue problem of equations (2.5) – (2.8) is solved. Therefore an iterative process must be used as follows. With an assumed failure diameter d_f, for a

given charge diameter d, the curvature of the detonation front can be estimated by equation (2.57). Then the source terms m, f and q can be calculated by equations (2.50), (2.60) and (2.65). With the same method as before, the eigenvalue problem of equations (2.5) – (2.8) with m, f, and q can be solved with the generalized C-J condition. Therefore, a new critical curvature and hence a new failure diameter can be derived. If this new failure diameter is close to the assumed value, the eigenvalue detonation problem in a weakly confining tube has been solved completely. Otherwise, another value of the failure diameter must be assumed. The above process is repeated until the calculated failure diameter is close to the assumed value, within a prescribed error. Fig. 2.5 shows the calculated result of detonation velocity-inverse diameter in NM with the weakly confining tube. The detonation velocity deficit obtained (i.e., less than 2% at the failure diameter) is consistent with the experimental results. As shown in Table 2.3, with an Arrhenius reaction rate law, failure diameters of 15-18 mm are obtained for activation energies in the range of 30-40 kcal/mol, which are consistent with experimental values. However, for E^* = 53.6 kcal/mol, the calculated failure diameter of 22 mm exceeds experimental values. This illustrates that the reaction rate constant $k = Ze^{-\frac{E^*}{RT}}$ plays a key role in determining the failure diameter. In other words, since Z is related to the detonation zone time and the term $e^{-\frac{E^*}{RT}}$ represents the sensitivity of the explosive, an explosive with a short reaction zone and high sensitivity will have a small failure diameter and vice versa.

Comparing these calculation results to the experimental value of failure diameter (18 mm) for weakly confined liquid NM reported by Dremin (1999), the corresponding activation energy in the calculations is E^*= 40 kcal/mol. This value will be continuously used in later chapters of this thesis. On the other hand, the simulation of detonation failure provides a new theoretical way to determine chemical kinetics of detonation taking account of experimental difficulty in high speed elapse process.

Fig. 2.6 shows the temperature and the pressure at the sonic point as a function of charge diameter. For a small charge diameter, the lateral expansion wave rapidly penetrates to the axis of the combustion products cone, producing a strongly curved detonation front. On the other hand, since the ratio of surface area to volume is large for a small charge diameter, friction and heat losses to the wall per unit volume are also large. The increase in the curvature, friction and heat losses results in a decrease in the detonation temperature and pressure as shown in Fig. 2.6.

According to Rosing and Chariton (1940), explosive detonation capability is governed by a relationship between the detonation chemical reaction time t_r and time θ necessary for the expansion wave to penetrate to the axis of the charge, as shown schematically in Fig. 2.7. The detonation propagates only if the explosive has had time to react completely before the expansion wave can cool the products, i.e.: $t_r < \theta$. If $t_r > \theta$, then the propagation fails. Since the lateral rarefaction wave propagates with the local sound velocity c, it follows that the critical conditions for detonation failure occurs when

$$\theta = \frac{d}{2c} \quad , \tag{2.66}$$

where d is the explosive charge diameter. The time-scale equality $t_r = \theta$ corresponds to the failure diameter. From this relation, Chariton (1947) proposed a formula to roughly estimate the failure diameter of an explosive:

$$d_f \approx 2ct_r \tag{2.67}$$

In essence, the formula is based on the flow pattern inside the reaction zone shown in Fig. 2.7., in which the rarefaction wave propagates from the lateral charge surface to its axis inside the reaction zone behind the plane detonation shock wave front, it is suggested that the reaction proceeds only in the region that the rarefaction wave has not reached. Our calculations also show the same trend as equation (2.67), i.e.: if there are two explosives with different chemical reaction rate constant $k_1 = Z_1 e^{-\frac{E_1^*}{RT}}$

and $k_2 = Z_2 e^{\frac{E_2^*}{RT}}$, the explosive with larger failure diameter such as the case of E^*=53.6 kcal/mol has longer detonation zone than the explosive with smaller failure diameter such as the case of E^*=30 kcal/mol. As shown in Fig. 2.5 and 2.6.

Although equation (2.67) is not quantitatively precise, the interpretation of the detonation failure related to detonation zone length is very useful. As a matter of fact, theoretical prediction is possible for the detonation zone time of heterogeneous explosives but it is difficult to predict the failure diameter. In contrast, experimentally it is *relatively* easy to determine the failure diameter of a given explosive but difficult to directly measure the detonation zone time. So equation (2.67) will frequently be used to interpret our two-phase flow model of non-ideal detonation in the aluminized liquid explosives which will be described next in Chapters 3 and 4.

CHAPTER 3 1-D TWO-PHASE FLOW MODEL OF DETONATION IN ALUMINIZED LIQUID EXPLOSIVE

3.1 Problem Description

Detonation of aluminized high explosives has been extensively studied experimentally and theoretically since the middle of the 20^{th} century. These studies are of practical interest because aluminum is incorporated in explosives to enhance air blast, increase bubble energies in underwater explosives, raise detonation temperature and create incendiary effects. On the other hand, this research is also of great scientific interest because detonation propagation in high explosives containing aluminum particles provides a number of challenges for modeling the role of the aluminum particles within the detonation zone.

The key theoretical question is whether the Al reacts in the reaction zone of a detonation wave or at a later time. The majority of researchers believe that for the case of powerful aluminized high explosives, aluminum behaves as an inert additive in the reaction zone and is oxidized only in the expanding detonation products. However, there are supporters of the opposite viewpoint stating that Al participates, at least partially, in the chemical reaction upstream of the C-J plane. The latter researchers generally make their conclusions by using equilibrium thermo-chemical codes. They calculate the detonation parameters of powerful aluminized high explosives and estimate the extent of Al oxidation, i.e.: the fraction of aluminum reacted within the reaction zone of a detonation wave, by adjusting the Al burn fraction to provide the best agreement between calculated and measured detonation velocities.

Previous calculations of Al burn fraction in the detonation zone have often been contradictory. For example, Imkhovik and Soloviev (1995) interpreted their results with RDX/Al explosives to lend support to the conclusion that aluminum does not

react within the detonation zone. Conversely, the estimation by Hobbs and Baer (1993) that 40% of Al in HMX/Al compositions is consumed is rather high in comparison. The result of Cowperthwaite (1993) for RDX/TNT/Al explosives yields even 70% for the amount of Al that reacted within the detonation zone. We have also carried out calculations with the Cheetah 2.0 equilibrium thermodynamic code to calculate the detonation parameters of NM/Al explosives. Figure 1.3 shows the comparison of the experiments and Cheetah calculations with the BKWC equation of state by assuming that the Al was either inert or totally reactive. From these calculations, it is not possible to infer the extent of the reaction of Al within the detonation zone since detonation velocities for both the inert Al and reactive Al cases are lower than those of experiments.

The above discrepancies may be due to the fact that the researchers apply different equations of state to describe the thermodynamics of the detonation products. In addition, the C-J detonation theory is not strictly applicable for the case of aluminized high explosives considering that the assumption of instantaneous thermodynamic equilibrium of the detonation products breaks down for non-ideal explosives. We also note from the experimental data (see Figs. 1.1 and 1.2), that Al particle size affects the detonation velocity of explosive compounds. The effect of size of the Al particles cannot be addressed by a thermodynamic equilibrium code. In fact, if we simply analyze the steady flow of suspensions of particles in liquid explosives with the possible existence of shock waves, we can compute the relaxation zone structure and length behind normal shock waves which generate velocity and temperature differences between the Al particles and the liquid phase. Therefore a more sophisticated non-equilibrium detonation theory should be developed to model non-ideal detonation of the aluminized explosives.

3.2 1- D Two-Phase Non-Equilibrium Detonation Model

3.2.1 Non-Equilibrium Flow Theory for Aluminized Liquid Explosives. The steady flow of suspensions of particles in compressible gases with the possible existence of shock waves has been analyzed by many investigators (e.g., Krier, 1978; Boiko, 1983; Veyssiere, 1986). Veyssiere et al. (1986, 1991) reported experimental results for the detonation of two-phase media which were composed of an explosive ethylene-air mixture with a suspension of 10 μm aluminum particles. They produced a qualitative description of the structure of a detonation in these mixtures using streak photography and measurement of velocity, pressure, and radiant emissions. According to their description, behind the detonation shock front, the aluminum particles are accelerated and behave as a chemically inert species as long as they have not reached their ignition temperature.

In the present study, the behavior of aluminum particles in the detonation products of a liquid explosive is investigated and the time scales of drag and heat transfer between the detonation products and the aluminum particles are important physical parameters in the model. Therefore, the problem of interest can be described as following: initially the two phases (liquid explosive and aluminum particles) are in total equilibrium at velocity $U_1 = U_2 = D$, temperature $T_1 = T_2 = T_0$ and pressure P_0, where U is the velocity with respect to laboratory coordinates, D is the detonation wave velocity, the subscript '*1*" refers to liquid properties and "*2*" refers to solid particle properties. A strong shock wave with constant velocity D propagates through the mixture and upsets the equilibrium between the two phases. In the non-equilibrium region, the velocity of the liquid drops whereas the particle velocity rises as a result of friction due to the difference in phase velocities. Particles now find themselves in a high temperature medium and their temperature rises due to heat transfer to the particles. At some downstream location, the particle temperature reaches its point of ignition, T_{ign}. The lapse of time from the shock wave front to the ignition of the particles is called the particle ignition delay time. After that, chemical

reaction of the metallic particles occurs until the particles burn out. While being heated, the particles are also accelerated until they reach the velocity of the liquid phase. The lapse of time from the shock wave front to the equilibrium of particle velocity of both phases is called the relaxation time. The time scales in this relaxation zone and ignition delay can be roughly estimated by the momentum and energy balance equation if the particle volume fraction is negligible.

From Stokes' law, a simple momentum balance in terms of drag-coefficient gives

$$(\frac{\pi}{6}d_2^{\,3})\rho_2\frac{dU_2}{dt}=(\frac{\pi}{4}d_2^2)(\frac{C_D}{2})\rho_1(U_1-U_2)|U_1-U_2| \tag{3.1}$$

For relatively large particles, the particle Reynolds number will not be small and the Stokes drag region will not apply, hence an alternative drag coefficient relation must be chosen. A "standard" drag coefficient given by Kessler (1999) is assumed to be

$$C_D=\begin{cases}\dfrac{24}{R_e}[1+0.15(R_e)^{0.687}] & R_e\le 1000\\ 0.44 & R_e>1000\end{cases} \tag{3.2}$$

where the Reynolds number is

$$R_e=\frac{\rho_1 d_2(U_1-U_2)}{\mu} \tag{3.3}$$

Equation (3.1) can be used to estimate the relaxation time scale when $U_1\approx U_2$

It should be pointed out that, *a priori*, the reaction mechanism of Al particles under the extreme pressure and temperature conditions immediately behind the detonation front is not known and is the subject of current intense experimental and theoretical investigation. Most experimental data on Al particle ignition is obtained in relatively quiescent conditions which may not be applicable to the high convective flow conditions experienced by the Al in the detonation products. Development of a new reaction model for Al particles is beyond the scope of this thesis, and in light of the current uncertainties in the literature, we will follow the approach of previous researchers and use a simple ignition threshold temperature criterion to "turn on" the

reaction of the Al with the detonation products. In this simple model, the ignition delay will therefore be governed by the assumption of the ignition temperature T_{ign} of the particles. According to Friedman and Macek (1962), ignition of an aluminum particle occurs when the temperature at the surface of the particle exceeds the melting point of aluminum oxide. They showed that the temperature within the particles can be considered spatially uniform. If we assume that the equalization of temperature inside the particle is attained instantaneously and neglect any reaction between the particles and their surroundings prior to ignition, the heat balance equation considering only convective heat transfer gives

$$(\frac{\pi}{6})d_2^{\,3}\rho_2 C_{p2}\frac{dT_2}{dt} = \pi d_2 \lambda_f N_u (T_1 - T_2) \tag{3.4}$$

where the Nusselt number Nu is of the form (Soo, 1990)

$$N_u = 2 + 0.459(R_e)^{0.55} P_r \tag{3.5}$$

and the Prandtl number P_r is

$$P_r = \frac{\mu C_{p1}}{\lambda_f} \tag{3.6}$$

where λ_f is the thermal conductivity of the liquid and C_p is the specific heat capacity.

3.2.2 Estimation of Characteristic Times. For numerical calculations of the characteristic time of momentum and thermal relaxation between the aluminum particles and nitromethane, it is simply assumed that the temperature of the fluid phase after the shock front is 3000 K which approximately equals the temperature of the detonation products. The viscosity and the thermal conductivity of the fluid phase are temperature dependence and are given by the following (Gladilin, 1996):

$$\mu = 0.000085\sqrt{\frac{T_1}{3000}} \tag{3.7}$$

$$\lambda_f = 0.32\sqrt{\frac{T_1}{3000}} \tag{3.8}$$

i) Estimation of Drag Timescale. As discussed above, the particle velocity evolution of the solid phase in the flow of the high temperature and pressure detonation products can be obtained from equation (3.1). In particular, the calculation procedure is as follows. For a given shock velocity D, the variables U_1, P and ρ_1 of the fluid phase immediately behind the shock front can be obtained from Rayleigh line (2.41) and shock Hugoniot equation (2.42). With the equilibrium pressure assumption for both phases, the variables U_2 and ρ_2 of the particle immediately behind the shock front are also obtained from Rayleigh line of the solid phase as the form of equation (2.41). Then R_e and C_D are known from equations (3.2) and (3.3). The 4th order of Runge-Kutta method is used to solve equation (3.1) with each small time interval (Δt =0.1 ns) until to the time when particle velocity equilibrium is reached. This time corresponds to particle velocity relaxation timescale. This estimation of the particle and fluid velocity after the shock is sufficient to illustrate the subsequent acceleration of the particles to the ambient flow velocity. However, a further discussion of the jump conditions across the shock is given in section 3.6 below. Following the procedure described above, for a detonation velocity of 6300 m/s, the corresponding particle velocities of Al and NM behind the shock front are about 610 and 2800 m/s, respectively. Due to this difference in the particle velocities, an exchange of momentum between the phases occurs. By solving equation (3.1), the characteristic timescales when the particle velocities reach 99% of fluid phase may be obtained. Fig. 3.1 shows the particle velocity evolution behind the shock front for different Al particle sizes. The drag between the two phases accelerates the motion of the solid phase until both phases have an identical velocity. This relaxation time from shock front to particle velocity equilibrium strongly depends on particle size (for a given particle density). Fig. 3.2 shows the timescale of drag for D = 5500 and 6300 m/s, which are typical detonation velocities of the aluminized nitromethane. For 100 nm size particles, the timescale of drag is about 9 ns which is smaller than the 20 ns detonation zone timescale of NM. However, for micron-sized particles, the timescale of drag is on the order of a

microsecond which is much longer than the detonation timescale. Therefore, it is essential to model the non-equilibrium process of velocity equilibration in the detonation of aluminized NM, at least for micron-sized metallic particles. Figure 3.2 also shows the drag timescale with different shock strengths but the same temperature of the fluid phase, e.g., D = 6300 and 5500 m/s and a 3000 K temperature of the detonation products. From this figure, it can be seen that the effect of shock strengths on the relaxation timescale is quite weak. The same conclusion can be drawn for the effect of the temperature of fluid phase. As shown in Fig. 3.3, with a D = 6000 m/s shock wave, the calculated relaxation times for a given particle size almost remain unchanged when the temperature of the fluid phase after the shock front is assumed to be 1350 K, the temperature of the shocked but unreacted liquid NM, and 3000 K, the typical temperature of the detonation products. This result illustrates that the temperature of the fluid phase has no significant effect on the drag timescale.

ii) Estimation of Ignition Delay Timescale. As mentioned above, the classical Al ignition criterion was proposed by Friedman and Macek (1962). This criterion is based on the presence of the oxide layer on the surface of the particle which impedes the diffusion of the oxidizing species. Hence they proposed that no ignition is possible before melting of this oxide film which occurs at a surface temperature of about 2310 K. The validity of this criterion may be questionable in some cases, and other criteria have been postulated. For example, in their model calculations, Veyssiere et al. (1983) chose 1350 K as the ignition temperature of 1-20 μm aluminum particles. Kuehl (1965) reported the ignition of aluminum particles in pure water vapor at 1427°C. In shock tube tests, Boiko et al. (1983) have shown that small fractions of aluminum powders may be ignited by a shock wave at a temperature of 1300 K, which is much lower than the 2300 K melting point of alumina. Grosse and Conway (1958) observed ignition of aluminum samples in oxygen at 1000°C which were heated beforehand in an inert atmosphere. Phillips and De Witt (1979) were even able to provoke ignition of aluminum powders at very low

temperatures (of the order of magnitude of the melting point of the metal) with the help of fluid dynamic oscillations generated by resonance tube oscillations. For nanoscale aluminum particles, the temperature for the onset of aluminum oxidation will likely be much lower (perhaps as low as the value of 825 K observed in thermal analysis experiments that will be described later in Chapter 4).

If we consider the ignition temperature as a parameter, and consider a typical detonation wave with a velocity of 6300 m/s, we obtain the ignition delay time scale as a function of particle size by solving the equation (3.4). As shown in Fig. 3.4, the ignition delay is strongly dependent on the Al particle sizes and the assumption of the threshold ignition temperature. Ignition delays assuming an 825 K ignition temperature are an order of smaller than with the assumption of Al ignition at 2350 K. For 100 nm sized particles, the ignition delay is only 1 ns or less, which is much smaller than the detonation zone length. This suggests that nanoscale aluminum particles may react within the detonation zone. However, other factors (e.g., particle agglomeration and sintering, excessive pre-oxidation of particles) may limit the degree to which nanoscale particles may practically react within the reaction zone. For a typical 10 μm sized particle, the ignition delay is on the order of 0.2 – 7 μs which is much longer than the time associated with the detonation zone. Therefore, considering the heat transfer between micron-sized Al particles and liquid explosive is essential in modeling the detonation of aluminized liquid NM.

Kato et al. (1981) measured the brightness temperature in NM-PMMA/Al mixtures with Al particles with an average size of 10 μm. From their experiments they found that the maximum brightness temperature of the detonation products occurred at a time of 1-1.5 μs. Hence they concluded that a considerable fraction of the Al reacted within the first 1 μs after passage of the detonation wave. From Fig. 3.4, we note that the ignition delay of a 10 μm Al particle is about 1 μs if a threshold ignition temperature of 1350 K is applied. A comparison with the experimental results from Kato et al. (1981) suggests that an ignition temperature threshold on the order of 1350 K is a reasonable estimation for 10 μm Al particles.

3.2.3 1-D Two Phase Non-Equilibrium Flow Model. When a detonation propagates in a liquid–solid particle system, energy release results from the reaction of the homogenous liquid phase as well as from heterogeneous reactions between the solid particles and the gaseous products. The characteristic times for the heat release from these two types of reactions may differ by several orders of magnitude. From the estimation above, the detonation of aluminized liquid explosives is apparently a non-equilibrium process in the detonation zone in terms of the relaxation of the particle velocity and temperature. This is perhaps the primary reason why the chemical equilibrium codes cannot predict the non-ideal detonation of this kind of explosive. Here, we propose a 1-D two-phase non-equilibrium flow model to predict the detonation of aluminized liquid explosives. In fact, two-phase flow models have been widely used in the study of shock or detonation waves in gas-droplet and bubbly media, gas–solid particles and gas-liquid film systems, and deflagration-to-detonation transition in solid explosives. Following these studies, we deal with the aluminized liquid explosive as a two-phase system. The unreacted liquid explosive and the detonation products of the liquid explosive are one phase called the fluid phase, denoted with the subscript "*1*". The aluminum particles are the other phase referred to as the solid phase, and denoted with the subscript "*2*". Initially the two phases are in complete equilibrium at zero velocity, and ambient temperature and pressure. A shock wave traveling with a constant velocity D (i.e., the detonation velocity of the aluminized liquid explosive), propagating through the mixture disturbs the equilibrium between the two phases. As depicted in Fig 3.5, in the non-equilibrium region, the particle velocity of the fluid phase drops whereas the particle velocity of solid phase increases as a result of drag due to the difference in the phase velocities. At the same time, the passage of the shock raises the temperature of the liquid which subsequently reacts forming high temperature products. The high temperatures generated eventually initiate the reaction of the solid phase. At some location downstream, the generalized CJ condition is satisfied which is followed by the

unsteady expansion zone. Depending on the size of the particles, they may or may not react within the detonation zone. If the ignition of the Al particles occurs within the detonation zone, the energy release will support the detonation of the fluid phase, otherwise the released energy only goes to increase the temperature of the expanding detonation products.

In the mathematical description of this two-phase system, we will apply the material continuum model in the following manner:

(i) Each phase is assigned a density ρ_a, a specific volume $v_a = 1/\rho_a$, particle velocity U_a, specific internal energy e_a, temperature T_a and volume fraction Φ_a, where the subscript "a" can be "*1*" or "*2*". These variables represent the local, mesoscale material specific average of the microscopic phase variables, and the volume fractions satisfy the condition $\Phi_1 + \Phi_2 = 1$.

(ii) On the mesoscale, each phase is in local thermodynamic equilibrium. Phase separation then indicates that averaged, material-specific variables for each phase (e.g., the internal energy e_a) depend only on the independent variables of that phase (e.g., the density, the temperature, etc.).

(iii) The motion of each phase is described by the balance laws for mass, momentum, and energy that are the same as those for single-phase materials. The interaction between the phases is described by source terms, which can be dependent on independent variables from both the phases.

3.3 ZND Detonation Structure Equations

The balance laws for this two-phase flow model are expressed in terms of a system of eight partial differential equations (Bdzil, 1981), six arising from the conservation of mass, momentum and energy for each phase, the seventh an evolution equation for the volume fraction, and the eighth the conservation of particle number, providing closure. The one-dimensional governing equations are as follows:

In laboratory coordinates (x', t') for the fluid phase, the conservation of mass is

$$\frac{\partial \overline{\rho}_1}{\partial t'} + \frac{\partial (\overline{\rho}_1 U_1)}{\partial x'} = m \tag{3.9}$$

The conservation of momentum is

$$\frac{\partial (\overline{\rho}_1 U_1)}{\partial t'} + \frac{\partial (\overline{\rho}_1 U_1^{\,2} + \overline{P}_1)}{\partial x'} = -P_1 \frac{\partial \Phi_2}{\partial x'} + m\, U_2 - f \tag{3.10}$$

The conservation of energy is

$$\frac{\partial (\overline{\rho}_1 E_1')}{\partial t'} + \frac{\partial [U_1 (\overline{\rho}_1 E_1' + \overline{P}_1)]}{\partial x'} = -P_1 U_2 \frac{\partial \Phi_2}{\partial x'} + m E_2' - U_2 f - q + \zeta_1 q_{ch} + (P_2 - \beta)\tau \tag{3.11}$$

For solid phase, the conservation of mass is

$$\frac{\partial \overline{\rho}_2}{\partial t'} + \frac{\partial (\overline{\rho}_2 U_2)}{\partial x'} = -m \tag{3.12}$$

The conservation of momentum is

$$\frac{\partial (\overline{\rho}_2 U_2)}{\partial t'} + \frac{\partial (\overline{\rho}_2\, U_2^{\,2} + \overline{P}_2\,)}{\partial x'} = P_1 \frac{\partial \Phi_2}{\partial x'} - m\, U_2 + f \tag{3.13}$$

The conservation of Energy is

$$\frac{\partial (\overline{\rho}_2 E_2')}{\partial t'} + \frac{\partial [U_2 (\overline{\rho}_2 E_2' + \overline{P}_2]}{\partial x'} = -(P_2 - \beta)\tau + P_1 U_2 \frac{\partial \Phi_2}{\partial x'} - m E_2' + U_2 f + q + \zeta_2 q_{ch} \tag{3.14}$$

The compaction equation for the solid phase is

$$\frac{\partial \Phi_2}{\partial t'} + U_2 \frac{\partial \Phi_2}{\partial x'} = \tau + \frac{m}{\rho_2} \tag{3.15}$$

The equation for the conservation of particle number is

$$\frac{\partial}{\partial t'}\left[\frac{\Phi_2}{r^3}\right] + \frac{\partial}{\partial x}\left[\frac{U_2 \Phi_2}{r^3}\right] = 0 \tag{3.16}$$

where $E' = e + \frac{U^2}{2}$, is the total energy of each phase, e is the specific internal energy, $\overline{P}, \overline{\rho}$, are the pseudo-pressure and bulk density, $\overline{\rho}_1 = \Phi_1 \rho_1$, $\overline{\rho}_2 = \Phi_2 \rho_2$, $\overline{P}_1 = \Phi_1 P_1$, $\overline{P}_2 = \Phi_2 P_2$; P, ρ, U and Φ are the pressure, true density, particle velocity and volume concentration, respectively; n is the number of particles in a unit volume,

$n = \dfrac{\Phi_2}{\frac{4}{3}\pi r^3}$; and the subscripts "*1*" and "*2*" denote the fluid and solid phases, respectively. The primes indicate values relative to the laboratory frame; *m*, *f*, and *q* are the mass, momentum and energy source terms. The subscript "*ch*" represents the chemical reaction term of the aluminum particles; r is the radius of the metal particles; ζ is the coefficient of the aluminum reaction heat release to each phase and τ is the rate of compaction with the empirical form (Bdzil, 1981):

$$\tau = \begin{cases} \dfrac{\Phi_1 \Phi_2 (P_2 - P_1 - \beta)}{\mu_c} & P_1 > \beta \\ \dfrac{\Phi_1 \Phi_2 P_1}{\mu_c} & P_1 \le \beta \end{cases} \tag{3.17}$$

where μ_c is compaction viscosity and β is the intragranular stress or configuration pressure.

In terms of a reference frame attached to the moving shock, and when the time derivatives are equated to zero for a steadily propagating wave, we obtain (see Appendix 2 for the details):

$$\frac{d(\rho_1 \Phi_1 u_1)}{dx} = m \tag{3.18}$$

$$\frac{d(\rho_1 \Phi_1 u_1^{\,2} + \Phi_1 P_1)}{dx} = m\, u_2 + f - P_1 \frac{d\Phi_2}{dx} \tag{3.19}$$

$$\frac{d[u_1 \rho_1 \Phi_1 (e_1 + \frac{u_1^2}{2} + \frac{P_1}{\rho_1})]}{dx} = m(e_2 + \frac{u_2^2}{2}) + u_2 f - (q - \zeta_1 q_{ch}) - u_2 P_1 \frac{d\Phi_2}{dx} + (P_2 - \beta)\tau \tag{3.20}$$

$$\frac{d(\rho_2 \Phi_2 u_2)}{dx} = -m \tag{3.21}$$

$$\frac{d(\rho_2\, \Phi_2 u_2^{\,2} + \Phi_2 P_2)}{dx} = -m\, u_2 - f + P_1 \frac{d\Phi_2}{dx} \tag{3.22}$$

$$\frac{d[u_2\rho_2\Phi_2(e_2+\frac{u_2^2}{2}+\frac{P_2}{\rho_2})]}{dx} = -m\,(e_2+\frac{u_2^2}{2}) - u_2 f + (q+\eta_2 q_{ch}) + u_2 P_1 \frac{d\Phi_2}{dx} - (P_2-\beta)\tau \quad (3.23)$$

$$\frac{d\Phi_2}{dx} = \frac{\tau}{u_2} + \frac{m}{\rho_2 u_2} \quad (3.24)$$

$$\frac{dr}{dx} = -\frac{mr}{3\Phi_2\rho_2 u_2} - \frac{r}{3\rho_2 u_2}\frac{d\rho_2}{dx} \quad (3.25)$$

Equations (3.18)-(3.23) are expressed in conservation form. In order to solve for each of the parameters explicitly, i.e., in operator form, a great deal of substitution and algebraic manipulations (see Appendix 2 in details) are required. The resultant equations are

$$\frac{du_1}{dx} = \frac{\psi}{\eta} \quad (3.26)$$

$$\frac{d\rho_1}{dx} = \frac{1}{u_1}(\frac{m}{\Phi_1} - \frac{\rho_1 u_1}{\Phi_1}\frac{d\Phi_1}{dx} - \rho_1\frac{du_1}{dx}) \quad (3.27)$$

$$\frac{dP_1}{dx} = \frac{1}{\Phi_1}[(u_2-u_1)m + f] - \rho_1 u_1\frac{du_1}{dx} \quad (3.28)$$

$$\frac{de_1}{dx} = H + \frac{P_1}{\rho_1^2}\frac{d\rho_1}{dx} \quad (3.29)$$

$$\frac{du_2}{dx} = -\frac{1}{\rho_2\Phi_2 u_2}[f + (P_2-P_1)\frac{d\Phi_2}{dx} + \Phi_2\frac{dP_2}{dx}] \quad (3.30)$$

$$\frac{d\rho_2}{dx} = \frac{1}{\Phi_2 u_2^2}[f + (P_2-P_1-\rho_2 u_2^2)\frac{d\Phi_2}{dx} + \Phi_2\frac{dP_2}{dx} - u_2 m] \quad (3.31)$$

$$\frac{de_2}{dx} = \frac{1}{\Phi_2\rho_2 u_2}[m\frac{P_2}{\rho_2} + u_2 P_2\frac{d\Phi_2}{dx} + \frac{\Phi_2 u_2 P_2}{\rho_2}\frac{d\rho_2}{dx} + q + \zeta_2 q_{ch} - (P_2-\beta)\tau] \quad (3.32)$$

where

$$\psi = u_1(\frac{\partial P_1}{\partial e_1})_{v_1,\lambda_1} H + u_1(\frac{\partial P_1}{\partial \lambda_1})_{v_1,e_1} \frac{d\lambda_1}{dx} - \frac{u_1}{\Phi_1}[m(u_2 - u_1 - \frac{c_1^2}{u_1}) + f - \rho_1 c_1^2 \frac{d\Phi_1}{dx}] \tag{3.33}$$

$$\eta = \rho_1(c_1^2 - u_1^2) \tag{3.34}$$

and the expression H is given by equation (51) in Appendix 2.

The determination of P_2 and β is difficult and subject to considerable debate to date. In the original Baer-Nunziato (BN) model (Baer & Nunziato, 1986), the aim was to describe a granular explosive in which a gas phase fills the interstitial pores between chemically reacting solid grains. The velocity, temperature, and pressure of the two phases are allowed to be unequal. A dissipation inequality for this mixture is employed to formulate the source terms, requiring that at each point the mixture entropy be non-decreasing with time. A drag source in the momentum equations equilibrates the velocities, a heat-transfer term in the energy equations equilibrates the temperatures, and a relaxation equation for the volume fraction serves to equilibrate the pressure. Due to the low-pressure material strength of the grains, modeled by the configuration pressure, the solid and gas pressures are offset by β at equilibrium. In contrast to the BN model, many conventional two-phase fluid models assume pressure equilibrium. We will follow the latter assumption, and assume pressure equilibrium for the detonation of aluminized explosives. And if we consider the dilute particle mixture, i.e. Aluminum particle are dispersed in liquid explosive, then intergranular stress β could be small even vanished., to apply the equations P_1=P_2 =P and $\beta = 0$ to equations (3.17), (3.24)-(3.32). Therefore, the final differential equations for solving the detonation of the aluminized liquid explosives are written as:

$$\frac{du_1}{dx} = \frac{\psi}{\eta} \tag{3.35}$$

$$\frac{d\rho_1}{dx} = \frac{1}{u_1}(\frac{m}{\Phi_1} - \frac{\rho_1 u_1}{\Phi_1}\frac{d\Phi_1}{dx} - \rho_1 \frac{du_1}{dx}) \tag{3.36}$$

$$\frac{dP}{dx} = \frac{1}{\Phi_1}[(u_2 - u_1)m + f] - \rho u_1 \frac{du_1}{dx} \tag{3.37}$$

$$\frac{de_1}{dx} = H + \frac{P}{\rho_1^2}\frac{d\rho_1}{dx} \tag{3.38}$$

$$\frac{du_2}{dx} = -\frac{1}{\rho_2 \Phi_2 u_2}[f + \Phi_2 \frac{dP}{dx}] \tag{3.39}$$

$$\frac{d\rho_2}{dx} = \frac{1}{\Phi_2 u_2^2}[f - \rho_2 u_2^2 \frac{d\Phi_2}{dx} + \Phi_2 \frac{dP}{dx} - u_2 m] \tag{3.40}$$

$$\frac{de_2}{dx} = \frac{1}{\Phi_2 \rho_2 u_2}[m\frac{P}{\rho_2} + u_2 P \frac{d\Phi_2}{dx} + \frac{\Phi_2 u_2 P}{\rho_2}\frac{d\rho_2}{dx} q + \zeta_2 q_{ch}] \tag{3.41}$$

$$\frac{d\Phi_2}{dx} = \frac{m}{\rho_2 u_2} \tag{3.42}$$

$$\frac{dr}{dx} = -\frac{mr}{3\Phi_2 \rho_2 u_2} - \frac{r}{3\rho_2 u_2}\frac{d\rho_2}{dx} \tag{3.43}$$

For a given shock strength, the states of both the phases behind the shock can be determined from the Rankine-Hugoniot relationship which serve as initial conditions for the integration of equations (3.35)–(3.43) for the thermodynamics profiles within the detonation structure.

3.4 Equations of State

The equations of states of the fluid phase have been discussed in Chapter 2. The expressions for the pressure, pressure derivative, internal energy, and local sound speed remain unchanged in this two-phase model.

For the solid phase, we use the simple equation of state

$$e_2 = C_{v2} T_2 \tag{3.44}$$

and take the specific heat capacity C_{v2} of aluminum as a constant in the detonation process.

3.5 Source Terms

The reaction of the aluminum with the high pressure and temperature detonation products is currently poorly understood. In detonation calculations for a solid-gas system and deflagration-to-detonation transition in a condensed explosive (Veyssiere et al., 1996; Powers, 1988), the mass change is usually modeled as a single, irreversible process from solid to inert gas. However, in the detonation of a liquid high explosive, due to the narrow detonation zone, for large metallic particles, no reaction of the particles is expected to occur in the detonation zone. Hence, in this case, the mass exchange term m vanishes. For very small (i.e., nanoscale) metallic particle, partial reaction of the particles within the detonation zone may be possible, but complete reaction is unlikely (Haskins, 2001). Given the uncertainty in the degree of reaction of even ultrafine particles within the reaction zone, we will simply assume that the mass exchange term m is vanishingly small. Hence, the Al reaction, if any, only contributes thermal energy to the detonation zone.

The source term f corresponds to an exchange of momentum due to the drag interaction between the phases. This interaction is modeled with a drag law in which the drag is proportional to the difference of particle velocity between the phases, and inversely proportional to the particle radius. From equation (3.1), the drag force on each aluminum particle is

$$f_n = (\frac{\pi}{4} d_2^2)(\frac{C_D}{2})\Phi_1 \rho_1 (u_2 - u_1)|u_2 - u_1| \tag{3.45}$$

The number of particles in unit volume is

$$n = \frac{\Phi_2}{\frac{1}{6}\pi d_2^3} \tag{3.46}$$

Therefore, total drag force in unit volume is

$$f = \frac{3}{4d_2}\Phi_1 \Phi_2 \rho_1 C_D (u_2 - u_1)|u_2 - u_1| \tag{3.47}$$

where the drag coefficient is still in the form of equation (3.2) and the Reynolds number has the form

$$R_e = \frac{\Phi_1 \rho_1 d_2 (u_2 - u_1)}{\mu} \tag{3.48}$$

The source term q accounts for the exchange of thermal energy between the fluid and the solid phases. The thermal energy exchange rate is assumed to be proportional to the temperature difference between the two phases, and inversely proportional to the square of the particle radius. From equation (3.4), the heat flux for each aluminum particle is

$$q_n = \pi d_2 \lambda_f N_u (T_1 - T_2) \tag{3.49}$$

Therefore, total heat exchange in unit volume is

$$q = \frac{6}{d_2^{\,2}} \Phi_2 N_u \lambda_f (T_1 - T_2) \tag{3.50}$$

where the Nusselt number N_u is given by equation (3.5).

The heat release rate associated with the aluminum particle reaction is q_{ch}. If the simple reaction rate law is assumed for the burning of the solid phase, i.e., equation (2.29) with the independence of reaction rate constant k on temperature and pressure, then the source term q_{ch} can be expressed as

$$q_{ch} = \rho_2 \Phi_2 k_2 (1 - \lambda_2) Q_{ch} \tag{3.51}$$

where k_2 is the burning rate constant of aluminum which depends on the particle size and shape; λ_2 is the degree of reaction, $\lambda_2 = 0$ corresponds to the unreacted solid phase, $\lambda_2 = 1$ corresponds to complete reaction of the aluminum particles; and Q_{ch} is the heat of reaction for the aluminum particles.

3.6 Shock Discontinuities

As in single-phase ZND theory, one must consider shock discontinuities when analyzing two-phase detonations. In this two-phase flow model a shock wave is

modeled as an infinitely thin zone where all flow variables change values discontinuously across the shock wave. Such discontinuities are admitted by the governing equations because they are hyperbolic. Mechanisms that would define a shock structure such as diffusive energy and momentum transfer have been neglected. It is assumed that the length scales where these processes are important are much smaller than the length scales associated with the chemical reaction, interphase drag, heat transfer, and compaction.

The shock equations can be derived by considering equations (3.18)-(3.24). Through the shock discontinuity, the reaction, drag, heat transfer and compaction processes have no time to occur and may thus are neglected. By neglecting these terms, a discontinuity analysis provides the following jump conditions when the condition $P_1=P_2=P$ is applied,

$$[\rho_1\Phi_1u_1]=0 \tag{3.52}$$

$$[\rho_2\Phi_2u_2]=0 \tag{3.53}$$

$$[\rho_1\Phi_1u_1+P\Phi_1]=0 \tag{3.54}$$

$$[\rho_2\Phi_2u_2+P\Phi_2]=0 \tag{3.55}$$

$$[\rho_1\Phi_1u_1(e_1+\frac{u_1^2}{2}+\frac{P}{\rho_1})]=0 \tag{3.56}$$

$$[\rho_2\Phi_2u_2(e_2+\frac{u_2^2}{2}+\frac{P}{\rho_2})]=0 \tag{3.57}$$

$$[\Phi_2]=0 \tag{3.58}$$

Here the brackets denote jump conditions as defined below for the general variable j:

$$[j] = j(\text{shocked state}) - j(\text{ambient state})$$

From equation (3.58) it is seen that the volume fraction does not change through a shock discontinuity. Using this result, the shock equations of the fluid phase along with its state equations are sufficient to determine the shocked state of the fluid phase. The solid shock equations along with the solid phase equations of state are sufficient to solve for the solid shocked state. In fact, when the constant factor of volume

fraction is removed from these equations, they are identical to two sets of single-phase shock equations. The shock states for the fluid phase and solid are thus identical to their single-phase equivalents.

Zhang et al. (2002) questioned the above conditions and pointed out that the classic assumption of a "non-momentum transfer shock" used in multiphase continuum detonation ignition and propagation models may not be valid. With a mesoscale model, they calculated particle velocities for metal particles subjected to a shock in liquid explosives and RDX as a function of particle material density, particle acoustic impedance and shock strength. Their results showed that immediately behind the shock front, the velocity of particles such as Al and magnesium may actually achieve 60-94% of the value of the shocked velocity of the explosive itself. The particle velocity after the shock-particle interaction strongly depends on the initial density ratio of explosive to metal, but is relatively insensitive to other parameters such as the particle acoustic impedance, shock strength and bulk explosive shock Hugoniot. A curve fit of the numerical data suggested the following velocity transmission factor immediately after shock front,

$$\alpha = \frac{\rho_{10}}{\rho_{20}} \frac{a + b\dfrac{\rho_{10}}{\rho_{20}}}{a+b} \tag{3.59}$$

where α is defined as the ratio of the particle velocity u_2 of the solid phase to the particle velocity u_1 of the shocked fluid phase; ρ_{10} and ρ_{20} are the initial density of the fluid phase and solid phase, respectively; a and b are the coefficients from the curve fit, i.e., a = 3.947 and b = -1.951. Given the uncertainties regarding the appropriate value of the Al particles immediately after the shock wave, the alternative jump condition for particle velocity given above will also be considered in Chapter 4.

3.7 Criterion to Determine the Detonation Solution

To solve the equations of the two-phase detonation model and determine the detonation structure, a criterion for determining the detonation end states must be considered first. In the classical C-J criterion, the steady-state detonation solution is the tangency of the Rayleigh line and the equilibrium Hugoniot curve. With the presence of source terms, the classical C-J criterion can no longer be used to select the unique detonation solution since the detonation products are no longer in equilibrium within the reaction zone when the sonic plane is reached. Moreover, in two-phase flow, different sonic planes can be defined since two particle velocities and several sound speeds exist (Fedorov, 1999). However, considering the solid phase is dispersed and the fluid phase is dominant, it is possible to describe the end state of two-phase non-equilibrium detonation as the state at which the particle velocity of the fluid phase is equal to its sound speed. From a physical point of view, for steady state detonation the end point is traveling at a sonic speed, and hence no rarefaction waves downstream of the detonation zone can catch and interfere with the detonation zone. From equation (3.35), when the particle velocity u_1 becomes sonic ($u_1 = c_1$), the denominator in equation (3.35) vanishes. For arbitrary values of the numerator, the solution becomes singular at the sonic plane. The derivatives of the thermodynamic variables then become singular at the sonic plane. This singularity can be removed if one seeks a particular integral curve in which the numerator also vanishes simultaneously with the denominator. This results in an indeterminate value for the derivative du_1/dx and permits a smooth transition through the sonic point. Therefore the condition of requiring that the numerator vanish when the sonic condition is reached is the criterion to determine the solution of two phase non-equilibrium detonation or is referred to as the "generalized C-J criterion, i.e., $\Psi=0$ when $\eta = 0$. With the "generalized CJ condition", convergence to the solution is reached by varying the value of detonation velocity, beginning, for example, from that of the mixture without aluminum particles. In such a way, different integral paths are

computed. In fact, the existence of possible solutions for the differential equations of the fluid phase has been discussed by Zel'dovich (1940). He pointed out that this system of differential equations has a peculiar saddle point, in which the Mach number of the fluid phase is equal to 1 and the effective heat release rate is equal to zero.

In the next chapter, the two phase model developed above is solved using the generalized C-J criterion and will be applied to the Al/NM system to determine the dependence of the solution on the various parameters (particle size, mass fraction, etc.). Of particular interest is the relative role of the momentum and heat transfer interaction terms on the detonation characteristics.

CHAPTER 4 NON-IDEAL DETONATION OF ALUMINIZED NITROMETHANE

4.1 Introduction

Detonation propagation in a heterogeneous explosive containing metal particles involves both exothermic and endothermic processes that proceed with different characteristic timescales. As a result, the detonation structure in these systems may differ significantly from the ideal C-J case, depending on the metal concentration and particle size. To elucidate the detonation characteristics of these multiphase explosive systems, a one-dimensional, steady-state, two-phase flow model has been developed in Chapter 3. Prior to considering the two-phase system, a model was first developed in Chapter 2 for detonation in pure liquid NM to validate the appropriate choice of the physical and chemical properties of the fluid phase. Table 4.1 summarizes the constants and parameters for nitromethane, aluminum and the detonation products which are utilized in the two-phase flow model. The remainder of this chapter is devoted to an exploration of the characteristics of the detonation of aluminized nitromethane which is chosen as a model of aluminized explosive. The choice of this explosive is motivated by the existence of relevant experimental data. Of particular interest is the dependence of the particle characteristics (e.g., ignition criterion, particle size and mass fraction) on the predicted detonation characteristics.

4.2 Ignition and Burning of Aluminum Particles

4.2.1 Aluminum Ignition Mechanism. The behaviour of aluminum particles when exposed to a highly transient, high temperature and pressure oxidizing environment is poorly understood. Under these conditions, the ignition and subsequent reaction of

the particles will depend not only on the particle characteristics (e.g., particle size, morphology, thickness of pre-existing oxide layer), but also on the ambient flow characteristics (e.g., P, T, relative velocity, concentration of oxidizing species). The particle size, the morphology, and the thickness of the pre-existing oxide coating will all influence the combustion behaviour of the particles. As reviewed earlier in section 3.1.2, there is considerable variation in the temperature at which ignition of an aluminum particle occurs, depending on the experimental arrangement used. In light of the earlier work, what is an appropriate ignition mechanism for Al particles exposed to high-(T, P) detonation products? For aluminum particles, it is worth noting the key role that the oxide layer that forms immediately on the metal surface with respect to limiting the diffusion of oxidizer to the metal. If the oxide film is disrupted for some reason, ignition of the particle may become possible. The oxide film can be disrupted by several causes. One of them is due to the difference between the thermal expansion coefficients of the metal and oxide. As noted by Veyssiere (1983), this coefficient is three times greater for aluminum than for aluminum oxide. As a result, even for a modest increase in temperature (e.g., ~50°C), the oxide film can begin to crack. Moreover, pressure and velocity gradients in the fluid phase downstream of the shock may induce deformation of the particle. Shear forces can lead to stretching and breaking of the oxide film. Also, initial irregularities on the particle surface may be another cause of loss of continuity of the oxide film. As a result of the above thermal and mechanical factors, oxidation of the aluminum particle may be initiated at temperatures that are considerably lower than the melting temperature of the aluminum oxide film.

Even in the absence of high flow velocity effects, very fine (i.e., nanoscale) aluminum particles may begin to oxidize also at relatively low temperatures in comparison with micron-sized Al particles. In the next section, the results from some thermal analysis experiments illustrate this effect.

4.2.2 Thermal Analysis of Nanoscale and Micro-Sized Al Particles. Much of the earlier work on the addition of nanoscale Al powder to energetic materials used the powder denoted "Alex" which was described in Chapter 1. Figure 4.1 shows a SEM (Scanning Electron Microscopy) photograph of a sample of Alex in comparison with conventional micron-sized Al powder (Ampal 611)*. The use of Alex for increasing the burning rate of propellants has been described by Ivanov and Tepper (1998). Mench et al. (1998) examined the thermal analysis of Alex in different gases using thermogravimetric (TGA) analysis and differential temperature analysis (DTA)

When they exposed a sample of Alex to air and gradually increased the temperature, they observed a rapid weight gain of the sample, which they attributed to the oxidation of the aluminum, i.e.

$$4Al + 3O_2 \rightarrow 2Al_2O_3. \qquad (4.1)$$

A second reaction at about 840°C was associated with the formation of aluminum nitride, i.e.,

$$2Al + N_2 \rightarrow 2AlN. \qquad (4.2)$$

The nitride formed can then oxidize at a higher temperature according to the reaction

$$4AlN + 3O_2 \rightarrow 2Al_2O_3 + 2N_2. \qquad (4.3)$$

Mench et al. (1998) speculated that the gradual weight gain observed above 1200°C corresponds to the above reaction. They found that the oxidation of Alex particles occurs at a lower onset temperature and attributed this effect to the greater surface area of the Alex particles.

To investigate particle sizes effects on ignition at different ambient temperatures, thermogravimetric analysis (TGA) and differential scanning calorimetry (DSC) have been carried out in the present investigation on Alex and Ampal 611 aluminum powder (Ampal 611 has a mean particle size of 50-60 μm) in air (a Setaram Setsys 1700 system was available within the Shock Wave Physics Group laboratory for the tests). These techniques involve measuring the response of the powders exposed to a

* The SEM images were obtained courtesy of the Microscopy Centre in the Department of Mining, Metals and Materials Engineering , Mcgill University.

given atmosphere and subjected to a slowly increasing ambient temperature (heating rate $\beta = 7^0 C$ /min). The variations of the sample mass and heat flow rate are measured to monitor the reaction of the aluminum with the atmospheric gas.

Fig. 4.2 shows the mass variation and heat flux from a sample of Alex in air. The initial oxidation of the nanoscale powders occurs at a lower temperature (about 823 K) than the melting peak. A second weight gain occurs for the nanoscale powders just above the melting point. This suggests that a suitable choice of temperature for the onset of oxidation of the Alex powder is on the order of 825 K – this value will be used later in calculation for detonation propagation in NM with nanoscale particles. It is likely that high pressure and flow effects will reduce, if at all, the onset temperature for oxidation, so this value is likely a conservative estimate for oxidation onset. For micron-sized aluminum particles, Fig. 4.3 shows that there is negligible oxidation under above the melting point of Al. At a temperature of about 1300 K, there is a small kink the heat flux and a corresponding mass gain associated with oxidation. This temperature value is consistent with the ignition temperature threshold chosen for micron-sized aluminum particles in calculations by Veyssiere (1983). A temperature of 1300 K will also be taken as a representative ignition threshold for micron-sized aluminum particles in later calculations. As a matter of fact, the calculations from the two-phase flow model to be presented below show that the temperature for micron-sized particles within the detonation zone is much lower than this threshold. Hence, to a large degree, the choice of ignition temperature for micron-sized particles will not affect the modeling results. The important conclusion from the TGA/DSC tests is that nanoscale aluminum powder indeed begins to react at significantly lower temperatures with a higher degree of reaction than conventional micron-sized powder.

Once the Al particles begin to react within the detonation zone, a corresponding burning rate must be specified for the calculations. The heat release as given in equation (3.51) still applies. What we don't know is the contribution of this heat release to heat each of the phases, and therefore some assumptions are needed. First,

we consider that all the thermal energy from the burning of aluminum particles contributes to heating the fluid phase, i.e., $\zeta_1=1$, $\zeta_2=0$. Secondly, the temperature of aluminum particles is assumed to remain constant during reaction. These assumptions allow the reaction model within the two-phase model to be specified.

4.3 Detonation Properties of Nitromethane with Dispersed Micron-Sized Aluminum Particles

In the present model, the compaction work associated with the aluminum particles is not considered. The compaction term becomes important only for very dense mixtures (Baer and Nunziato, 1986), i.e., for mixtures near maximum particle loading. In the present calculations, the particle mass fraction will be limited to values less than about 35%, a value less than that for maximum particle loading by a factor of about 2. The governing equations are then in the form of equations (3.35)-(3.43). For the fluid phase, the jump conditions across shock front are equations (3.52), (3.54) and (3.56). The particle velocity and temperature of the fluid phase right behind the shock front are determined by equation (2.11) and equation (2.27). For the solid phase, the particle velocity across shock front is determined by equation (3.59) and no temperature jump is assumed considering the solid phase is dispersed in the fluid phase. The two-phase model was computed for several aluminum loadings (5, 10, 15, 20, 25, and 30% on a mass basis) with an assumed reaction onset temperature of 1300 K. The reaction kinetics of the fluid phase are assumed to have an Arrhenius form with activation energy of 40 kcal/mole and reaction rate constant of 2.2×10^{12}.

Here we define nitromethane with the dispersed micron-sized Al particles as the conventional aluminized nitromethane. Figures 4.4 to 4.6 present the typical results for the detonation propagation of conventional aluminized nitromethane with 10 μm particles. These profiles show that the detonation pressure, temperature and particle velocity change relatively slowly for most of the detonation zone. Very near the

sonic point, these detonation parameters have exhibit a sharp decrease or increase due to the nature of Arrhenius reaction rate law (i.e., a long induction time). It is this sharp decrease of the particle velocity that results in the velocity equilibrium of both phases at the end of the detonation zone as shown in Figure 4.6. However, due to the continuous increase in the temperature of the combustion products and the relatively slow heat transfer to the micron-sized aluminum particles, temperature equilibrium between the phases is not achieved by the end of the detonation zone as shown in Figure 4.7. From this figure, it is seen that the overall temperature increase of the aluminum particles is quite small in the relatively narrow detonation zone. The temperature (< 450 k) of Al particles attained is far below the ignition threshold criterion, which eliminates the possibility of aluminum particle reaction within the detonation zone. Figure 4.10 shows the calculated detonation temperatures at the sonic point for 10, 20, and 50 μm aluminum particles as a function of Al mass fraction. The larger the particles, and the higher the Al mass fraction, the lower the temperatures at the sonic point. Therefore, for conventional aluminum additives, which typically have diameters in the range of 10-100 μm, the particles cannot react within detonation zone, i.e., the particles are effectively inert within the reaction zone. The inert property of 10 μm Al particles in the detonation zone has been experimentally demonstrated by Brousseau et al. (2002) in TNT/Al explosives.

It is desirable to compare the model predictions with the available experimental data for aluminized liquid explosives. The experimental detonation velocity for a NM/PMMA gel with 10 μm aluminum particles was reported by Kato (1983). Figure 4.8 shows the detonation velocity of aluminized nitromethane predicted by the two-phase model in comparison with Kato's experiments. The predicted detonation velocity is in reasonable agreement with the experiment for an aluminum mass fraction of up to 15%. If the experimental data are interpolated to larger values of aluminum mass fraction, the results of the model will not fit with the experimental trend. This suggests that when the mass loading of aluminum particles is high, other effects such as the compaction work of aluminum particles and the hot-spot effect of

the aluminum particles on the chemical kinetics of the fluid phase may play a role in the detonation process. The modification of the reaction rate model to simulate the hot-spot effect of aluminum additives will be addressed in section 4.6.

With this two-phase flow model, Figure 4.8 clearly shows the effects of aluminum concentration and particle size on the predicted detonation velocity. Due to the low temperature attained within the reaction zone, the micron-sized aluminum particles are effectively inert within the whole detonation zone and hence provide no thermal contribution to the detonation products. The effect of micron-sized particles is therefore endothermic, i.e., the particles absorb momentum and energy. Therefore, the larger the concentration and smaller the aluminum particle size, the more the momentum and heat losses influence the detonation process, and hence the larger the decrease in the detonation velocity. As seen from Fig. 4.8, for typical 10 μm aluminum additives up to a mass fraction of 15%, the detonation velocity decreases up to 7% in comparison with that of pure nitromethane. Compared with the velocity deficit of less than 2.1% that occurs near failure for pure NM (see Chapter 2), the effects of momentum and heat exchange on the detonation process are obvious and contribute to a significant detonation velocity deficit in aluminized liquid explosives.

Figures 4.9 and 4.10 show the detonation pressure and temperature at the sonic point as functions of aluminum mass fraction. The detonation temperature and pressure at the sonic point both decrease for an increase in aluminum concentration or decrease in particle size, due to the particle/fluid interaction in the detonation zone. For typical 10 μm aluminum additives within a 15% mass concentration the decreases in detonation pressure and temperature are up to 4.4% and 2.9% compared with the values for pure nitromethane.

It is interesting to note from the calculations of the two-phase flow model that the increase in the detonation zone timescale is quite significant as the aluminum mass fraction increases and the aluminum particle size decreases. For typical 10 μm size particles, Figure 4.11 shows that the detonation zone time may be up to 320 ns with a 30% aluminum mass fraction, 16 times longer than the value for pure nitromethane.

So far no data is available to determine the change of the detonation zone time due to the addition of aluminum into explosives. However, the experiments by Haskins (2002) in 35%NM/65%Al explosive with 10.3 μm Al particles on detonation failure diameter have demonstrated that the addition of aluminum increases the sensitivity and decreases the failure diameter from 20 mm for pure NM to less than 15 mm for aluminized NM. Since the failure diameter for a given explosive is proportional to its detonation zone time from equation (2.67), this indicates that the detonation zone time should decrease with the addition of aluminum particles rather than increase as predicted by the Arrhenius law. Lee et al. (1995) also measured the failure diameter of NM in packed beds of glass beads with different sizes. They found that in the "small-bead" regime (from 66 μm to 1 mm) the failure diameter decreases as the particle size decreases. Following the relationship that the failure diameter for a given explosive is proportional to its detonation zone time, the experimental results from Lee indicate that micron sized particle additives reduce the detonation zone time of the explosive. However, our calculations with the Arrhenius reaction law show the opposite result. As shown in Fig. 4.11, the detonation zone time of the aluminized NM with 10 μm particles is longer than that with 50 μm particles. This indicates that the calculations for the detonation zone time assuming an Arrhenius reaction rate law do not capture the correct reaction mechanism and hence a more sophisticated reaction rate law must be considered.

4.4 Detonation Properties of Nitromethane with Dispersed Nano-Sized Aluminum Particles

As calculated for micron-sized particles, the detonation properties of aluminized nitromethane with nano-sized particles (with a small mass loading) can also be predicted by the two-phase flow model with an assumed ignition temperature of 825 K. Since the reaction rate of nano-sized aluminum is not clear, the reaction rate will be considered a parameter and several arbitrary values of the reaction rate constant k_2

ranging from 0 to 2×10^7 will be assumed in the calculations. Figures 4.12 and 4.13 show the profiles of detonation pressure and temperature when reaction rate constant for the aluminum particles is $k_2=1\times10^7$. As for the case of micron-sized particles, the concave shape and the sudden drop near the sonic point in detonation pressure and temperature are characteristic of the assumed Arrhenius rate law. Unlike the case of micron-sized particles, momentum balance of both phases for nano-sized particles is quickly reached within half of the detonation zone time due to the violent momentum exchange for small particles. For example, with $k_2=1\times10^7$, the times for accelerating the particle velocity of the solid phase to that of the fluid phase are 12 and 22 ns for the cases of 5 and 35% Al concentrations, respectively, as shown in figure 4.14. The most important characteristic of nano-sized aluminum particles in comparison with micron-sized particles is their ignition within the detonation zone. As shown in Fig. 4.15, nano-sized aluminum particles are heated to their assumed ignition temperature (825 K) and start to react with the fluid phase within 2 nanosecond after the shock front due to the violent heat exchange which is inversely proportional to the square of the particle diameter (Equation (3.50)). Although the exact reaction rate of the aluminum particles is not clear, that the temperature of the detonation products is increased by the heat release of aluminum particle reaction is clearly demonstrated in Fig. 4.13 and 4.16 for the case of $k_2=1\times10^7$. With the assumed values of the reaction rate constant, the increase of the detonation temperature at the sonic point is proportional to the aluminum concentration as shown in Fig. 4.16. If it is deliberately assumed that the nanoscale aluminum particles remain inert (i.e., $k_2=0$) within the detonation zone, the calculated detonation temperature at the sonic point is always lower than if some reaction of the Al occurs (see Fig. 4.16). The temperature at the sonic point for 80%NM/20%Al explosive may be as low as 2000 K if the Al particles are inert. Compared with the detonation temperature for pure NM of about 3677 K temperature of pure liquid explosive, it is unlikely that a steadily propagating detonation could be sustained with a 45% decrease of the detonation temperature. For the cases of aluminum particle reaction as seen in Fig. 4.16, the larger the

reaction rate constant k_2, the more violent the reaction, and hence the higher the detonation temperature at the sonic point. For a typical value of $k_2 = 1\times10^7$, the detonation temperature of aluminized nitromethane at the sonic point is as high as 4124 K, compared with 3677 K for pure nitromethane.

Fig. 4.17 shows the aluminum consumption in the detonation zone. It is expected that with a higher reaction rate, more Al will be consumed within the reaction zone. However, the results show that the dependence of aluminum consumption within detonation zone on Al mass fraction has a different trend, depending on the reaction rate. For the slower reaction case $k_2 = 5\times10^6$, the particle consumption increases monotonically with particle concentration. However the opposite result is obtained for the faster reaction case $k_2 = 1\times10^8$. The main factor for this behavior is perhaps due to the variation in the detonation zone time, as shown in Fig. 4.18 for several reaction rate constants. This figure clearly shows that increasing the Al reaction rate narrows the detonation zone. Combining the information in Figs. 4.17 and 4.18, it can be shown that increasing the detonation zone time leads to an increase in the Al consumption within the detonation zone, as shown in Fig. 4.19.

Although nano-sized aluminum particles are reactive and are expected to release heat within the detonation zone, the calculated detonation velocities and pressure of aluminized nitromethane explosives still decrease with an increase of aluminum mass fraction, as shown in Figs. 4.20 and 4.21, respectively. Experiments with Alex by Baudin et al. (1998) also demonstrated this characteristic of aluminized explosives. This phenomenon may be explained from the point of view of the two-phase model. According to the two-phase model, the detonation velocity is determined by the competition between the heat release from both detonation products and aluminum reaction and the heat loss to heating the particles prior to particle reaction and the momentum loss that goes to accelerating the particles. For small particles such as nano-sized aluminum, although the thermal energy from the particle reaction supports the detonation propagation, the large drag from the particles and the rapid heat exchange between both phases may surpass the positive contribution of the particle

reaction and result in a continuous decrease in the detonation velocity with an increase of Al particle concentration in the liquid explosive mixture. Due to the relatively narrow detonation zone for liquid NM, the extent of the reaction of the aluminum is not sufficient to dominate the heat and momentum losses. For explosives with a long reaction zone (such as ADN), the detonation velocity may actually increase with the addition of nanoscale Al particles as demonstrated in the experiments by Miller (1998).

If we compare the calculated detonation velocity with the experimental data from Baudin et al. (1998) in Fig. 4.20, the model results are consistent with the experiments with a choice of the reaction rate constant k_2 in the range of 5×10^6 to 1×10^7. Fig. 4.20 also shows that the measured detonation velocities are always higher than if the powder is assumed to be inert within the reaction zone.

4.5 Detonation of Aluminized Nitromethane with Heat Transfer only

The effect of aluminum on the propagation of a detonation has been analyzed by drawing the analogy with steady one-dimension compressible fluid flow subjected to drag and heat transfer. Momentum and heat losses are thought to be responsible for the velocity decrease of aluminized liquid explosives. On the other hand, heat release from the aluminum reaction will possibly counteract these velocity deficits. An attempt is made in the present section to model the propagation of the aluminized nitromethane subject to including a heat transfer source term only (i.e., ignoring momentum transfer between the phases). To consider this change, it is simply assumed that f=0 and $u_1 = u_2$ exist in equations (3.35)-(3.43). The generalized C-J conditions, Arrhenius reaction rate law and particle ignition criterion and burning rate are kept the same as sections 4.2 and 4.3.

The calculated detonation velocity and other parameters at the sonic point are shown in Figs. 4.22 - 4.25. Unlike for the non-equilibrium model of both particle velocity and temperature which results in a large deficit of detonation velocity, the

two-phase flow model with temperature non-equilibrium between the phases only predicts a very small decrease in the detonation velocity for the case of 10 μm aluminum particles as shown in Fig. 4.22. A small decrease (for $k_2 = 0$) or a slight increase (for $k_2 = 1\times10^7$) in the detonation velocity for 100 nm particles can also be seen in this figure. These results for detonation velocities as a function of aluminum mass fraction are not in agreement with the trends of the experimental data. This illustrates that heat losses alone could not account for the large departure in detonation velocity for aluminized liquid explosives in comparison with their pure liquid counterparts. Large momentum losses to accelerate the aluminum particles are therefore primarily responsible for the velocity deficits of detonation waves observed experimentally.

Figs. 4.23 and 4.24 show the detonation pressure and temperature at the sonic point, again with the assumption of velocity equilibration in whole detonation zone. Once again, only slight changes in detonation pressure and temperature can be seen when 10 μm particles are added to the liquid explosive. Since they are inert within the detonation zone, 10 μm aluminum particles provide no heat contribution to the detonation zone, and heat losses to the 10 μm size particles are not sufficient to affect the detonation as well. For the case of 100 nm aluminum particles, the heat release from the particles burning within detonation zone may overcome the heat losses to the particles and result in a slight increase of detonation pressure and temperature for the case of $k_2=1\times10^7$. Even if the 100 nm particles are assumed to be inert within the detonation zone (i.e., setting $k_2 = 0$), heat losses do not result in a large decrease of detonation pressure and temperature at the sonic point. For example, for aluminized nitromethane with a 35% aluminum concentration, the detonation pressure decreases only 3.6%, from 12.84 GPa for pure liquid nitromethane to 12.35 GPa; while the detonation temperature only decreases from 3677 K for pure nitromethane to 3400 K. This 8% decrease in temperature is relatively smaller than the 45% decrease for the case in which both momentum and heat losses are considered. However, heat transfer can significantly affect the detonation zone time, as shown in Fig. 4.25. For 10 μm

aluminum particles, the detonation zone time for aluminized nitromethane is about 40 ns, twice as much as for pure liquid nitromethane. For 100 nm particles, heat losses for the case of $k_2 = 0$ can extend the detonation zone of aluminized nitromethane to a value triple that of liquid nitromethane. On the other hand, heat release from the aluminum reaction accelerates the detonation process and reduces the detonation zone time as seen in Fig. 4.25 for $k_2=1\times10^7$.

Overall, the heat transfer source term by itself does not affect the detonation velocity, pressure and temperature as strongly as observed in experiments. Hence, the non-ideal detonation characteristics of aluminized liquid explosives are primarily due to the mechanism of momentum transfer between the phases.

4.6 Detonation of Aluminized Nitromethane with a Hot-Spot Reaction Rate Law

As an additive of to explosives, the effects of aluminum particles to the detonation of explosive mixtures have been simulated through a two-phase momentum and heat transfer model with a simple reaction rate law of aluminum for the case of aluminum temperature beyond the ignition point. The reaction rate law for the fluid phase is kept in the same Arrhenius form as for pure nitromethane. Chemical kinetics effects on explosives due to the addition of aluminum particles are not assumed in the previous calculations. It has long been known that adding particles to explosives influences the detonation behavior of condensed-phase explosives through the generation of "hot spots". The most commonly observed hot-spot effect is the sensitization of a homogenous liquid explosive with the addition of micron-sized particles and the reduction of failure diameter in heterogeneous liquid explosives compared with homogenous liquid explosives (Engelke, 1983, Haskins, 2002). This sensitizing effect exists for different particle materials over a wide range of particle concentrations (Lee et al., 1995). These hot-spot effects have also been observed directly in pioneering experiments by Campbell et al. (1961), in which they reported that 150 μm heterogeneities separated by 200 μm reduced the initiation distance of

NM by 15%. Therefore a modified chemical reaction law to account for the hot-spot effect for the fluid phase is proposed. This hot-spot reaction rate law of the fluid phase consists of two parts:

$$\frac{d\lambda}{dt} = \dot{R}_{bulk} + \dot{R}_{hs} \tag{4.4}$$

The first part of equation (4.4) is the Arrhenius law of pure nitromethane with the form of

$$\dot{R}_{bulk} = Z(1-\lambda)e^{-\frac{E^*}{RT}} \tag{4.5}$$

The second part is due to the hot-spot effect of aluminum particles, which is related to the detonation pressure, particle size and the numbers of particles per unit volume. The more particles per unit volume and the larger the contact surface of both phases, the stronger the hot-spot effect. Therefore,

$$\dot{R}_{hs} = K(1-\lambda)PA_0 n = 6K(1-\lambda)P\frac{\Phi_2}{d} \tag{4.6}$$

Where P is the detonation pressure; A_0 is the surface area of the particle, $A_0 = \pi d^2$; n is particle number per unit volume, $n = \dfrac{\Phi_2}{\frac{1}{6}\pi d^3}$; and K is a reaction rate constant.

Substituting (4.5) and (4.6) into (4.4), the hot-spot reaction rate law for the fluid phase has the final form

$$\frac{d\lambda}{dt} = Z(1-\lambda)[e^{-\frac{E^*}{RT}} + k_{hs}P\frac{\Phi_2}{d}] \tag{4.7}$$

Here k_{hs} is the single variable parameter due to hot-spot effect, which mainly depends on the particle shape and material. Through matching the calculated detonation velocities to the measured data, $k_{hs} = 3\times10^{-20}$ is an appropriate choice for spherical Al additives.

With the new chemical kinetics equation (4.7), jump conditions for the two-phase flow across the shock, equations (3.52)-(3.58), and the no-temperature jump condition of the solid phase across the shock front considering that the solid phase is dispersed

in the fluid phase, the detonation of aluminized nitromethane explosives is simulated by solving equations (3.35)-(3.43). Figure 4.26 shows the comparison of the calculated detonation velocities with the experimental results. The good agreement is achieved even for large Al concentrations (up to 35%). The calculations with this two-phase flow model and hot-spot reaction rate law also clearly demonstrate the characteristics of aluminized liquid explosives, i.e., the effect of aluminum mass fraction and particle size on the detonation properties. In general, the detonation velocity decreases with increasing particle concentration and decreasing particle size.

Unlike the Arrhenius law, the calculated detonation zone time with the hot-spot law decreases with increasing aluminum mass fraction, as shown in figure 4.27. For a given aluminum concentration, the detonation zone time with the small particles (i.e., 100 nm) is shorter than the one with the large particles (i.e., 10 μm). This is perhaps due to the fact that more hot spots per unit volume exist when the size of the particles is small and the aluminum concentration is large. Therefore, hot spots indeed have the effect of accelerating the detonation process. This conclusion could also be demonstrated if we compare the results for the hot-spot law with that using the Arrhenius rate law. For example, for a 70% NM/30% Al explosive with 10 μm particles, the detonation zone time with hot-spot chemical kinetics is only 5 ns, which is much shorter than the 320 ns with Arrhenius law.

So far, there is still no experimental data of detonation zone timescale to quantitatively verify the proposed hot-spot reaction rate law, However, experimental data on detonation failure diameter may provide useful information since the failure diameter for a given explosive is proportional to its detonation zone time as in equation (2.67) (Chariton, 1947, Dremin, 1999). The change of detonation zone time should have the same trend as the failure diameter when the heterogeneity is added to an explosive.

It is worth recalling the experiments of Engelke (1983). He examined the dependence of the failure diameter of NM/glass bead explosives on the number density of heterogeneities. The results showed that the addition of 35-45 μm and 105-

125 μm diameter glass beads in amounts up to 9.0 wt. % produces no evident critical-diameter reduction. In contrast, the addition of 1-4 μm diameter beads, in amounts as small as 0.5 wt. %, produced a failure diameter reduction. The effect was enhanced as the number density of 1-4 μm diameter heterogeneities was increased up to, at least, 9.0 wt. %.

Although the failure diameter, d_f, for a given explosive cannot be directly obtained by this two-phase flow model, the detonation zone timescale of the explosives with various sizes of particle additives can be calculated as long as the initial density ρ_0 and the specific heat capacity C_v of the heterogeneities are known. For glass beads, the values $\rho_0 \approx 2450$ kg/m^3 and C_v=835 J/(kg.k) are applied. Fig. 4.28 shows the calculated detonation zone time with the two-phase flow model and the measured failure diameter d_f by Engelke (1983) with various mass fractions of heterogeneities. The trend of the calculated detonation zone time with the mass fraction of heterogeneities agrees with the measured detonation failure diameter vs. mass fraction of heterogeneity. On the other hand, the sizes of the particle additives play an important role in accelerating the detonation process. As shown in Fig. 4.29, glass beads from 120 to 30 μm result in no evident reduction of the detonation zone time. The detonation zone time with 3 μm glass beads is much shorter than that with 30-120 μm silica beads. The change of the calculated detonation zone time with glass beads almost reproduces the trend of the measured failure diameter with these sizes of heterogeneity. The same results are obtained with Al particles as shown in Fig. 4.30. These comparisons with the experimental data provide additional support that the hot-spot reaction rate law is qualitatively reproducing the correct dependence on particle size and number density.

As prediction using the Arrhenius rate law, the calculation on the behavior of aluminum particles in detonation zone with the hot-spot rate law also shows that 10 μm aluminum particles are effectively inert and cannot be heated to the assumed threshold ignition temperature of 1300 K as shown in Fig. 4.31. In contrast, 100 nm

particles are quickly heated to the assumed 825 K ignition temperature within the first 2 nanosecond due to the heat exchange which is proportional to the inverse of particle diameter as shown in Fig. 4.32.

The rapid reaction of nano-sized aluminum in NM has been experimentally demonstrated by Haskins (2002). Figure 4.33 contains single frames from the high–speed record showing the detonation of cylindrical charges of NM and NM/Alex in 25 and 15 mm diameter glass tubes, respectively. From the photographs, we can see that the brightness of the detonation zone for NM/Alex is much stronger than that of pure NM. Although we cannot determine if there is any significant reaction of Alex within the detonation zone from this figure, the afterburning of the aluminum is clearly visible and appears to be present just downstream of the detonation front. The effect of aluminum particle size on the detonation process in Tritonal (80%TNT/20%Al) explosives is shown dramatically in the photographs of aquarium tests presented by Dorsett et al. (2001). As shown in figure 4.34, at times Δt =18 and 37 μs, both the detonation zone and the expansion zone for Alex-Tritonal explosive show considerably more luminosity (presumably due to the burning of the nanoscale Al) that those of regular Tritonal with 17 μm aluminum particles. The reaction of Alex in the detonation zone immediately after the detonation front as well as in the expansion zone is clearly visible. In contrast, no apparent "specks" of light due to the burning of micron-sized aluminum particles can be seen in the expansion zone at both Δt = 18 and 37 μs. The "specks" of light due to the burning of regular aluminum are evident only at a time of Δt = 82 μs, as shown in figure 4.35. Therefore, these experiments (as well as our theoretical model) demonstrate that nano-sized aluminum particles react significantly more quickly than micron-sized particles within the detonation products.

If particles are reactive within the detonation zone, the heat release from the particle reaction generally increases the detonation temperature (at the sonic point), depending on the reaction rates, as shown in Fig. 4.36 for the cases $k_2 = 1\times10^8$ and $k_2 = 5\times10^7$. From this figure, it is evident that there exists a particular nanoscale

aluminum mass fraction, i.e., about 10%, that leads to a maximum in the detonation temperature. For nanoscale particle mass fractions greater than this value, energy losses to the particles dominate over the energy release from the particle reaction. If nanoscale particles do not react within the detonation zone (i.e., $k_2 = 0$), then the detonation temperature decreases monotonically with increasing Al mass fraction.

Figs. 4.37 and 4.38 show the particle velocity profiles within the detonation zone for the solid and fluid phases, for 10 μm and 100 nm particles, respectively. For 10 μm sized aluminum (Fig. 4.37), no equilibrium between the particle velocities is attained within the detonation zone. The momentum transfer to the 10 μm particles is not sufficient for the particle velocity to equilibrate with the flow before the end of the detonation zone. In contrast to the case of micron-sized particles, the rapid momentum transfer for the case of nano-sized particles results in particle velocity equilibrium within the detonation zone (Fig. 4.38).

With this two-phase model, the detonation pressure profiles for aluminized nitromethane are quite different from the classical ZND theory as shown in Fig. 4.39. In the classical ZND structure, the detonation pressure continuously decreases from the Von Neumann spike to the C-J pressure as for the case of pure NM (i.e., 0% Al concentration). The calculated results with the two-phase flow model shows that a corresponding Von Neumann spike does not exist for detonation in aluminized nitromethane. Instead, the pressure behind the shock front remains relatively constant for some time, then abruptly drops near the end of the detonation zone for Al particle concentrations from 5-35%.

In general, with the proposed hot-spot reaction rate law, the qualitative predictions of the two-phase flow model agree well with experimental results for detonation velocity, Al behavior and failure diameter in aluminized NM. However, to determine if the predicted structure within the detonation zone (i.e., variation in temperature, pressure, and particle velocity) is realistic, more detailed experimental results are required.

CHAPTER 5 CONCLUSIONS AND RECOMMENDATIONS

In this thesis, a detailed investigation of detonation propagation in liquid and aluminized liquid explosives has been carried out by solving the 1-D conservation equations with source terms for mass, momentum and energy exchange. The detonation of these explosives may be an ideal detonation (governed by the classical C-J criterion) or non-ideal. In the latter case, to choose among the spectrum of possible solutions to the differential equations for the detonation structure, the so-called "generalized C-J condition" is applied, i.e., when source term are present in the conservation equations, a regular solution can be found for which the numerator and denominator of the particle velocity equation vanish simultaneously, which corresponds to the detonation products flowing at a sonic velocity relative to the shock front.

For liquid explosives (e.g., NM) with an infinite diameter, the ideal C-J detonation solution can be found from the global conservation laws and equilibrium thermodynamics. In this thesis, for liquid NM, the detonation parameters and detailed ZND structure were determined using an appropriate JWL equation of state and reaction rate law. The calculated detonation velocity and C-J pressure are in good agreement with the experimental data. With different chemical kinetic rate laws, the same Von Neumann peak and C-J state are obtained, but the variation of the fluid properties within the detonation zone are different. A realistic reaction rate law for the explosive cannot be determined without measuring detonation profiles or having data for the failure diameter of the explosive.

For finite diameter liquid explosive charges, small detonation velocity deficits and failure diameters have been observed experimentally. The eigenvalue behaviour is accounted for by including source terms in the 1-D conservation equations in differential form. These source terms of mass, momentum and energy represent the detonation front curvature, wall friction and heat loss to the wall. Regular solutions are found when the numerator of the du/dx equation vanishes as the rates of the

chemical heat release and heat losses from the shock front curvature, wall friction and heat transfer to the wall balance each other at the sonic point. A detonation velocity deficit near failure of less than 2.1% is predicted, which agrees well with the experimental results. The most important result obtained from solving the differential conservation equations with source terms is the prediction of the critical curvature and failure diameter of the explosive. For a finite diameter explosive, the detonation front is no longer plane but curved due to the lateral rarefaction wave. The flow downstream the shock front is radial. Although it is impossible to discern the exact nature of the radial flow without solving the fully coupled 2-D hydrodynamic problem, it is possible to roughly estimate its magnitude with source terms in the 1-D hydrodynamic equations. The radial flow model of Wood and Kirkwood is applied in this thesis to predict the existence of a critical curvature for the liquid explosive. The empirical relationship between detonation front curvature and charge diameter is used to convert the critical curvature value to a failure diameter. Although the calculated results shows that the detonation front curvature provides the primary contribution to the detonation failure, the effects of wall friction and heat loss play a lesser role and may modify the calculated failure diameter for NM. If the so-called simple reaction law is used, the existence of a failure diameter is not predicted, and hence this reaction law does not reproduce the detonation failure behavior of NM. With the Arrhenius reaction law, failure diameters of 15 – 22 mm are predicted for activation energies in the range of 30-53 kcal/mol. If we take the experimental value of failure diameter (about 18 mm), this corresponds to an activation energy for nitromethane of about 40 kcal/mol.

Detonation propagation in liquid explosives containing dispersed aluminum particles is much more complicated than in pure liquid explosives. Some experimental results for the detonation velocity in aluminized nitromethane are available, e.g., the velocity decreases from 6300 to 5760 m/s for a variation from 0 to 40% concentration of nanoscale Alex powder. The velocity deficit also depends on the size of the aluminum particles. The dependence of velocity on particle size cannot

be predicted by standard equilibrium codes such as Cheetah. Many researchers have indicated that endothermic effects that are present in these complicated flows are responsible for the velocity deficits observed.

A consideration of the characteristic times for momentum and heat transfer in the detonation zone shows that relaxation times will typically be longer than the characteristic reaction zone times. Hence non-equilibrium effects are important within the detonation zone. The combination of endothermic processes due to momentum and heat transfer between the liquid explosive and aluminum particles, and exothermic processes due to heat release from the aluminum reaction accounts for the variation of the detonation properties in the aluminized liquid explosives, in comparison with a homogeneous liquid explosive.

A two-phase flow model was proposed to predict the non-ideal detonation properties of aluminized liquid explosives. The principle of phase separation is invoked and each phase is separately assumed to be in local thermodynamic equilibrium, described by a density, specific internal energy and particle velocity and characterized by a separate equation of state. The phases are not, however, in equilibrium with each other. The dynamics are determined by a system of differential equations. Each phase separately satisfies conservation of mass, momentum and energy. The non-equilibrium interactions between the phases are described by source terms for the exchange of mass, momentum, and energy between the phases. A regular solution of these differential equations is determined by the generalized C-J criterion in the fluid phase. Regardless of the computing approach, the specification of the interphase interactions remains the essence and challenge of multiphase continuum modeling. To simplify the problem, pressure equilibrium and insignificant mass exchange between the two phases are assumed. The energy source term consists of an endothermic effect due to heating of the aluminum particles and an exothermic effect from heat release of aluminum reaction, if any. Regardless of the detailed mechanism of the aluminum reaction, TGA tests were carried out to determine the dependence of particle size on the temperature at which a significant

degree of oxidation occurs in a quiescent atmosphere. The thermal analysis experiments with 100 nm and 50 μm aluminum particles in air exhibited reaction onset temperatures for the particles of about 825 and 1350 K, respectively. With the specification of these reaction onset temperatures in the two-phase flow model, the dependence of the detonation profiles on particle size was then determined. The calculated results in aluminized nitromethane show that typical micron-sized aluminum particles (10 μm or larger) are effectively inert within detonation zone while 100 nm Alex particles start to react within 2 nanosecond of the passage of the detonation wave front. For inert particles of micron size, it is the dissipative effects occurring during the particle acceleration and heating that contribute to the decrease in the detonation velocity, pressure and temperature. Smaller particles and larger particle mass concentration lead to a larger decrease in the detonation properties noted above. The qualitative theoretical predictions regarding the effects of particle size and mass on the detonation properties are in agreement with the experimental data. For nano-sized particles, reaction within the detonation zone counteracts to some extent the endothermic processes. As a result, an increase of the detonation temperature is predicted although detonation velocity and pressure are still lower than that for pure liquid.

To determine the relative contribution of momentum and heat exchange to the detonation properties, detonation of aluminized nitromethane was simulated with the two-phase flow model including only the energy source term. The results show that the heat loss to the solid phase plays a relatively minor role and hence the momentum transfer is the primary factor in determining the deficit in the detonation properties.

Besides introducing non-equilibrium effects, addition of aluminum particles to a liquid explosive also may influence the chemical kinetics of the liquid explosive. Due to shock interactions with the particles, so-called "hot-spot" mechanisms are important and a strictly Arrhenius form for the reaction rate law for the fluid phase is no longer appropriate. A new hot-spot reaction rate law for the fluid phase which depends on the number density of the particles, and contains a single adjustable

constant is proposed. Calculations of the two-phase flow model with this hot-spot reaction rate law show that the predicted trends for the variation of detonation velocity of aluminized nitromethane with Al mass fraction are in agreement with experimental results. One parameter that is particularly sensitive to the choice of the reaction rate law is the predicted detonation zone timescale which is a function of particle concentration and size. The hot-spot reaction law predicts a decrease of detonation zone timescale with an increase in particle concentration, while the Arrhenius rate law predicts the inverse. Similar contradictory results are obtained for the dependence of reaction zone timescale on particle size. From past experiments on failure diameter, the addition of small solid particles sensitizes the explosive and reduces the failure diameter which implies a reduction in the detonation zone time according to Chariton's failure diameter theory. As a result, the proposed hot-spot reaction law, rather than the Arrhenius law, captures the failure diameter behavior for the NM/Al system.

Although the two-phase flow model predicts well the non-ideal detonation of aluminized liquid explosives and demonstrates the detailed detonation structure, there are several modifications to the model that could be made. Compressibility of the solid phase could be incorporated into the existing model to predict the detonation properties of heterogeneous explosives with concentrations of the additives that approach the maximum (i.e., packed-bed) case. The criterion for onset of the metal reaction mechanism and the subsequent reaction rate for the solid particles are treated in a simplistic manner in the present model. Additional, well-characterized experimental results for particle reaction rates are needed to refine these particle heat release terms. However, obtaining appropriate measurements of the particle reaction rates within the hostile, high pressure and temperature environment in the detonation reaction zone remains a formidable experimental challenge.

CONTRIBUTIONS TO KNOWLEDGE

The non-ideal behavior of the detonation of liquid explosives containing metal particle additives has been observed experimentally but is poorly understood from a theoretical standpoint. The contribution of this study is a thorough analysis of the dependence of detonation parameters and structure predicted by the proposed two-phase flow model on Al particle properties (e.g., particle size and concentration), and a theoretical determination of aluminum behavior in detonation zone. The results of the model indicate that the velocity deficit observed experimentally with metal additives is primarily due to momentum losses to the particles, with heat losses playing a relatively minor role. For a homogenous charge of liquid nitromethane, it is shown that with an appropriate choice for the reaction rate law of an Arrhenius form and accounting for detonation front curvature from the lateral expansion of the products, predicted values for the detonation failure diameter agree well with experimental results. In contrast, for an aluminized liquid explosive, an Arrhenius reaction rate fails to reproduce the dependence of failure diameter on particle size and concentration. In this case, a simple hot-spot reaction rate law is proposed which is in qualitative agreement with the observed behaviour of the failure diameter.

APPENDIX 1 1-D STEADY STATE ZND EQUATIONS OF EIGENVALUE DETONATION MODEL

1-D conservation equations of mass, momentum and energy with source terms can be written as the following form in laboratory coordinate (x', t')

$$\frac{\partial \rho}{\partial t'} + \frac{\partial (\rho U)}{\partial x'} = m \tag{1}$$

$$\frac{\partial (\rho U)}{\partial t'} + \frac{\partial (\rho U^2 + P)}{\partial x'} = mU - f \tag{2}$$

$$\frac{\partial [\rho (e + \frac{U^2}{2})]}{\partial t'} + \frac{\partial [\rho U (e + \frac{U^2}{2} + \frac{P}{\rho})]}{\partial x'} = m(e + \frac{U^2}{2} + \frac{P}{\rho}) - Uf - q \tag{3}$$

Where e is the specific internal energy; P and ρ are the pressure and density. The primes indicate values relative to the laboratory frame; m, f and q are the mass, momentum and energy source terms.

In reference frame (x, t) attached to the shock, the following transformations are made.

$$x = Dt' - x' \ , \ t = t' , \ u = D - U \tag{4}$$

Therefore

$$\frac{\partial}{\partial t'} = \frac{\partial}{\partial t} + D\frac{\partial}{\partial x} \ , \ \frac{\partial}{\partial x'} = -\frac{\partial}{\partial x} \tag{5}$$

Substituting the transformation equations (4) and (5) into conservation equations (1)-(3), we get

$$\frac{\partial \rho}{\partial t} + \frac{\partial (\rho u)}{\partial x} = m \tag{6}$$

$$\frac{\partial \rho u}{\partial t} + \frac{\partial (\rho u^2 + P)}{\partial x} = mu + f + \rho \frac{\partial D}{\partial t} \tag{7}$$

$$\frac{\partial[\rho(e+\frac{u^2}{2})]}{\partial t}+\frac{\partial[\rho u(e+\frac{u^2}{2}+\frac{P}{\rho})]}{\partial x}=m(e+\frac{u^2}{2}+\frac{P}{\rho})+uf-q+\rho D\frac{\partial D}{\partial t} \quad (8)$$

To obtain a steady state solution, all the time derivative are set equal to zero, i.e., $\frac{\partial}{\partial t}=0$, the governing equations are reduced to a much simpler system

$$\frac{d(\rho u)}{dx}=m \quad (9)$$

$$\frac{d(\rho u^2+P)}{dx}=mu+f \quad (10)$$

$$\frac{d[\rho u(e+\frac{u^2}{2}+\frac{P}{\rho})]}{dx}=m(e+\frac{u^2}{2}+\frac{P}{\rho})+uf-q \quad (11)$$

To further simplify equations (9)-(11) and derive the explicit expression of derivatives of u, ρ, P and e, we do the following manipulation. Rearranging equation (11), we have

$$\frac{d}{dx}(e+Pv+\frac{u^2}{2})=\frac{1}{\rho u}(uf-q) \quad (12)$$

where $v=\frac{1}{\rho}$, is the specific volume.

We may write equation (12) as

$$\frac{de}{dx}+u\frac{du}{dx}+P\frac{dv}{dx}+v\frac{dP}{dx}=\frac{1}{\rho u}(uf-q) \quad (13)$$

From equation (10), we have

$$u\frac{d(\rho u)}{dx}+\rho u\frac{du}{dx}+\frac{dP}{dx}=um+f \quad (14)$$

or

$$u\frac{du}{dx}+v\frac{dP}{dx}=\frac{f}{\rho} \quad (15)$$

Substituting equation (15) into (13) yields

$$\frac{de}{dx} = -P\frac{dv}{dx} - \frac{q}{\rho u} \tag{16}$$

Recall that

$$c^2 = -v^2\left(\frac{dP}{dv}\right)_s \tag{17}$$

if we consider specific energy e to be a function of P and v, we have

$$de = E_v dv + E_p dP \tag{18}$$

where

$$E_v = \left(\frac{de}{dv}\right)_p \quad , \quad E_p = \left(\frac{de}{dP}\right)_v$$

At constant isentropic s, $de = -Pdv$. This means that

$$-Pdv = E_v dv + E_p dP \tag{19}$$

Which can be rearranged to yield the result

$$c^2 = v^2\frac{P + E_v}{E_p} \tag{20}$$

For *e=constant*, from equation (18) we have

$$\left(\frac{dP}{dv}\right)_e = -\frac{E_v}{E_p} \tag{21}$$

Since

$$\frac{dP}{dx} = \left(\frac{\partial P}{\partial v}\right)_{e,\lambda}\frac{dv}{dx} + \left(\frac{\partial P}{\partial e}\right)_{v,\lambda}\frac{de}{dx} + \left(\frac{\partial P}{\partial \lambda}\right)_{e,v}\frac{d\lambda}{dx} \tag{22}$$

Substituting equations (16), (21) into equation (22) yields

$$\frac{dP}{dx} = -\frac{c^2}{v^2}\frac{dv}{dx} - \frac{q}{\rho u}\left(\frac{\partial P}{\partial e}\right)_{v,\lambda} + \left(\frac{\partial P}{\partial \lambda}\right)_{e,v}\frac{d\lambda}{dx} \tag{23}$$

Substituting equation (23) into equation (14) yields

$$\rho u\frac{du}{dx} - \frac{c^2}{v^2}\frac{dv}{dx} - \frac{q}{\rho u}\left(\frac{\partial P}{\partial e}\right)_{v,\lambda} + \left(\frac{\partial P}{\partial \lambda}\right)_{e,v}\frac{d\lambda}{dx} = f \tag{24}$$

From equation (9), we have

$$u\frac{d\rho}{dx}+\rho\frac{du}{dx}=m \tag{25}$$

i.e.,

$$-\frac{1}{v^2}\frac{dv}{dx}=\frac{d\rho}{dx}=\frac{m}{u}-\frac{\rho}{u}\frac{du}{dx} \tag{26}$$

Substituting equation (26) into equation (24) and then rearranging give the final form of differential equation of particle velocity

$$\frac{du}{dx}=\frac{\psi}{\eta} \tag{27}$$

Where

$$\psi=u(\frac{\partial P}{\partial\lambda})_{v,e}\frac{\partial\lambda}{\partial x}-[uf-mc^2+\frac{q}{\rho}(\frac{\partial P}{\partial e})_{v,\lambda}] \tag{28}$$

$$\eta=\rho(c^2-u^2) \tag{29}$$

Rearranging equations (15), (16) and (26), we have the final differential forms of the density, pressure and specific internal energy

$$\frac{d\rho}{dx}=\frac{m}{u}-\frac{\rho}{u}\frac{du}{dx} \tag{30}$$

$$\frac{dP}{dx}=f-\rho u\frac{du}{dx} \tag{31}$$

$$\frac{de}{dx}=\frac{P}{\rho^2}\frac{d\rho}{dx}-\frac{q}{\rho u} \tag{32}$$

Equations (27), (30), (31) and (32) are the differential forms to solve the eigenvalue detonation of liquid explosives

APPENDIX 2 STEADY STATE ZND EQUATIONS OF TWO-PHASE DETONATION MODEL

The model under consideration treats the aluminized liquid explosive as a chemically reacting mixture with a fluid phase and a solid phase. Unreacted liquid explosive and detonation products are the fluid phase, and the aluminum particles are the solid phase. Since the full derivation of the governing equations is detailed elsewhere (Baer and Nunziato, 1986), we shall be content here with a very brief outline and focus on the case of steady state. In the sense of the continuum theory of mixtures, the two phases are assumed to coexist at each spatial location, and are assigned individual state variables such as density, velocity, specific internal energy, and so on. Intra-phase diffusive thermal and momentum transport are ignored. Since it is assumed that each phase is a continuum, consequently the partial differential equations resembling single-phase equations are written to describe the evolution of mass, momentum and energy in each constituent. An exchange of these phase variables across the phase boundaries appears as interaction terms in the balance equations. The heat release of the two-phase reaction will be considered as a source term in energy balance equations. Pressure disequilibrium between the phases is accommodated by introducing a compaction law. The model is described by the following set of equations in laboratory coordinate (x', t'). Conservation of mass, momentum and energy for the fluid phase are

$$\frac{\partial \overline{\rho}_1}{\partial t'} + \frac{\partial (\overline{\rho}_1 U_1)}{\partial x'} = m \tag{1}$$

$$\frac{\partial (\overline{\rho}_1 U_1)}{\partial t'} + \frac{\partial (\overline{\rho}_1 U_1^{\,2} + \overline{P}_1)}{\partial x'} = -P_1 \frac{\partial \Phi_2}{\partial x'} + mU_2 - f \tag{2}$$

$$\frac{\partial (\overline{\rho}_1 E_1')}{\partial t'} + \frac{\partial [U_1(\overline{\rho}_1 E_1' + \overline{P}_1)]}{\partial x'} = (P_2 - \beta)\tau - P_1 U_2 \frac{\partial \Phi_2}{\partial x'} + mE_2' - U_2 f - q + \zeta_1 q_{ch} \tag{3}$$

Conservation of mass, momentum and energy for the solid phase are

$$\frac{\partial \overline{\rho}_2}{\partial t'} + \frac{\partial (\overline{\rho}_2 U_2)}{\partial x'} = -m \tag{4}$$

$$\frac{\partial(\bar{\rho}_2 U_2)}{\partial t'}+\frac{\partial(\bar{\rho}_2 U_2^{\,2}+\bar{P}_2)}{\partial x'}=P_1\frac{\partial \Phi_2}{\partial x'}-mU_2+f \tag{5}$$

$$\frac{\partial(\bar{\rho}_2 E_2')}{\partial t'}+\frac{\partial[U_2(\bar{\rho}_2 E_2'+\bar{P}_2)]}{\partial x'}=-(P_2-\beta)\tau+P_1U_2\frac{\partial \Phi_2}{\partial x'}-mE_2'+U_2 f+q+\zeta_2 q_{ch} \tag{6}$$

The compaction equation for the solid phase is

$$\frac{\partial \Phi_2}{\partial t'}+U_2\frac{\partial \Phi_2}{\partial x'}=\tau+\frac{m}{\rho_2} \tag{7}$$

The equation for the conservation of particle number is

$$\frac{\partial}{\partial t'}\left[\frac{\Phi_2}{r^3}\right]+\frac{\partial}{\partial x'}\left[U_2\frac{\Phi_2}{r^3}\right]=0 \tag{8}$$

where $E'=e+\dfrac{U^2}{2}$ is the total energy of each phase, e is the specific internal energy; $\bar{P},\bar{\rho}$, are pseudo-pressure and bulk density, $\bar{\rho}_1=\Phi_1\rho_1$, $\bar{\rho}_2=\Phi_2\rho_2$, $\bar{P}_1=\Phi_1P_1$, $\bar{P}_2=\Phi_2P_2$; P, ρ, and U are the pressure, true density and velocity respectively; Φ is the volume concentration, for continuity, $\Phi_1+\Phi_2=1$; n is the number of particles in unit volume, $n=\dfrac{\Phi_2}{\frac{4}{3}\pi r^3}$; Subscripts "*1*" and "*2*" denote the fluid phase and the solid phase, respectively; The primes indicate values relative to the laboratory frame; *m*, *f*, and *q* are the mass, momentum and energy source terms, respectively. The subscript "*ch*" represents the chemical reaction term for aluminum; r is the radius of the metal particles; ζ is the effective coefficient of aluminum reaction heat release to each phase. τ is the rate of compaction with the following empirical form (Bdzil, 1999):

$$\tau=\begin{cases}\dfrac{\Phi_1\Phi_2(P_2-P_1-\beta)}{\mu_c} & P_1>\beta \\ \dfrac{\Phi_1\Phi_2P_1}{\mu_c} & P_1\le\beta\end{cases} \tag{9}$$

where μ_c is compaction viscosity; β is the intragranular stress or configuration pressure.

By combining the solid mass evolution equation (4) with the particle number conservation equation (8), an explicit equation is obtained for particle radius evolution:

$$\frac{\partial r}{\partial t'}+U_2\frac{\partial r}{\partial x'}=-\frac{rm}{3\Phi_2\rho_2}-\frac{r}{3\rho_2}\left(\frac{\partial \rho_2}{\partial t'}+U_2\frac{\partial \rho_2}{\partial x'}\right) \tag{10}$$

In the reference frame (x, t) attached to the shock, the following transformations are made:

$$\begin{aligned} &x = Dt'-x' \ , \quad t=t' \\ &u_1 = D-U_1, \quad u_2 = D-U_2 \end{aligned} \tag{11}$$

Therefore the following transformations exist

$$\begin{aligned} &\frac{\partial}{\partial t'}=\frac{\partial}{\partial t}+D\frac{\partial}{\partial x} \\ &\frac{\partial}{\partial x'}=-\frac{\partial}{\partial x} \end{aligned} \tag{12}$$

Substituting the transformation equations (11) and (12) into the conservation equations (1)-(10), we get conservation equations of mass, momentum and energy in the shock frame.

For the fluid phase, the conservation equations of mass, momentum and energy are

$$\frac{\partial \overline{\rho}_1}{\partial t}+\frac{\partial(\overline{\rho}_1 u_1)}{\partial x}=m \tag{13}$$

$$\frac{\partial \overline{\rho}_1 u_1}{\partial t}+\frac{\partial(\overline{\rho}_1 u_1^{\,2}+\overline{P}_1)}{\partial x}=mu_2+f-P_1\frac{\partial \Phi_2}{\partial x}+\overline{\rho}_1\frac{\partial D}{\partial t} \tag{14}$$

$$\begin{aligned} \frac{\partial \overline{\rho}_1 E_1}{\partial t}+\frac{\partial[u_1(\overline{\rho}_1 E_1+\overline{P}_1)]}{\partial x}&=\tau(P_2-\beta)+mE_2+u_2 f \\ &-(q-\zeta_1 q_{ch})-u_2 P_1\frac{\partial \Phi_2}{\partial x}+\overline{\rho}_1 u_1\frac{\partial D}{\partial t} \end{aligned} \tag{15}$$

For the solid phase, the conservation equations of mass, momentum and energy are

$$\frac{\partial \bar{\rho}_2}{\partial t} + \frac{\partial (\bar{\rho}_2 u_2)}{\partial x} = -m \tag{16}$$

$$\frac{\partial \bar{\rho}_2 u_2}{\partial t} + \frac{\partial (\bar{\rho}_2 u_2^{\,2} + \bar{P}_2)}{\partial x} = -m u_2 - f + P_1 \frac{\partial \Phi_2}{\partial x} + \bar{\rho}_2 \frac{\partial D}{\partial t} \tag{17}$$

$$\begin{aligned} \frac{\partial \bar{\rho}_2 E_2}{\partial t} + \frac{\partial [u_2 (\bar{\rho}_2 E_2 + \bar{P}_2)]}{\partial x} &= -(P_2 - \beta)\tau - m E_2 - u_2 f + (q_e + \zeta_2 q_{ch}) \\ &\quad + P_1 u_2 \frac{\partial \Phi_2}{\partial x} + \bar{\rho}_2 u_2 \frac{\partial D}{\partial t} \end{aligned} \tag{18}$$

$$\frac{\partial r}{\partial t} + u_2 \frac{\partial r}{\partial x} = -\frac{rm}{3\Phi_2 \rho_2} - \frac{r}{3\rho_2}\left(\frac{\partial \rho_2}{\partial t} + u_2 \frac{\partial \rho_2}{\partial x}\right) \tag{19}$$

$$\frac{\partial \Phi_2}{\partial t} + u_2 \frac{\partial \Phi_2}{\partial x} = \tau + \frac{m}{\rho_2} \tag{20}$$

where $E = e + \frac{u^2}{2}$ is the total energy of each phase in the shock frame.

To obtain a steady-state solution, all the time derivatives are set equal to zero, i.e., $\frac{\partial}{\partial t} = 0$, and the governing equations (13)-(20) are reduced to a much simpler system:

$$\frac{d(\rho_1 \Phi_1 u_1)}{dx} = m \tag{21}$$

$$\frac{d(\rho_1 \Phi_1 u_1^{\,2} + \Phi_1 P_1)}{dx} = m u_2 + f - P_1 \frac{d\Phi_2}{dx} \tag{22}$$

$$\begin{aligned} \frac{d[u_1 \rho_1 \Phi_1 (e_1 + \frac{u_1^2}{2} + \frac{P_1}{\rho_1})]}{dx} &= m(e_2 + \frac{u_2^2}{2}) + u_2 f - (q - \zeta_1 q_{ch}) \\ &\quad - u_2 P_1 \frac{d\Phi_2}{dx} + (P_2 - \beta)\tau \end{aligned} \tag{23}$$

$$\frac{d(\rho_2 \Phi_2 u_2)}{dx} = -m \tag{24}$$

$$\frac{d(\rho_2 \Phi_2 u_2^{\ 2} + \Phi_2 P_2)}{dx} = -mu_2 - f + P_1 \frac{d\Phi_2}{dx} \tag{25}$$

$$\frac{d[u_2 \rho_2 \Phi_2 (e_2 + \frac{u_2^2}{2} + \frac{P_2}{\rho_2})]}{dx} = -m(e_2 + \frac{u_2^2}{2}) - u_2 f + (q + \zeta_2 q_{ch}) + P_1 u_2 \frac{d\Phi_2}{dx} - (P_2 - \beta)\tau \tag{26}$$

$$\frac{dr}{dx} = -\frac{rm}{3\Phi_2 \rho_2 u_2} - \frac{r}{3\rho_2 u_2}\frac{d\rho_2}{dx} \tag{27}$$

$$\frac{d\Phi_2}{dx} = \frac{\tau}{u_2} + \frac{m}{\rho_2 u_2} \tag{28}$$

To further simplify equations (21)-(23) and derive the explicit expression of derivatives of u, ρ, P and e, we do the following manipulation. To make the expression simpler, we omit the subscript "1".

Rearranging equation (23), we have

$$\frac{d[u\rho\Phi(e + \frac{u^2}{2} + Pv)]}{dx} = H_1 \tag{29}$$

or

$$\frac{d}{dx}(e + Pv + \frac{u^2}{2}) = H_2 \tag{30}$$

where

$$H_1 = m(e_2 + \frac{u_2^2}{2}) + u_2 f - (q - \zeta_1 q_{ch}) - u_2 P_1 \frac{d\Phi_2}{dx} + (P_2 - \beta)\tau \tag{31}$$

$$H_2 = \frac{1}{\Phi\rho u}[H_1 - m(e + \frac{u^2}{2} + Pv)] \tag{32}$$

and $v = \frac{1}{\rho}$, is the specific volume.

We may write equation (30) as

$$\frac{de}{dx}+u\frac{du}{dx}+P\frac{dv}{dx}+v\frac{dP}{dx}=H_2 \tag{33}$$

$$u\frac{d(\Phi\rho u)}{dx}+\Phi\rho u\frac{du}{dx}+\Phi\frac{dP}{dx}+P\frac{d\Phi}{dx}=u_2m+f-P\frac{d\Phi_2}{dx} \tag{34}$$

or

$$u\frac{du}{dx}+v\frac{dP}{dx}=\frac{m(u_2-u)+f}{\Phi\rho} \tag{35}$$

Substituting equation (35) into (33) yields

$$\frac{de}{dx}=H-P\frac{dv}{dx} \tag{36}$$

where

$$H=H_2-\frac{m(u_2-u)+f}{\Phi\rho} \tag{37}$$

Recall that

$$c^2=-v^2\left(\frac{dP}{dv}\right)_s \tag{38}$$

if we consider specific energy e to be a function of P and v, we have

$$de=E_v dv+E_p dP \tag{39}$$

where

$$E_v=\left(\frac{de}{dv}\right)_p \quad , \quad E_p=\left(\frac{de}{dP}\right)_v$$

At constant entropy (*s=constant)*, $de = -Pdv$. This means that

$$-Pdv=E_v dv+E_p dP \tag{40}$$

which can be rearranged to yield the result

$$c^2=v^2\frac{P+E_v}{E_p} \tag{41}$$

For *e=constant*, we have

$$(\frac{dP}{dv})_e = -\frac{E_v}{E_p} \tag{42}$$

Since

$$\frac{dP}{dx} = (\frac{\partial P}{\partial v})_{e,\lambda}\frac{dv}{dx} + (\frac{\partial P}{\partial e})_{v,\lambda}\frac{de}{dx} + (\frac{\partial P}{\partial \lambda})_{e,v}\frac{d\lambda}{dx} \tag{43}$$

Substituting equations (41), (42) into equation (43) yields

$$\frac{dP}{dx} = -\frac{c^2}{v^2}\frac{dv}{dx} + (\frac{\partial P}{\partial e})_{v,\lambda}H + (\frac{\partial P}{\partial \lambda})_{e,v}\frac{d\lambda}{dx} \tag{44}$$

Substituting equation (44) into equation (35) yields

$$\rho u\frac{du}{dx} - \frac{c^2}{v^2}\frac{dv}{dx} + (\frac{\partial P}{\partial e})_{v,\lambda}H + (\frac{\partial P}{\partial \lambda})_{e,v}\frac{d\lambda}{dx} = \frac{1}{\Phi}[m(u_2 - u) + f] \tag{45}$$

From equation (21), we have

$$u\frac{d\rho}{dx} + \rho\frac{du}{dx} = \frac{1}{\Phi}(m - \rho u\frac{d\Phi}{dx}) \tag{46}$$

i.e.,

$$-\frac{1}{v^2}\frac{dv}{dx} = \frac{d\rho}{dx} = \frac{1}{\Phi u}(m - \rho u\frac{d\Phi}{dx}) - \frac{\rho}{u}\frac{du}{dx} \tag{47}$$

Substituting equation (47) into equation (45) and then rearranging them give the final form of differential of particle velocity with subscript "1"

$$\frac{du_1}{dx} = \frac{\psi}{\eta} \tag{48}$$

Where

$$\begin{aligned}\psi = {} & u_1(\frac{\partial P_1}{\partial e_1})_{v_1,\lambda_1}H + u_1(\frac{\partial P_1}{\partial \lambda_1})_{v_1,e_1}\frac{d\lambda_1}{dx} \\ & -\frac{u_1}{\Phi_1}[m(u_2 - u_1 - \frac{c_1^2}{u_1}) + f - \rho_1 c_1^2\frac{d\Phi_1}{dx}]\end{aligned} \tag{49}$$

$$\eta = \rho_1(c_1^2 - u_1^2) \tag{50}$$

$$H = \frac{1}{\Phi_1 \rho_1 u_1}\{ m[e_2 - e_1 + \frac{(u_2 - u_1)^2}{2} - P_1 v_1] + (u_2 - u_1) f \\ -(q - \zeta_1 q_{ch}) - u_2 P_1 \frac{d\Phi_2}{dx} + (P_2 - \beta)\tau\} \tag{51}$$

Substituting equation (48) into equations (35), (36) and (47), we have the final differential forms of the density, pressure and specific internal energy in the fluid phase:

$$\frac{d\rho_1}{dx} = \frac{1}{u_1}(\frac{m}{\Phi_1} - \frac{\rho_1 u_1}{\Phi_1}\frac{d\Phi_1}{dx} - \rho_1 \frac{du_1}{dx}) \tag{52}$$

$$\frac{dP_1}{dx} = \frac{1}{\Phi_1}[(u_2 - u_1)m + f] - \rho_1 u_1 \frac{du_1}{dx} \tag{53}$$

$$\frac{de_1}{dx} = H + \frac{P_1}{\rho_1^2}\frac{d\rho_1}{dx} \tag{54}$$

To solve ordinary differential equations (48), (52), (53) and (54), u_2, e_2, ρ_2 and P_2 are needed to be determined *a priori*.

From equation (25) by means of equation (24), the rate of particle velocity in the solid phase can be expressed as

$$\frac{du_2}{dx} = -\frac{1}{\Phi_2 \rho_2 u_2}[f + (P_2 - P_1)\frac{d\Phi_2}{dx} + \Phi_2 \frac{dP_2}{dx}] \tag{55}$$

From equation (24), the derivative of particle velocity in solid phase may also be expressed as

$$\frac{du_2}{dx} = -\frac{1}{\rho_2 \Phi_2}(m + \Phi_2 u_2 \frac{d\rho_2}{dx} + \rho_2 u_2 \frac{d\Phi_2}{dx}) \tag{56}$$

Comparing equation (55) with equation (56), we obtain

$$\frac{d\rho_2}{dx} = \frac{1}{\Phi_2 u_2^2}[f + (P_2 - P_1 - \rho_2 u_2^2)\frac{d\Phi_2}{dx} + \Phi_2 \frac{dP_2}{dx} - u_2 m] \tag{57}$$

Through some manipulations, we can also reduce equation (26) to a simple ordinary differential equation:

$$\frac{de_2}{dx} = \frac{1}{\Phi_2 \rho_2 u_2}[m\frac{P_2}{\rho_2} + u_2 P_2 \frac{d\Phi_2}{dx} + q + \zeta_2 q_{ch} - (P_2 - \beta)\tau + \frac{\Phi_2 u_2 P_2}{\rho_2}\frac{d\rho_2}{dx}] \quad (58)$$

To close the system requires equations of state of the constituents.

REFERENCES

Akhavan, J., The chemistry of explosives, *RSC Paperbacks, The Royal Society of Chemistry*, UK, 1998

Arkhipov, V. I., Makhov, M.N., Pepekin, V.I., Shchetinin, V.G., Investigation into detonation of aluminized high explosives, *Chem. Phys. Reports*, 18(12): 2329-2337, 2000

Bdzil, J.B., Steady-state two-dimensional detonation, *J. Fluid Mech.* 108:195-226, 1981

Bdzil, J.B., Menikoff, R., Son, S.F., Kapila, A.K., Stewart, D.S., Two-phase modeling of deflagration-to-detonation transition in gradual materials: A critical examination of modeling issues, *Phys. Fluids*, 11(2):378-402, 1999

Baer, M.R., Nunziato, J.W., A two-phase mixture theory for the deflagration-to-detonation transition (DDT) in reactive granular materials, *Int. J. Multiphase Flow*, 12(6):861-889, 1986

Baudin, G., Lefrancois, A., Bogot, D., Champion, Y., Combustion of nanophase aluminum in the detonation of nitromethane, *11th Symp. on Detonation*, 1998

Baudin, G., Bergues, D., A reaction model for aluminized PBX applied to underwater explosion calculations, *10th Symp. on Detonation*, 1994

Blais, C.N., Engelke, R., Sheffield, S.A., Mass spectroscopic study of the chemical reaction zone in detonating liquid nitromethane, *J. Phys. Chem.*, A, 101(44), 1997

Boiko, V.M., Fedorov, A.V., Fomin, V.M., Papyrin, A.N., Soloukhin, R.I., Ignition of small particles behind shock wave, *Shock Wave, Explosion, and Detonation*, Progress in astronautics and aeronautics, 87:71-83, 1983

Brailovsky, I., Sivashinsky, G., Effects of momentum and heat losses on the multiplicity of detonation regimes, *Combustion and Flame* 128:191-196, 2002

Brousseau, P., Anderson, C. H., Nanometric aluminum in explosives, *Propellants, explosives, pyrotechnics* , 27: 300-306, 2002

Burton, J.A., Hawkins, S.J., Hooper, H., Detonation temperature of some liquid explosives, *7th Symp. on Detonation*, 1982

Campbell, A.W., Davis, W.C., Travis, J.R., Shock initiation of detonation in liquid explosives, *Phys. Fluids*, 4:495-510, 1961

Chan, S.K., Theoretical prediction of the velocity-diameter relation of bubble sensitized liquid explosives, *Propellants, Explosives and Pyrotechnics*, 8, 1983

Chapman, D.L., On the rate of explosion in gases. *Philos. Mag.* 47:90-104, 1899

Chariton, Y.B., Problem of explosive theory, *Izd-vo Akad. Nauk* SSSR, Moskva-Leningrad, 1947.

Cooper, Paul W., Explosives engineering, *Wiley-VCH*, New York, 1996

Cowperthwaite, M., Nonideal detonation in a composite CHNO explosive containing aluminum, *10th Symp. on Detonation*, 1993

Cowperthwaite, M., Steady-state detonation in ammonium perchlorate/aluminum compositions with components in mechanical but not thermal equilibrium, *11th Symp. on Detonation*, 1998

Craig, B.G., Measurements of the detonation-front structure in condensed-phase explosives, *10th Symp. on Combustion*,1965

Davis, W.C., Shock waves; rarefaction waves; equations of state, *Explosive Effects and Applications*, Edited by Jonas A. Zukas and William P. Walters, 2000

Dionne, J.P., Theoretical study of the propagation of non-ideal detonations, *Ph.D. Thesis*, Mcgill University, Canada, 2000

Dobratz, B.M., Crawfort, P.C., LLNL explosives handbook, *Technical Report UCRL-52997*, Lawrence Livermore National Laboratory, 1985

Döring, W., On detonation processes in gases, *Ann. Phys.* 43:421-436, 1943

Dorsett, H.E., Brousseau, P., Cliff, M.D., The influence of ultrafine aluminum upon explosives detonation, *28th Int. Pyrotechnics Seminar*, South Australia, 2001

Dremin, A.N., Toward detonation theory, *Spring-Verlag New York Inc*,1999

Duff, R.L., Houston, E., Measurement of the Chapman-Jouguet pressure and reaction zone length in a detonating high explosive, *J. of Chem. Phys.*, 23(7), 1955

Dunnett, J.D., Swift, D.C., Braithwaite, M., Comparison of Williamsburg and JWL equations of state for nitromethane, *11th Symp. on Detonation*,1998

Engelke, R, Effect of a physical inhomogeneity on steady-state detonation velocity, *Phys. Fluids* , 22(9):1623-1630, 1979

Engelke, R., Bdzil, J. B., A study of the steady-state reaction-zone structure of homogenous and heterogeneous explosive, *Phys. Fluids*, 26(5):1210-1221, 1983

Engelke, R, Effect of the number density of heterogeneities on the critical diameter of condensed explosives, *Phys. Fluids*, 26(9):2420-2424,1983

Erpenbeck, J.J., Stability of steady-state equilibrium detonation, *Phys. Fluids* 5:604-614, 1962

Fedorov, A.V., Khmel, T.A., Numerical simulation of shock-wave initiation of heterogenous detonation in aerosuspensions of aluminum particles, *Combustion, Explosion, and Shock Waves*, 35(3), 1999

Fedorov, A.V., Khmel, T.A., Numerical simulation of detonation initiation with a shock wave entering a cloud of aluminum particles, *Combustion, Explosion, and Shock Waves*, 38(1), 2002

Fickett, W., Davis, W.C., Detonation, *University of California Press*, 1979

Finger, M., Hornig, H.C., Lee, E.L., Kury, J. W., Metal acceleration by composite explosives, *5th Symp. On Detonation*, 1970

Foelsche, R.O., Ignition and combustion of aluminum particles in $H_2/O_2/N_2$ combustion products, *J. of Propulsion and Power*, 14(6), 1998

Fried, L.E., Howard, W. M., Souers, P. C., Cheetah 2.0 user's manual, *Lawrence Livermore National Lab., Energetic Materials Center*, 1998

Friedman, R., Macek, A., Ignition and combustion of aluminum particles in hot ambient gases, *Combustion and Flame*, 6(1), 1962

Frost, D. L., Aslam, T., Hill, L.G., Application of detonation shock dynamics to the propagation of detonation in nitromethane in a packed inert particle bed, *Shock Compression of Condensed Matter*, CP505, 1999

Frost, D. L., Kleine, H., Blast waves from heterogeneous explosives, *22th Int. Sypm. on Shock Wave* , 2001

Frost, D.L., Goroshin, S., Li, Y., Zhang, F., Murray, S., Lee, J., Brouille, M., Hill, L., Aslam, T., Dremin, A., Detonation in heterogeneous explosive: experimental results and modeling issues, Gordon research conference on energetic materials, 2002

Frost, D.L., Detonation of NM in packed bed of aluminum particles, *Private Communication*, 2005

Gibson, F.C., Bowser, M.L., Summers, C.R., Scott, F.H., Mason, C.M., Use of an electro-optical method to determine detonation temperature in high explosives, *J. of Applied Phys.*, 29(4):628-632, 1958

Gladilin, A.M., Detonation processes in two-phase media, *Nova Science Publishers Inc.*, New York, 1996

Gogulya, M.F., Detonation waves in HMX/Al mixtures (pressure and temperature measurements), *11th Symposium on Detonation* ,1998

Gogulya, M.F., Dolgoborodov, A, Makhov, M.N., Brazhnikov, M.A.., Shchetinin, V.G., Detonation performance of aluminized compositions based on BTNEN, *12th Symp. On Detonation*, 2002

Gonor, A., Hooton, I., Narayan, S., Steady-state model of heterogeneous detonation with reactive metallic particles, *12th Symp. on Detonation*, 2002

Grishkin, A. M., Doubnov, L. V., Davodov, V. Yu, Levshina, Yu. A., Mikhailova, T. N., Effect of powdered aluminum additives on the detonation parameters of high explosives, *Fizika Goreniya Vzryva*, 2992:115-117, 1993

Grosse, A.V., Conway, J.B., Combustion of metals in oxygen, *Ind. Eng. Chem.*, 50:663-672, 1958

Haskins, P. J., Cook, M. D., Briggs, R.I., The effect of additives on the detonation characteristics of a liquid explosive, *CP620, Shock Compression of Condensed Matter - 2001*, Edited by Furnish, M.D., Thadhani, N.N., and Horie,Y., 2002, American Institute of Physics.

Havard, W.M. et al., Kinetic modeling of non-ideal explosives with Cheetah, *11th Symp. on Detonation*, 1998

Hawken, D., Modeling support to heterogeneous blast waves from a condensed charge with metal particles, *Combustion Dynamics Ltd. Internal Report*, 2002

Imkhovik, N.A, Soloviev, V.S., *21th Int. Pyrotechnics Seminar; Inst. Chem. Phys, RAS, Moscow*, 1995

Ishida, T., Haykawa, T., Tokita, K., Kato, Y., Detonation pressure measurements of aluminized explosives by means of shock-induced polarization, *22th Int. Annual Conference on ICT*, 71:1 -12, 1991

Jouguet, E., On the propagation of chemical reactions in gases, *J. de Math. Pures et Appliquees* 1:347-425, 1905, 2:5-85, 1906

Kato,Y., Mori, N., Sakai, H., Tanaka, K., Sakurai, T., Hikita, T., Detonation temperature of nitromethane and some solid high explosives, *8th sym. on detonation*, 1985

Kato,Y., Brochet, C., Detonation temperatures of nitromethane aluminum gels, *Dynamics of Shock Wave, and Detonation, Progress in Astronautics and Aeronautics*, 94,1984

Kato, Y., Bauer, B., Brochet, C., Bouriannes, B., Brightness temperature of detonation wave in nitromethane-tetranitromethane mixture and in gaseous mixtures at a high initial pressure, *7th Symp. on Detonation*, 1981

Kato, Y., Brochet, C., Cellular structure of detonation in nitromethane containing aluminum particles, *Dynamics of Shock Wave and Detonation, Progress in Astronautics and Aeronautics*, 93,1983

Kennedy, D.L., The challenge of non-ideal detonation, *J. de Physique IV, Colloque C4, supplement au J. de Physique III*, 5, 1995

Kennedy, D.L., Jones, D.A., Modeling shock initiation and detonation in non-ideal explosive PBXW-115, *10th Symp. on Detonation*, 1993

Kessler, D. P., Greenkorn, R.A., Momentum, heat and mass transfer fundamentals, *Marcel Decker*, New York, 1999

Krier, H., Mozaffarian, A., Two-phase reactive particle flow through normal shock waves, *Int. J. Multiphase Flow*, Vol.4, pp. 65-79, 1978

Kuehl, D.K., *Pyrodynamics*, 3:65-79,1965

Leal, B., Baudin, G., Goutelle, J.C., Presles, H.N., An optical pyrometer for time resolved temperature measurements in detonation wave, *11th Symp. On Detonation*, 1998

Lee, J.J., Brouillette, M., Frost, D.L., Lee, J.H.S., Effect of diethylenetriamine sensitization on detonation of nitromethane in porous media, *Combustion and Flame*, 100:292-300, 1995

Leiper, G.A., Cooper, J., Reaction of aluminum and ammonium nitrate in non-ideal heterogeneous explosives, *10th Symp. on Detonation*, 1994

Mader, C.L., Numerical simulation of explosives and propellants, *CRC Press*, 1998

Mcguire R.R., Finger, M., Composite explosives for metal acceleration: the effect of detonation temperature, *8th Symp. on Detonation*, 1985

Mench, M.M., Kuo, K. K., Yeh, C.L., Lu, Y.C., Comparison of thermal behavior of regular and ultra-fine aluminum powder (Alex) made from plasma explosion process, *Combust. Sci. and Tech*, 135:269-292, 1998

Miller, P.J., Bedford, C.D., Davis, J.J., Effect of metal particle size on the detonation performance of various metallized explosives, *11th Symp. on Detonation*, 1998

Miller P. J., Guirguis, R.H., Experimental study and model calculations of metal combustion in Al/AP underwater explosives, *Mat. Res. Soc. Symp. Proc.*, 296, 1993

Orth, L.A., Shock physics of non-ideal detonations for energetic explosives with aluminum particles, *Ph.D. Thesis*, University of Illinois at Urbana-Champaign, 1999

Pastine, D. J., Cowperthwaite, M., Solomon, J.M., Enig, J. W., A model of nonideal detonation in aluminized explosives, *11th Symp. on Detonation*, 1998

Persson, P. A., Rock blasting and Explosives Engineering, *CRC Press*, 1994

Phillips, B.R., De Witt, K.J., Resonance-tube ignition of aluminum, *Combustion and Flame*, 35:249-258, 1979

Powers, J.M., Theory of detonation structure for two-phase materials, *Ph.D. thesis*, University of Illinois at Urbana-Champaign, U.S., 1988

Presles, H.N., Vidal, P., Detonation generation and propagation in homogenous liquid explosives, *J. De Physique IV, Colloque C4, Supplement au Journal de Physique III*, 5, 1995

Presles, H.N., Brochet, C., Kato, Y., Tanaka, K., Influence of additives on nitromethane detonation characteristics, *7th Symp. on Detonation*, 1981

Ritter, H., Braun, S, High explosives containing ultrafine aluminum ALEX, *Propellant, Explosives, Pyrotechnics*, 26: 311-314, 2001

Rosing, V.O., Chariton, Y.B., Explosive detonation at small charge diameter, *Dokl. Akad. Nauk USSR*, 26(4):360-361,1940

Sheffield, S.A., Davis, L.L., Engelke, R., Detonation properties of nitromethane, deuterated nitromethane and bromonitromethane, *APS Topical Group on Shock Compressed of Condensed Matter Meeting*, 1999

Sheffield, S.A., Engelke, R., Alcon, R.R., Gustavsen, R.L., Robbins, D.L., Stahl, D.B., Stacy, H.L., Whitehead, M.C., Particle velocity measurements of the reaction zone in nitromethane, *12th Symp. On Detonation*, 2002

Soo, S.L., Multiphase fluid dynamics, *Science Press and Gower Technical*, Beijing, 1990

Stewart, D.S., The shock dynamics of multidimensional condensed and gas-phase detonations, *27th Symp. on Combustion*, pp.2189-2205, 1998

Sun, Y.B., Explosive mixtures in military, *China Weapon Industry Press*, 1995

Taylor, J., Detonation in condensed Explosives, *Oxford at the Clarendon Press*, 1952

Tao, W.C, Tarver, C.M., Kury, J.W., Lee, C.G., Ornellas, D.L., Understanding composite explosive energetics: IV. Reactive flow modeling of aluminum reaction kinetics in PETN and TNT using normalized product equation of state, *10th Symp. on Detonation*, 1993

Tepper, F., Ivanov, G., Lerner, M., Davidovich, V., Energetic formulations from nanosize metal powders, *24th Int. Pyrotech. Seminars*, pp.519-530, 1998

Veyssiere, B., Ignition of aluminum particles in gaseous detonation, *Shock Wave, Explosion, and Detonation, Progress in astronautics and aeronautics*, 87, 1983

Veyssiere, B., Structure of the detonation in gaseous mixtures containing aluminum particles in suspension, *Dynamics of Explosions, Progress in Astronautics and Aeronautics*, 106, 1986

Veyssiere, B., Khasainov, B.A., A model for steady, plane, double-front detonations (DFD) in gaseous explosive mixtures with aluminum particles in suspension, *Combustion and Flame*, 85: 241-253, 1991

Von Neumann, J., Theory of detonation waves, *Off. Sci. Res. Dev. Rep.* 549*Balist. Res. Lab. File No. X-122*, Aberdeen Proving Ground, MD, 1942

Winey, J. M., Duvall, G. E., Knudson, M. D., and Gupta, Y. M., Equation of state and temperature measurements for shocked nitromethane, *J. of Chem. Phys.*, 13(17), 2000

Wood, W.W., Kirkwood, J.G., Diameter effect in condensed explosives- The relation between velocity and radius of curvature of the detonation wave, *J. of Chem. Phys.*, 22(11),1954

He, X., The measurement of detonation temperature of condensed explosives with two color optical fiber pyrometer, *8th Symp. on Detonation*, 1985

Zel'dovich, Ya. B., On the theory of the propagation of detonation in gaseous system. *Zh. Eksp. Teor. Fiz.* 10:542-568, 1940

Zel'dovich, Ya. B., Gelfand, B.E., Borisov, A.A, Reaction zone in low-velocity detonation of gases in tube with rough walls, *Sov. J. Chem. Phys.* (4) 2:447:464, 1986

Zhang, F., Lee, J. H.S., Friction-induced oscillatory behavior of one-dimensional detonations, *Proc. R. Soc. Lond. A*, 446, 87-105, 1994

Zhang, F., Thibault, P.A., Link, R., Gonor, A.L., Momentum transfer during shock interaction with metal particles in condensed explosives, *Shock Compression of Condensed Matter-2001, 2002 American Institute of Physics*, 2002

TABLES

Table 2.1 Coefficients of heat capacity as a function of temperature

Name of Products	*a*	*b*	*c*
CO_2	37.792	0.0047012	-4.1865×10^{-7}
H_2O	23.242	0.0067768	-5.6263×10^{-7}
H_2	18.543	0.0024436	-1.5978×10^{-7}
N_2	21.543	0.0022379	-1.9585×10^{-7}
CO	21.572	0.0021387	-1.8778×10^{-7}

Table 2.2 Detonation parameters of NM

Detonation Parameters	This model				Cheetah BKWC	Sheffield (1999)	Blais (1997)
	Simple law	Arrhenius law E^* (kcal/mol)					
		30	40	53.6			
D m/s	6316.5	6316.6	6316.5	6316.8	6064	6335	6300
Pcj GPa	12.84	12.85	12.84	12.84	11.37		13
Tcj K	3718.7	3676	3674.7	3676.5	3664		
ρ_{cj} g/m^3	1580	1580.5	1580	1579.8	1556		
U_{cj} m/s	1799.2	1800.7	1798.9	1800.2	1666		

Table 2.3 Failure diameters (mm) of NM

E^* kcal/mol	Considering Curvature only	Considering m, F and q	Data in Engelke (1979) & Dremin (1999)
30	13.31	15	16.2
40	14.54	18	~
53.6	15.91	22	18

Table 4.1 Constants and initial conditions of NM, Al and detonation

Names of Parameters		Numbers	Units
Heat capacity of fluid phase at constant volume:	C_{v1}	1800	J/(kg·k)
Heat capacity of Al particles at constant volume:	C_{v2}	1000	J/(kg·k)
Heat capacity of fluid phase at constant pressure:	C_{p1}	2400	J/(kg·k)
Heat capacity of solid phase at constant pressure:	C_{p2}	1200	J/(kg·k)
Chemical energy of NM:	Q_{NM}	5×10^6	J/kg
Chemical energy of Al:	Q_{al}	3.1×10^7	J/kg
Initial density of Al:	ρ_{20}	2700	Kg/m^3
Initial density of NM:	ρ_{10}	1130	Kg/m^3
Gruneisen gamma of NM:	Γ	2.1	
Initial temperature of both phases:	T_0	300	
Coefficients of JWL EOS:	A	2.092×10^{11}	K
	B	5.689×10^9	Pa
	R_1	4.4	Pa
	R_2	1.2	
	Ω	0.3	
Coefficient of NM shock Hugoniot:	c_0	1760	
	s_0	1.56	m/s
Coefficient of Al shock Hugoniot:	c_0	5325	
	s_0	1.338	m/s
Efficiency of Al heat release:	ζ_1	1	
	ζ_2	0	

FIGURES

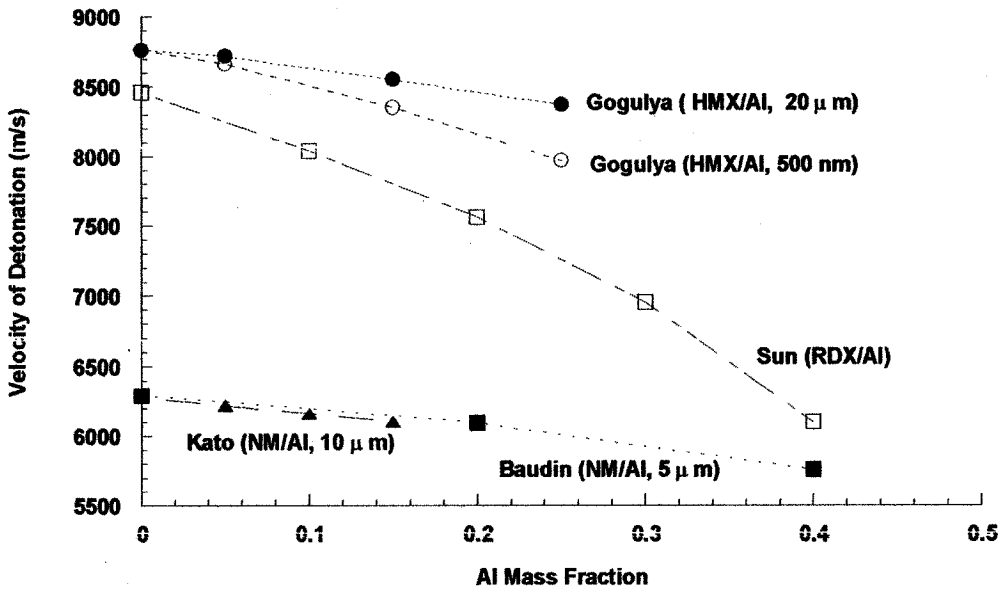

Figure 1.1 Measured detonation velocity in some high explosives

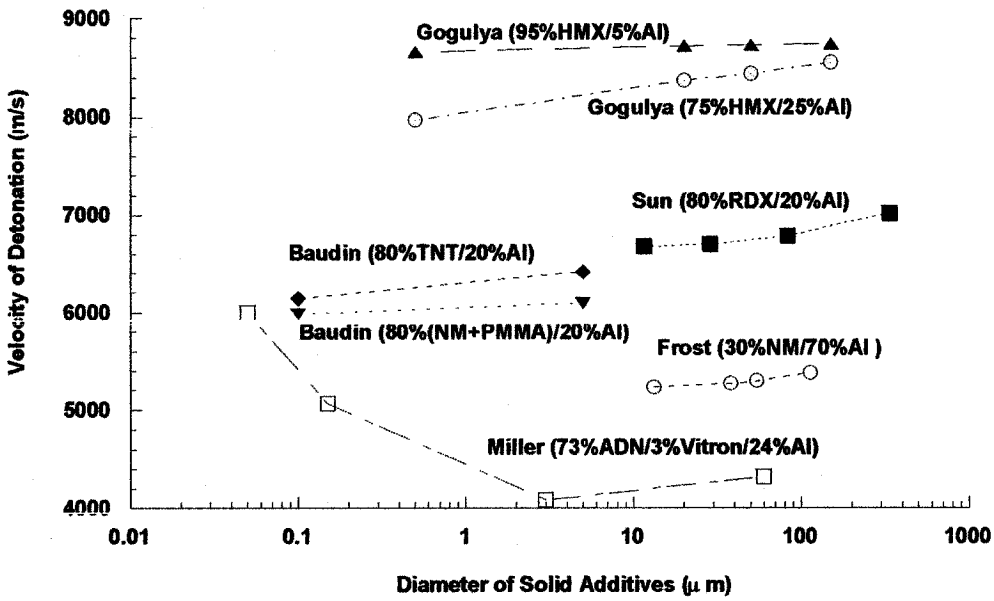

Figure 1.2 Detonation velocity with different particle sizes of additives in some explosives

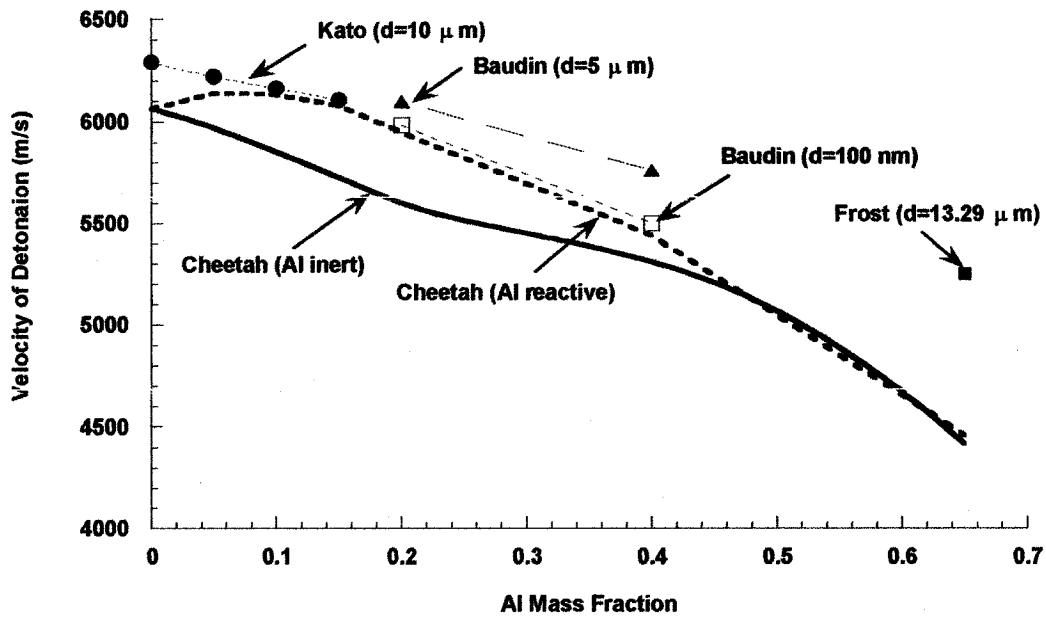

Figure 1.3 Detonation velocity of aluminized nitromethane

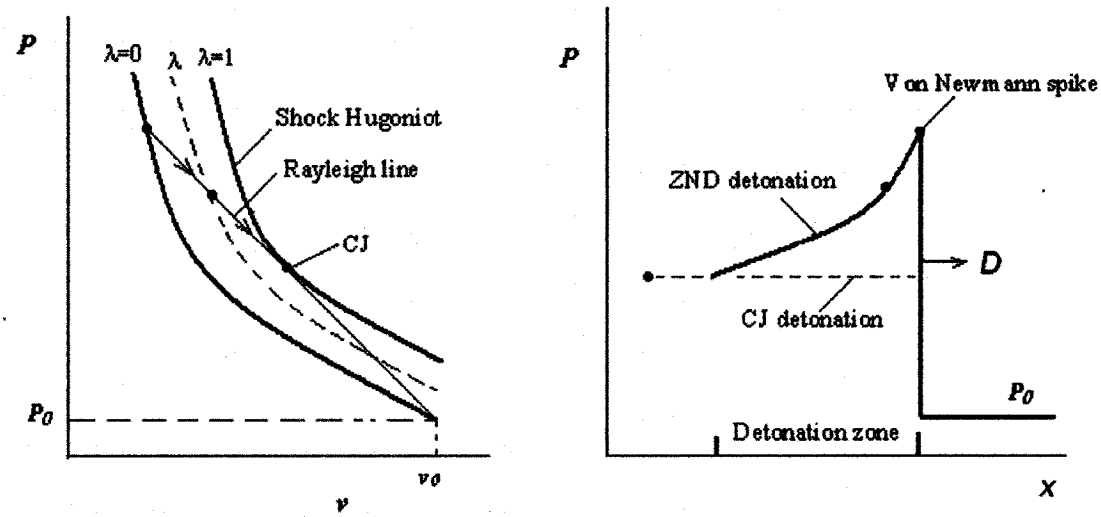

Figure 2.1 Shock pressure in ZND and CJ detonation theory

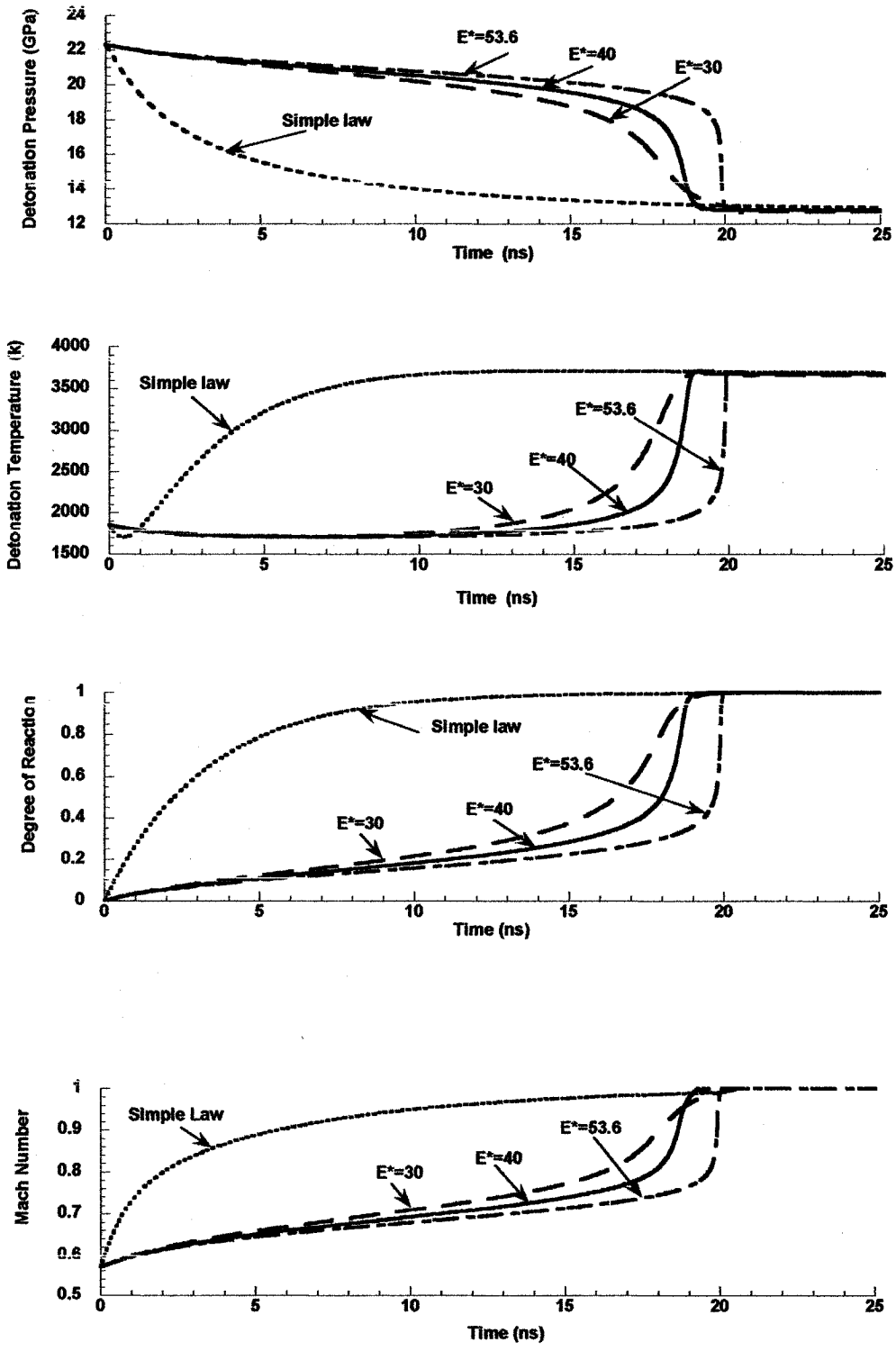

Figure 2.2 Steady-state detonation profile with various reaction rate laws in infinite diameter NM

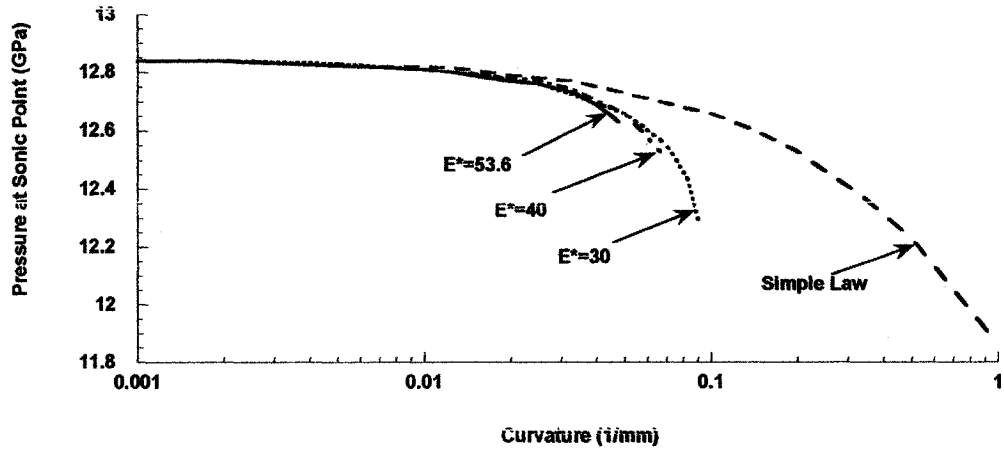

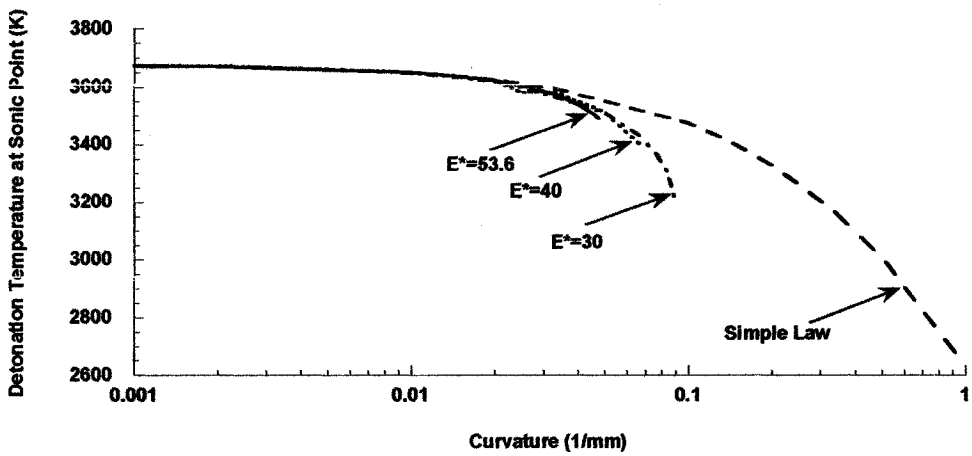

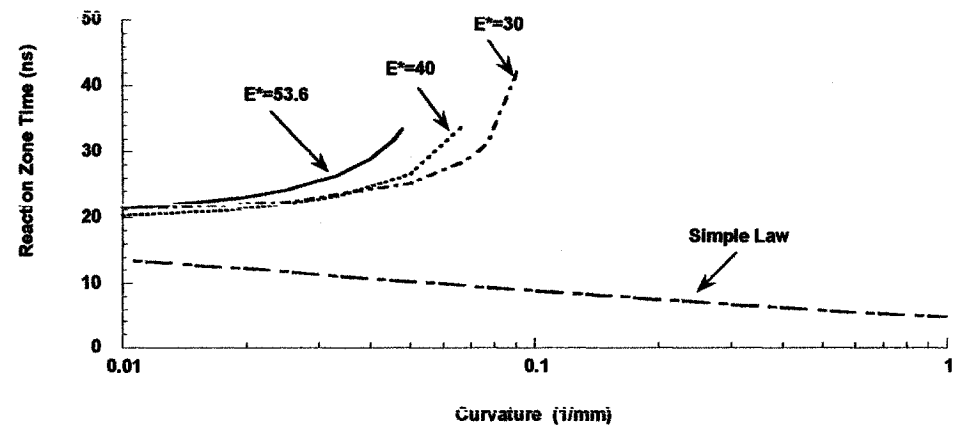

Figure 2.3 Detonation eigenvalue at sonic point for finite diameter NM with curvature only

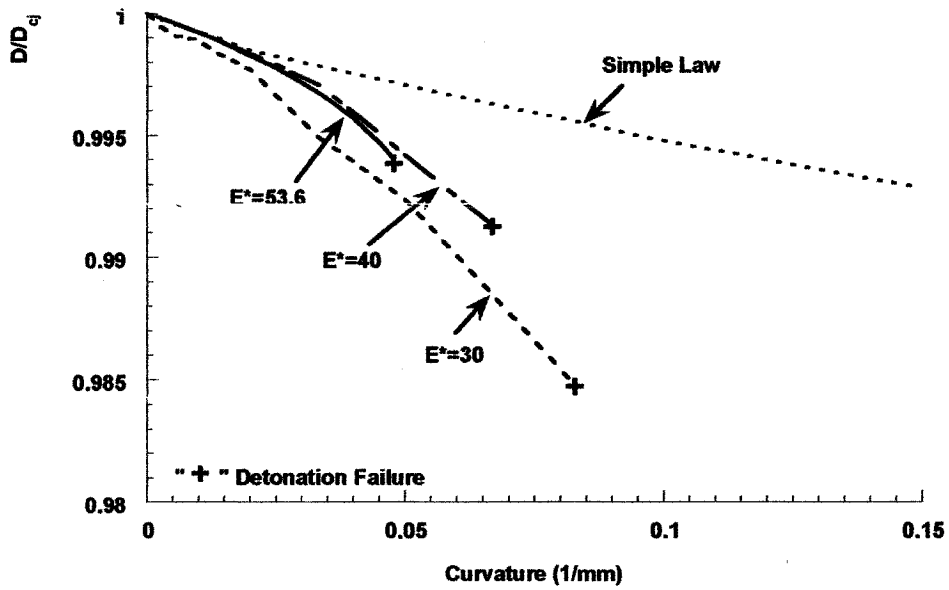

Figure 2.4 Detonation velocity of NM with curvature only

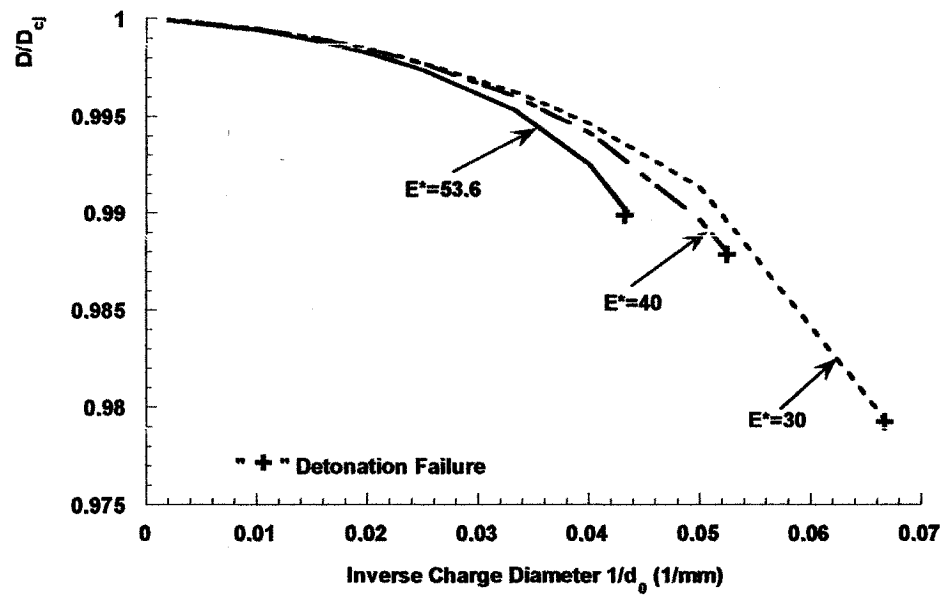

Figure 2.5 Detonation velocity of finite diameter NM with curvature, wall friction and heat loss

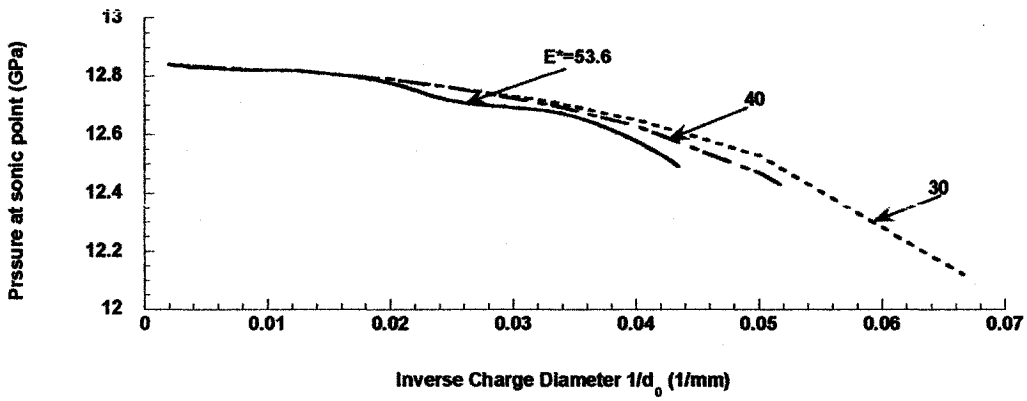

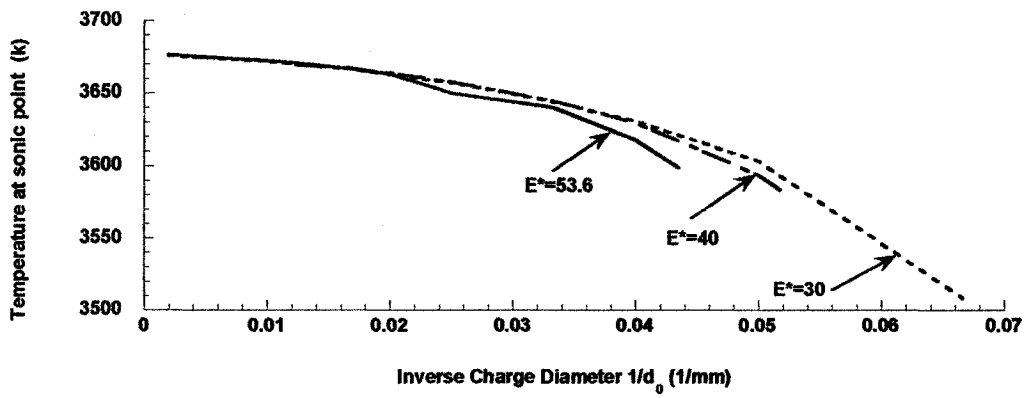

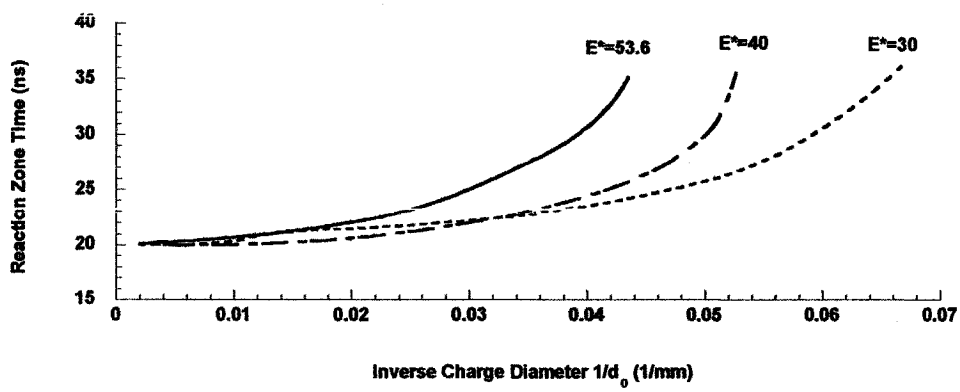

Figure 2.6 Eigenvalue at sonic point vs. inverse charge diameter for NM with curvature, wall friction and heat loss

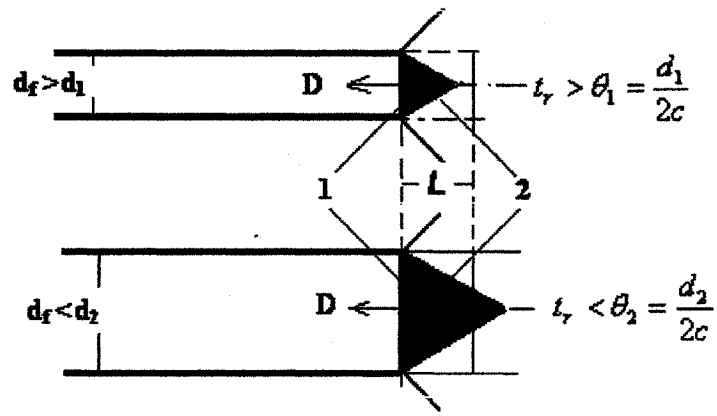

Figure 2.7 Rosing and Chariton detonation ability concept (1- detonation front; 2-lateral rarefaction wave front; d- charge diameter; d_f- failure diameter, D- detonation velocity; L- detonation zone length)

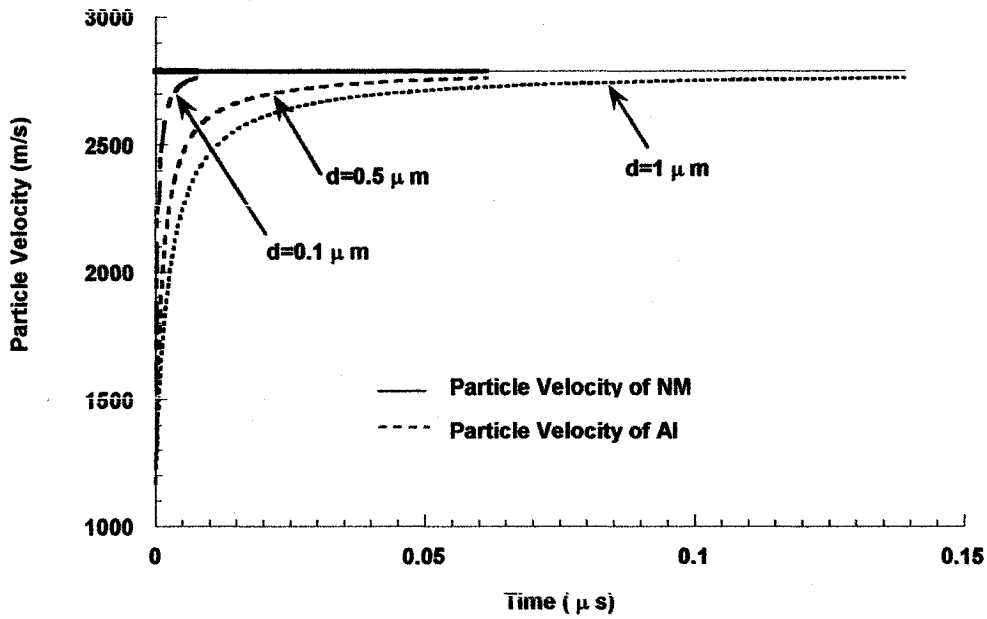

Figure 3.1 Particle velocity evolution of liquid NM and aluminum by 6300 m/s shock wave

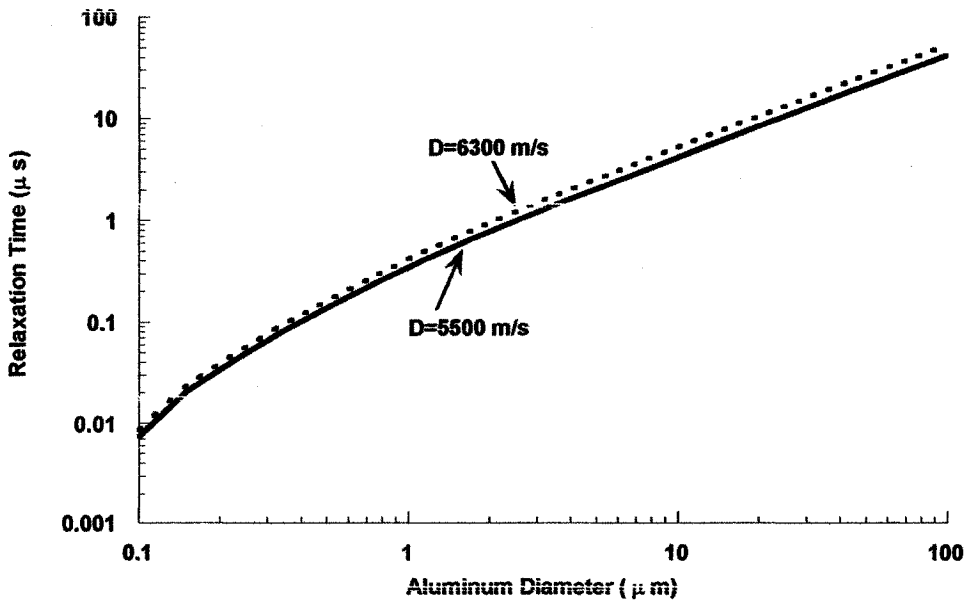

Figure 3.2 Particle velocity relaxation time of single Al particle in NM detonation products (Temperature of detonation products T=3000 k)

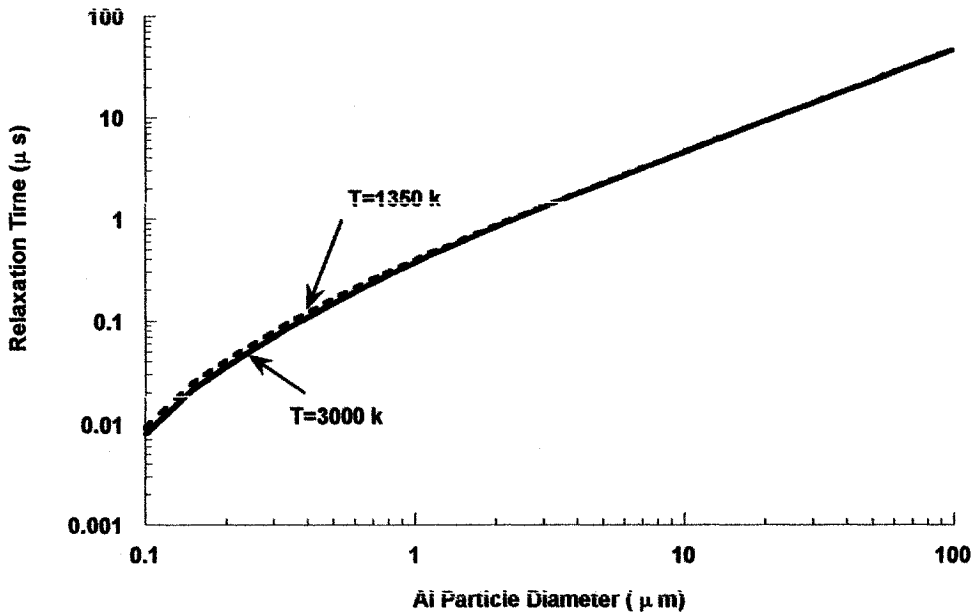

Figure 3.3 Particle velocity relaxation time with different temperatures of fluid phase

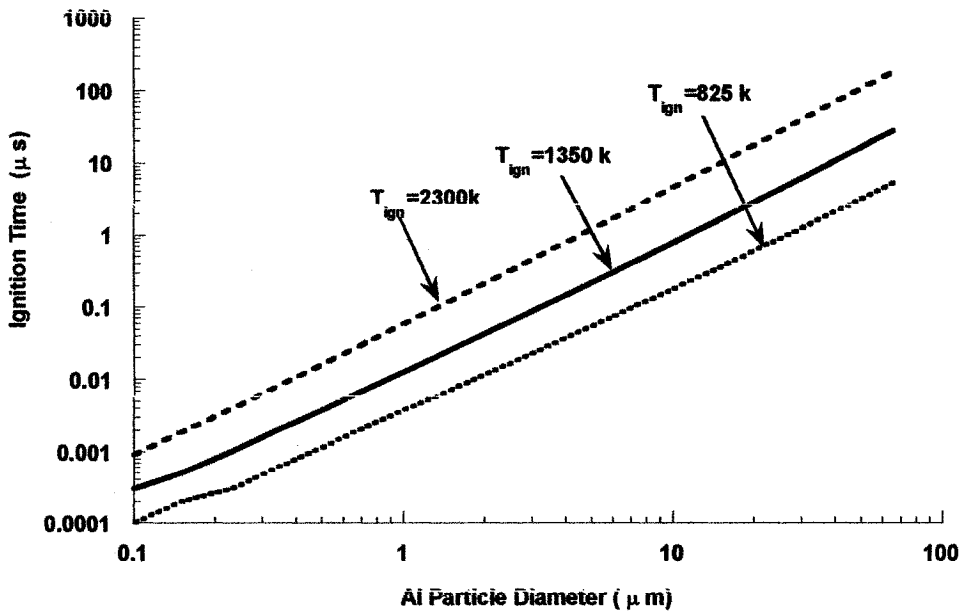

Figure 3.4 Ignition time of Al particles with different ignition criteria (Shock velocity D=6300 m/s, Temperature of NM T=3000 k)

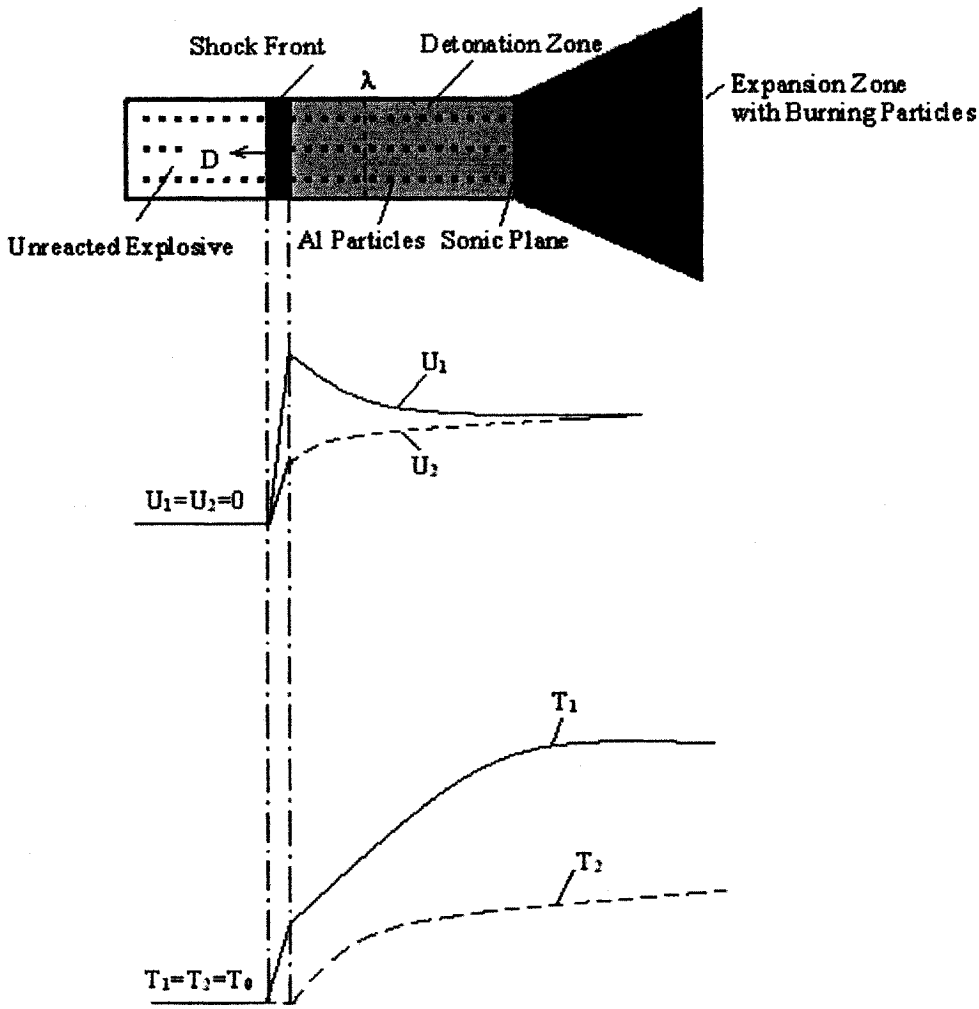

Figure 3.5 1-D two-phase flow model of detonation for aluminized liquid explosives

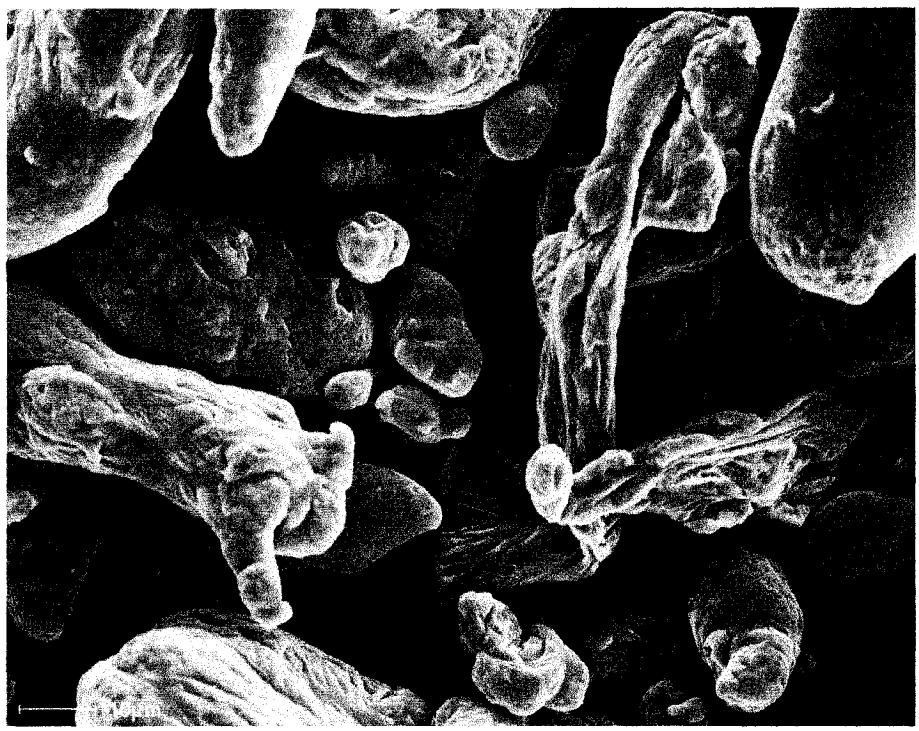

Conventional Al powder (Amp 611)

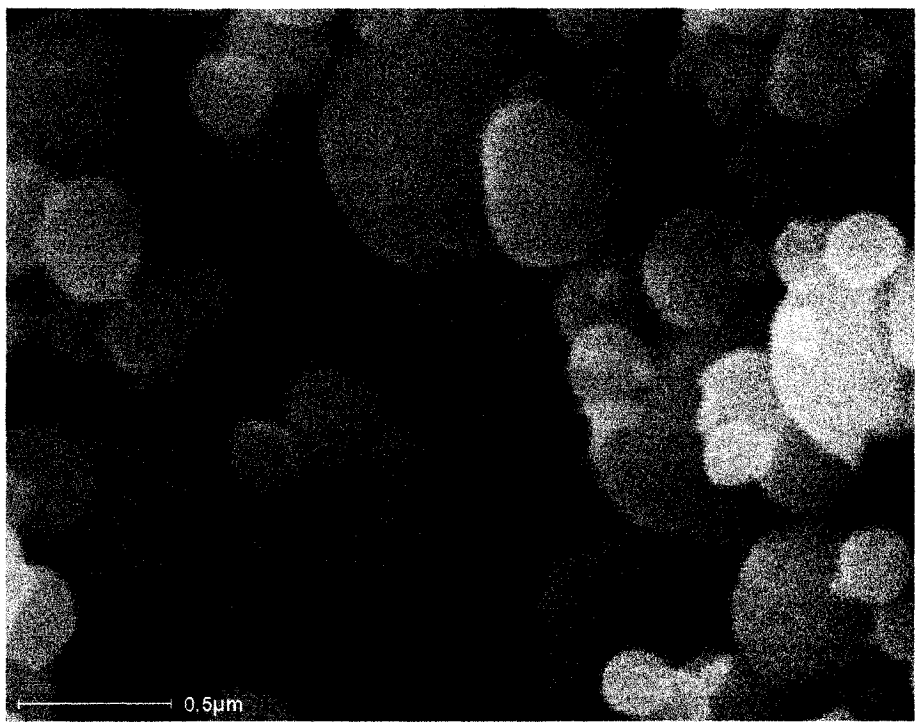

Nanoscale Al powder (Comb. Syn.)

Figure 4.1 SEM (Scanning electron Microscopy image) of Alex and conventional aluminum particles

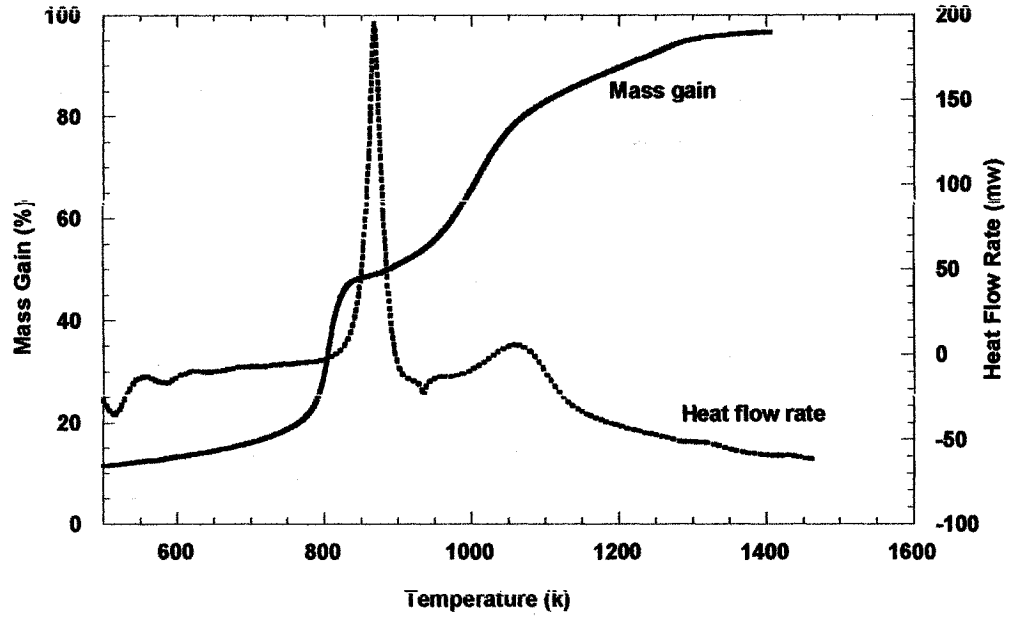

Figure 4.2 Mass gain and heat flow rate of Alex in air (β=7 ^{0}C/min.)

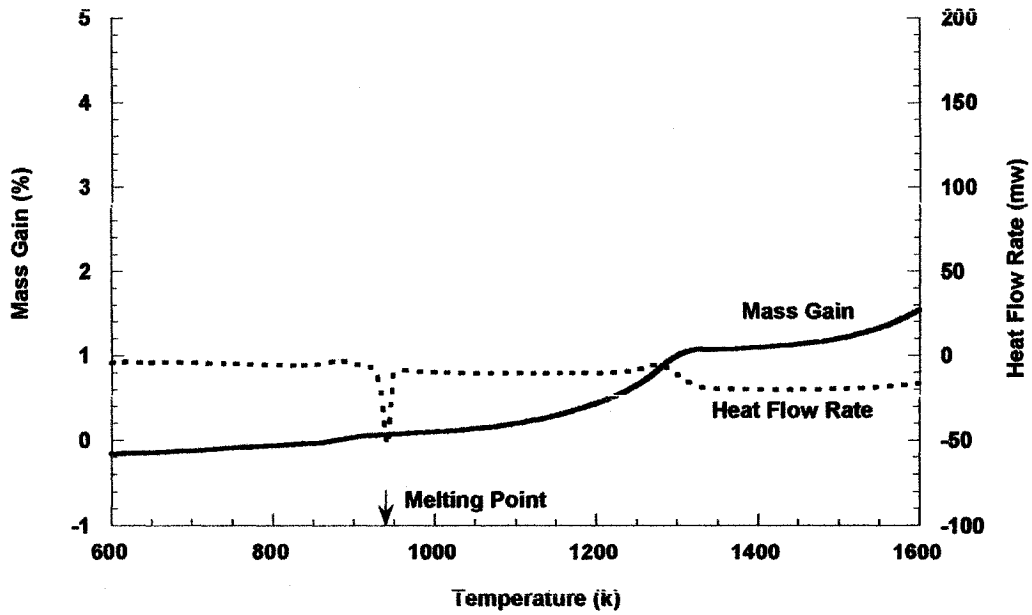

Figure 4.3 Mass gain and heat flow rate of Amp611 in air (β=7 ^{0}C/min.)

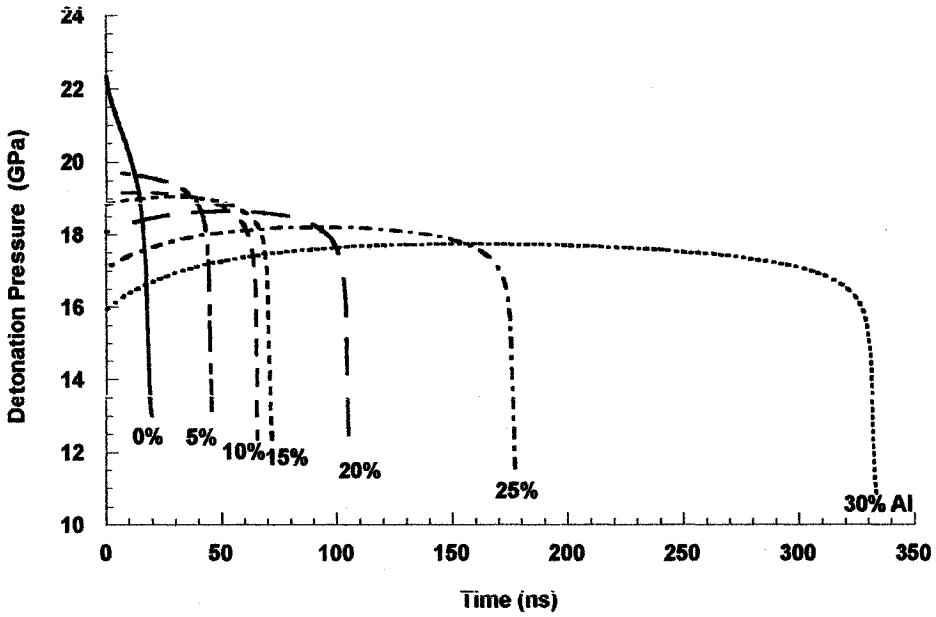

Figure 4.4 Pressure profile of aluminized nitromethane with Arrhenius law ($d = 10$ μm)

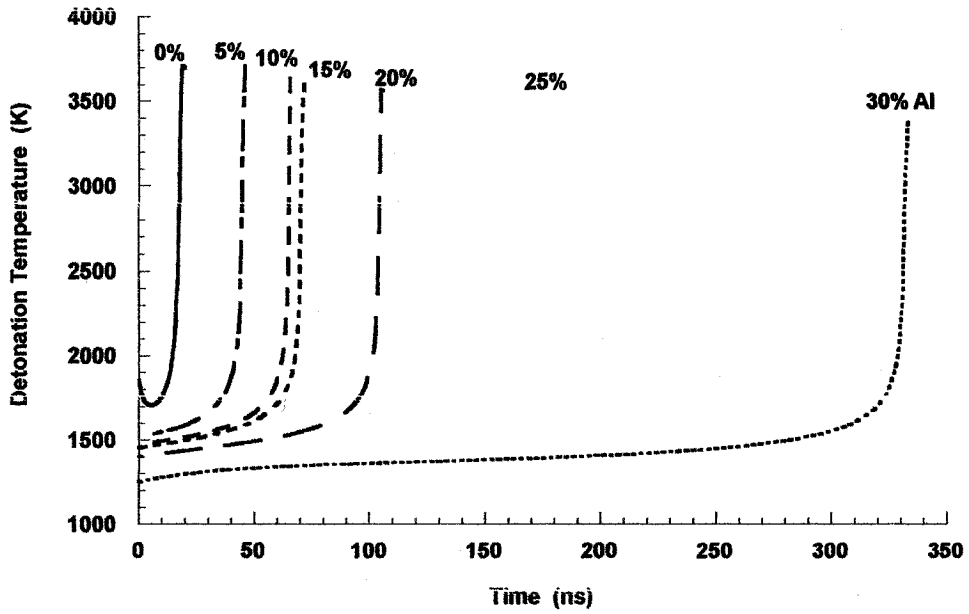

Figure 4.5 Temperature profile of aluminized nitromethane with Arrhenius law ($d = 10$ μm)

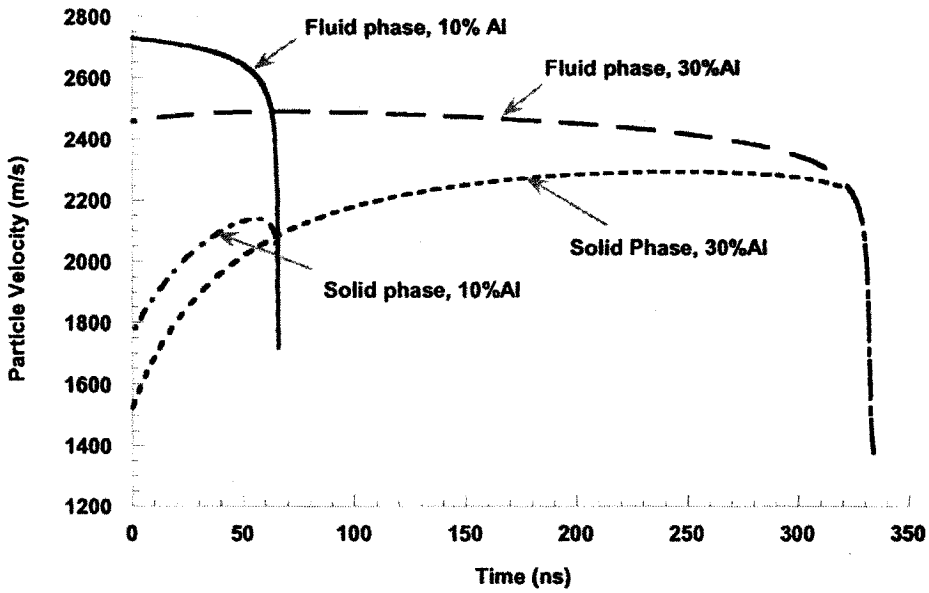

Figure 4.6 Particle velocity profile of aluminized nitromethane with Arrhenius law (d =10 μm)

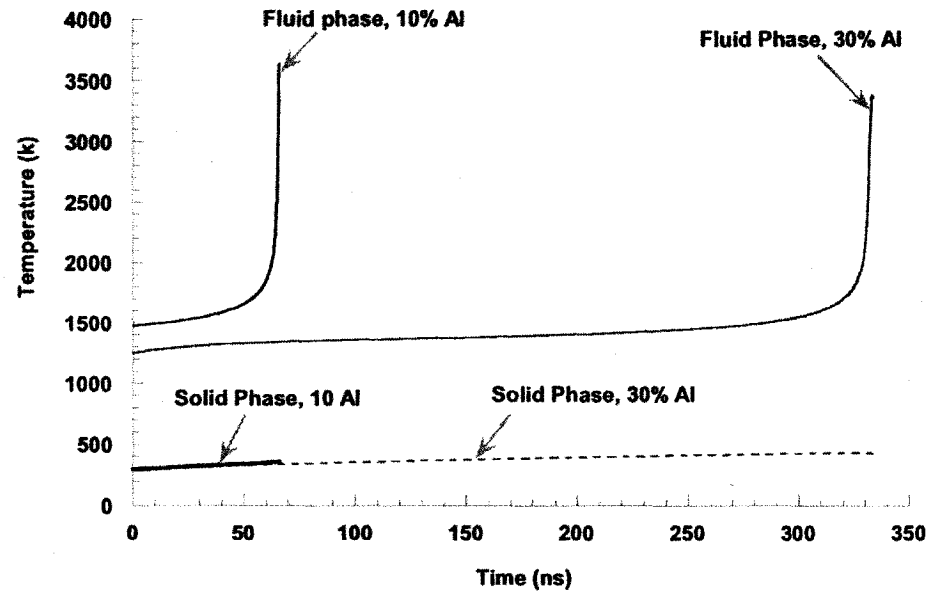

Figure 4.7 Temperature profile of two phases with Arrhenius law (d = 10 μm)

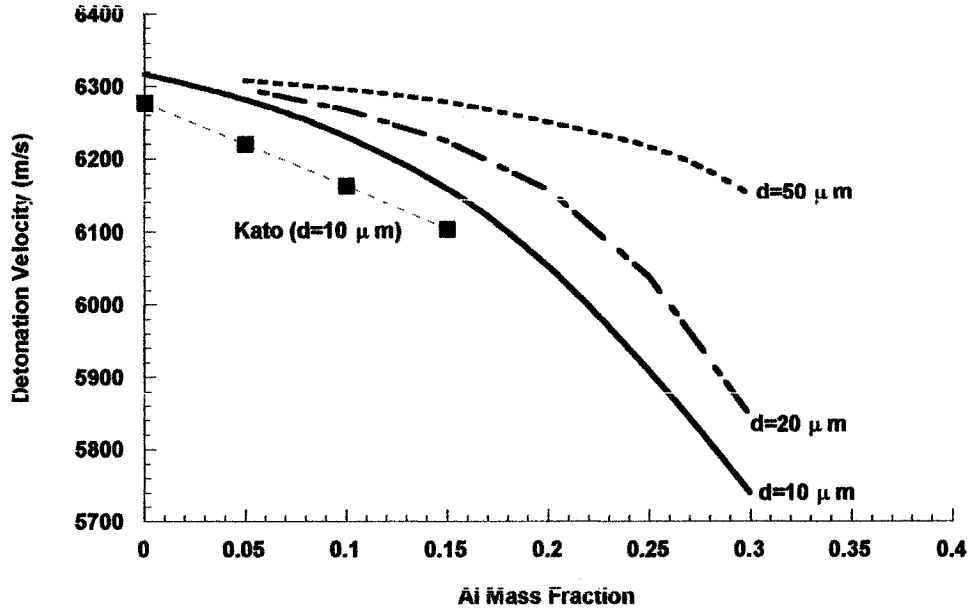

Figure 4.8 Detonation velocity of conventional aluminized nitromethane with Arrhenius law

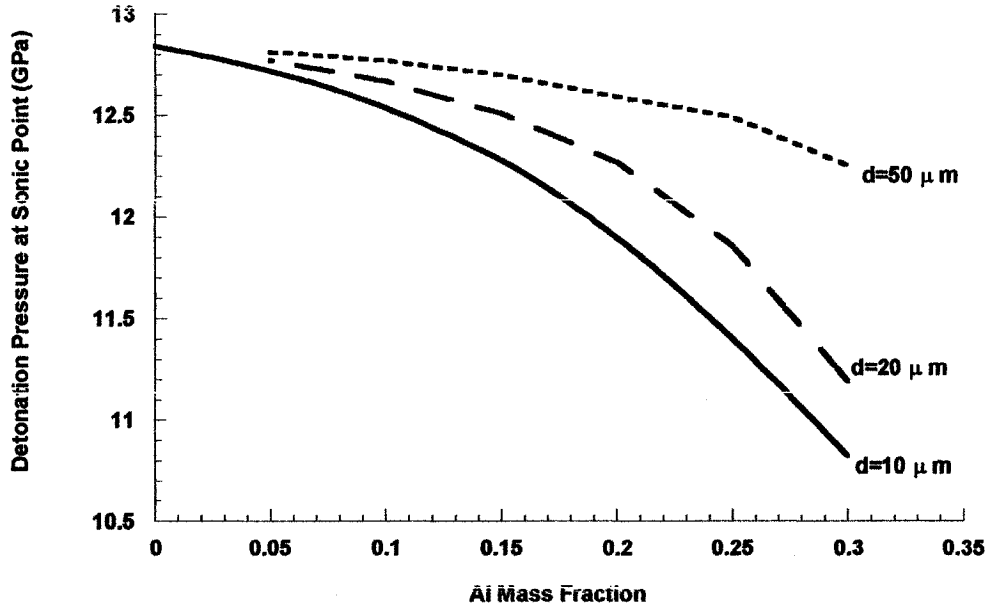

Figure 4.9 Detonation pressure at sonic point for conventional aluminized nitromethane with Arrhenius law

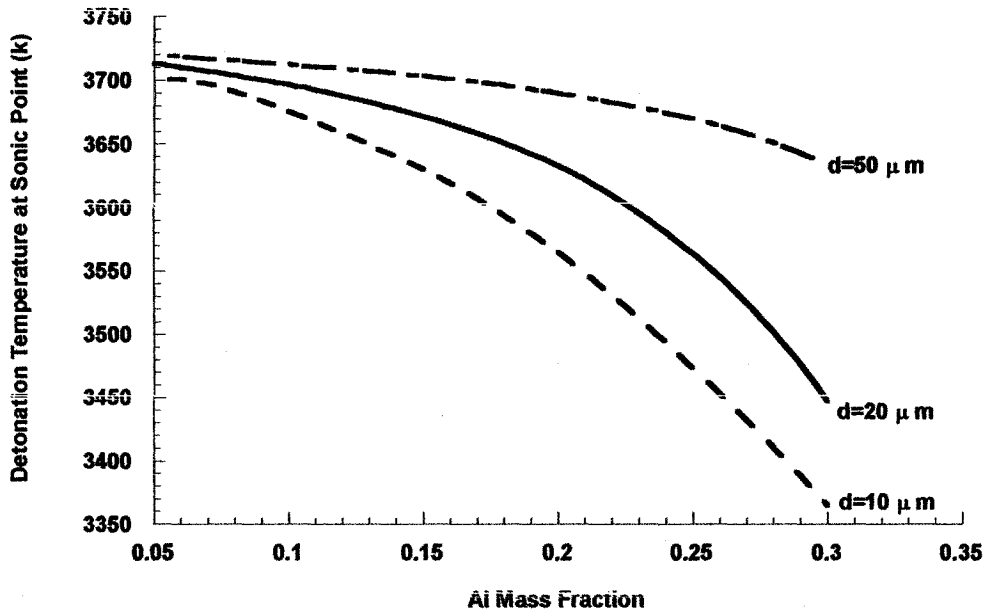

Figure 4.10 Detonation temperature at sonic point for conventional aluminized nitromethane with Arrhenius law

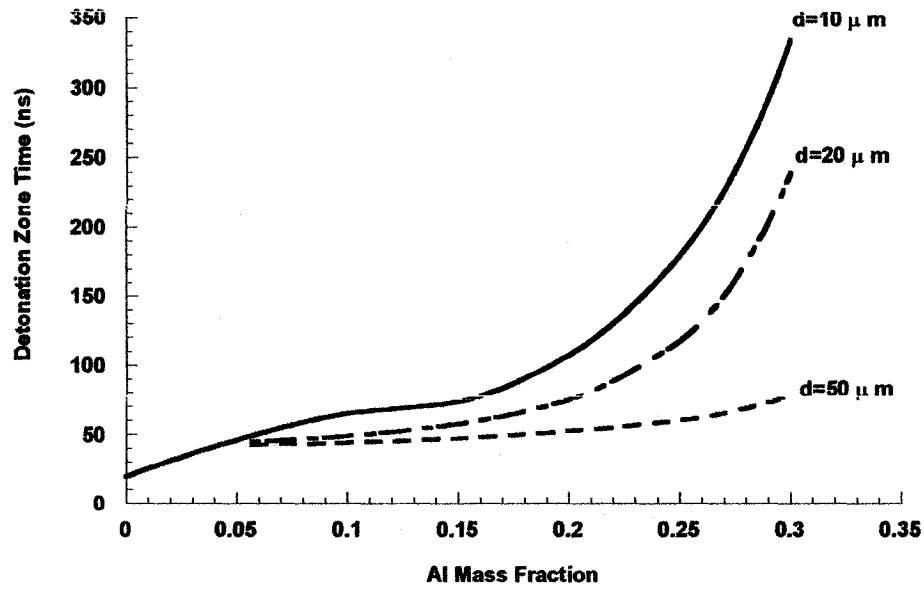

Figure 4.11 Detonation zone time of conventional aluminized nitromethane with Arrhenius law

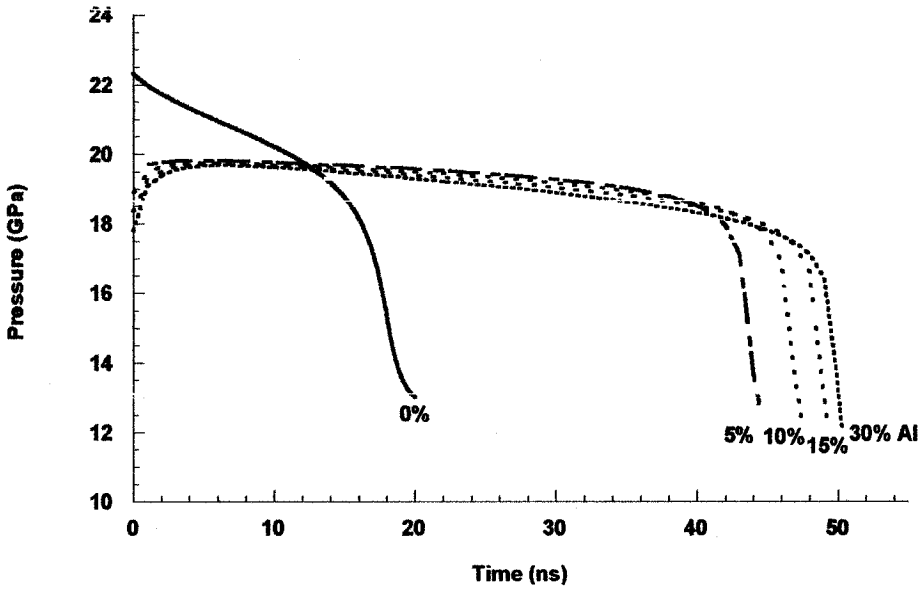

Figure 4.12 Pressure profile of aluminized nitromethane in detonation zone with Arrhenius law (d=100 nm, k_2=1×10^7)

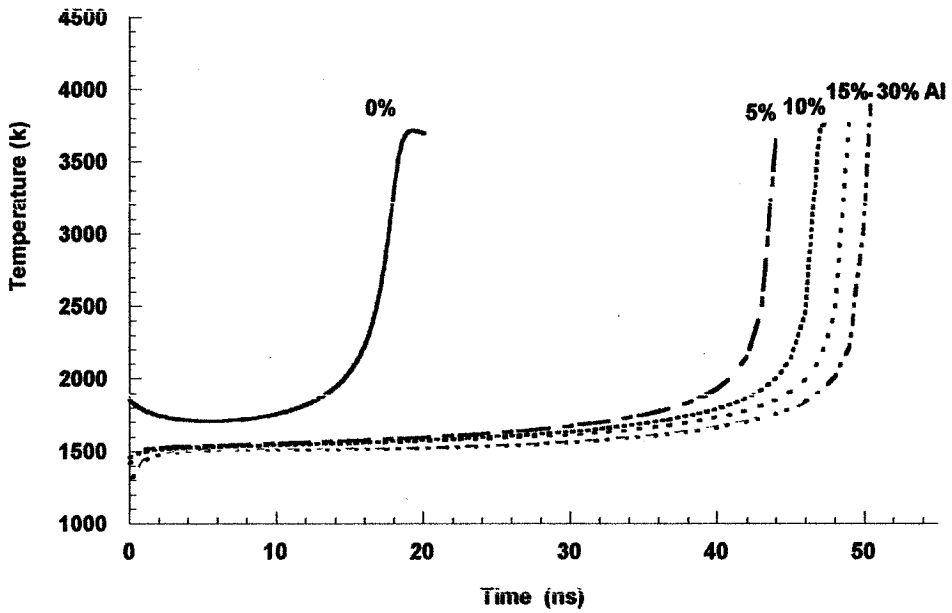

Figure 4.13 Temperature profile of aluminized nitromethane in detonation zone with Arrhenius law (d=100 nm, k_2=1×10^7)

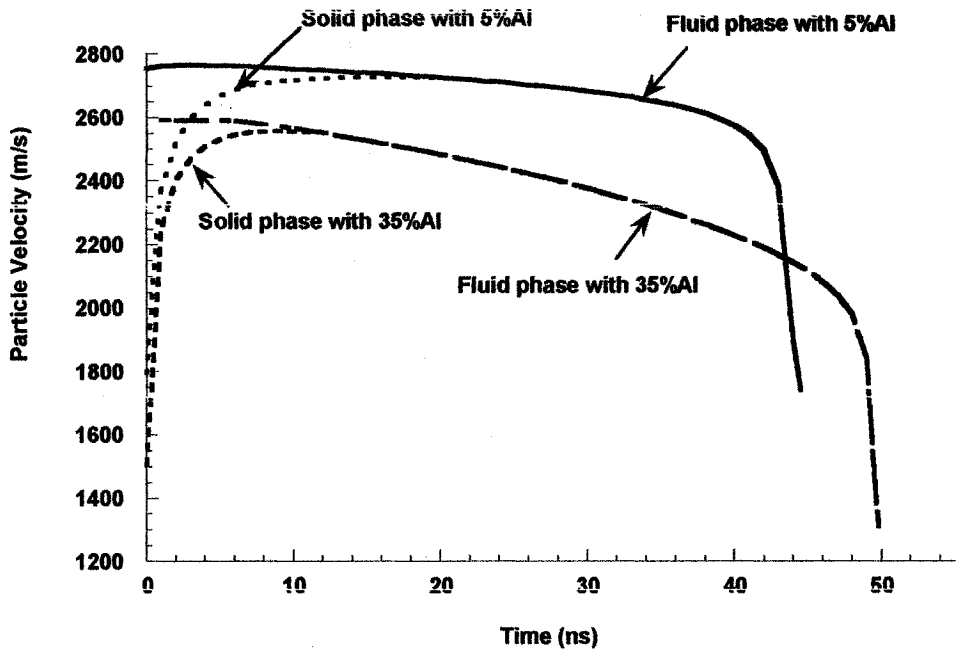

Figure 4.14 Particle velocity profile of aluminized nitromethane with Arrhenius law (d =100 nm, k_2=1×10^7)

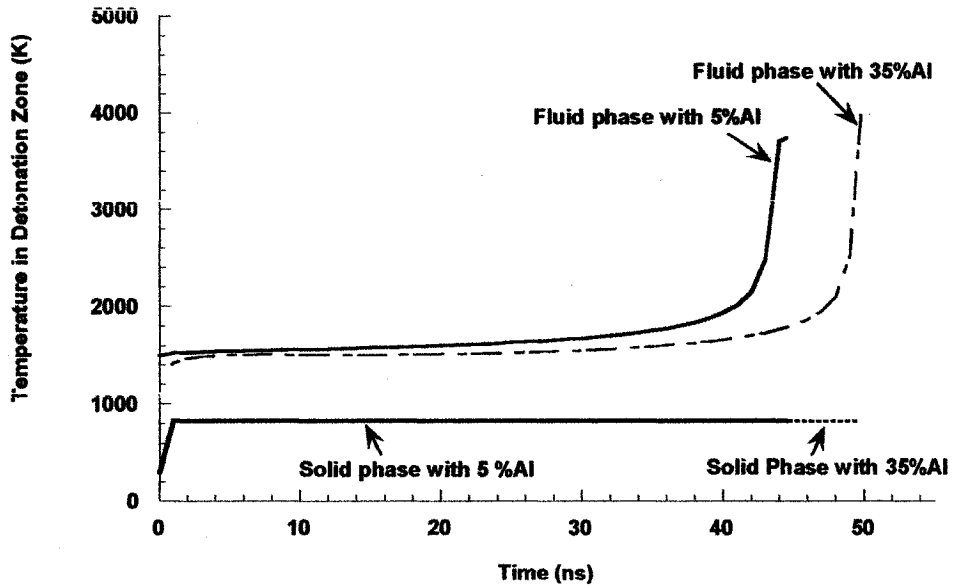

Figure 4.15 Temperature profile of aluminized nitromethane with Arrhenius law (d =100 nm, k_2=1×10^7)

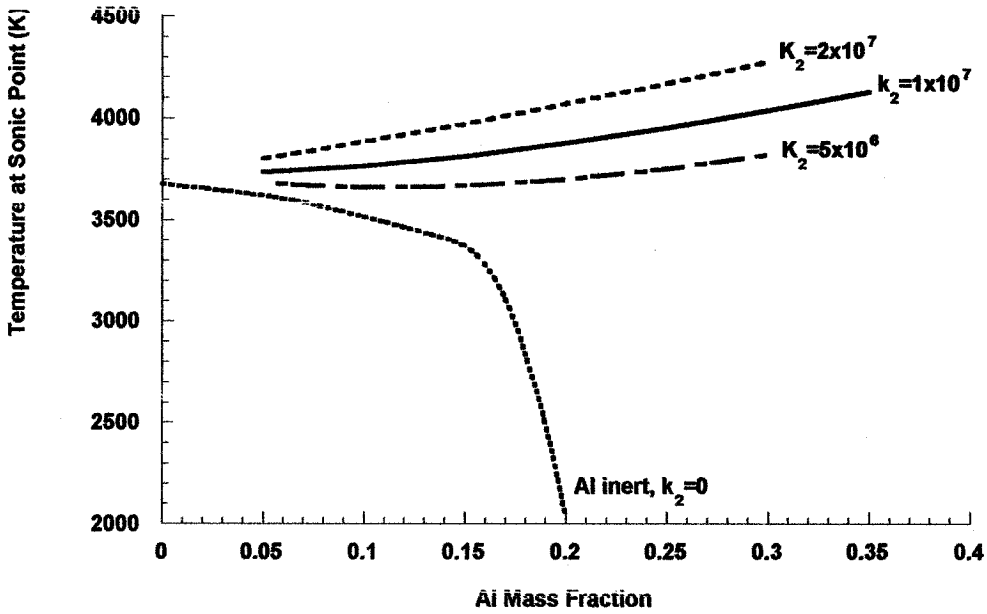

Figure 4.16 Detonation temperature at sonic point for aluminized nitromethane with Arrhenius law ($d = 100$ nm)

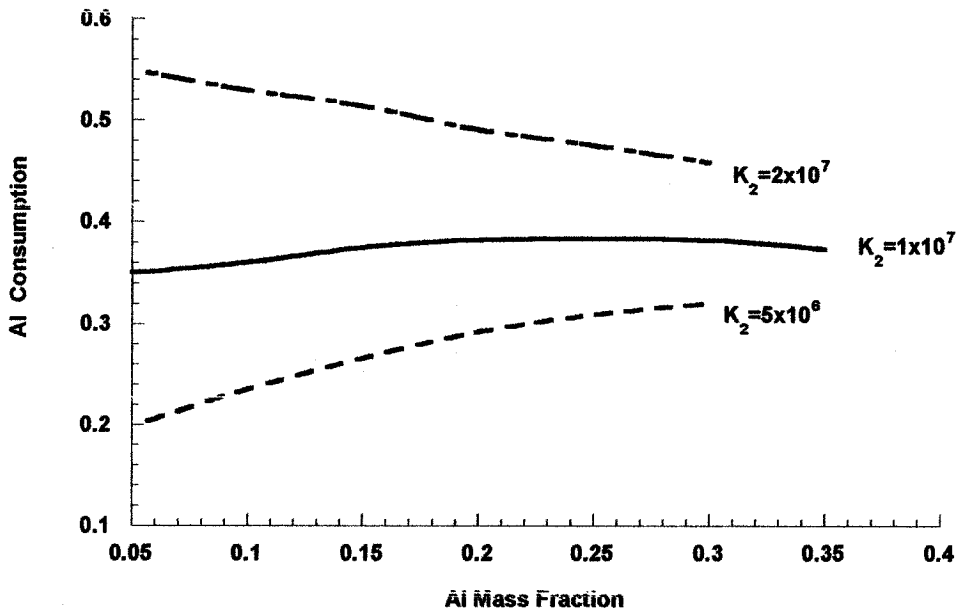

Figure 4.17 Al consumption at sonic point for aluminized nitromethane with Arrhenius law (d =100 nm)

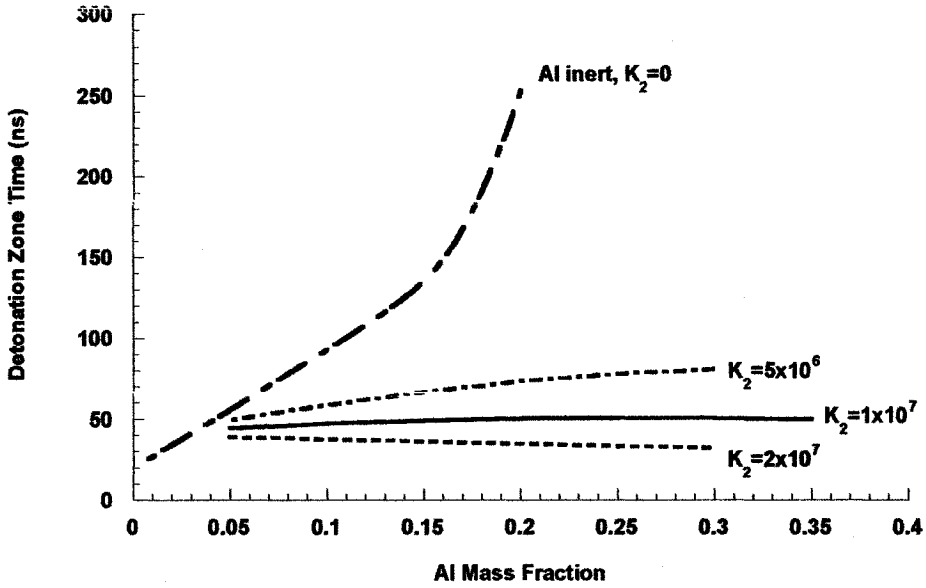

Figure 4.18 Detonation zone time of aluminized nitromethane with Arrhenius law (d=100 nm)

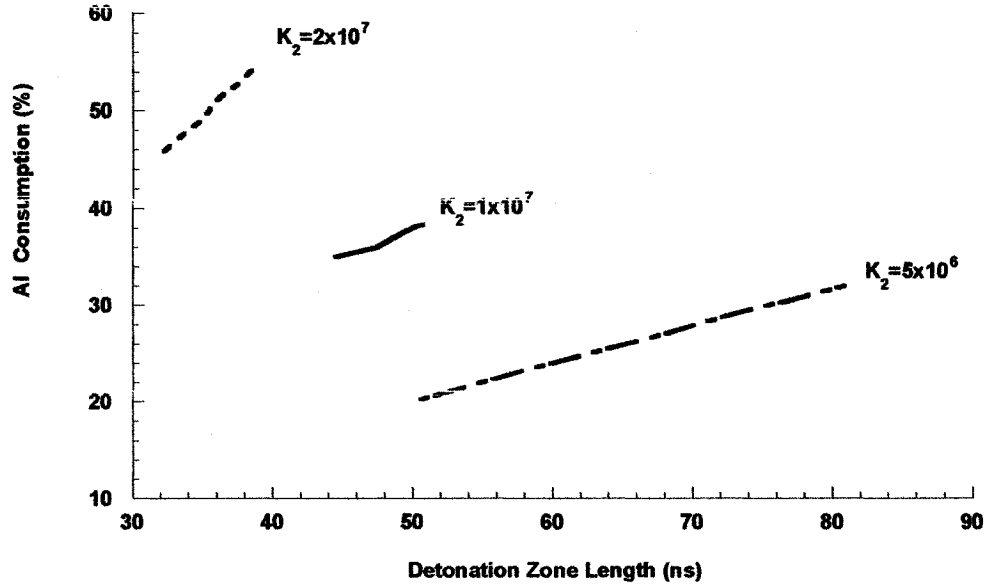

Figure 4.19 Al consumption in detonation zone of aluminized nitromethane (d=100 nm)

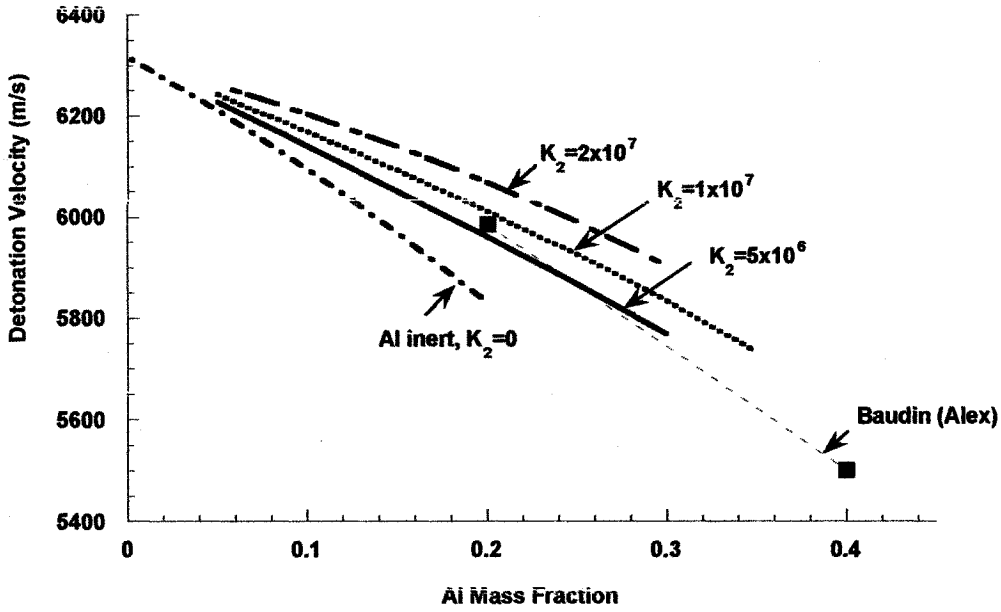

Figure 4.20 Detonation velocity of aluminized nitromethane with Arrhenius law (d=100 nm)

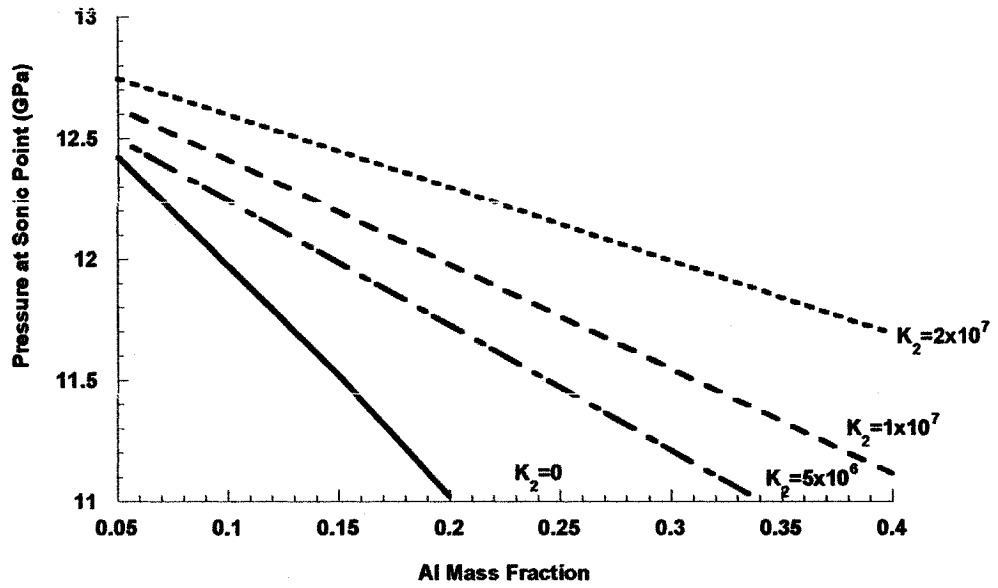

Figure 4.21 Detonation pressure of aluminized nitromethane at sonic point with Arrhenius law (d=100 nm)

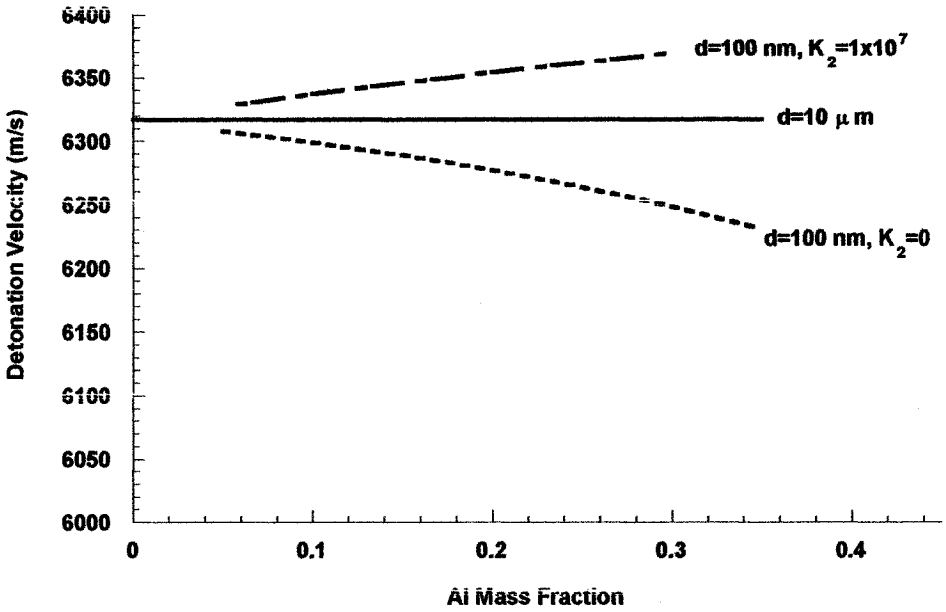

Figure 4.22 Detonation velocity of aluminized nitromethane with heat transfer only

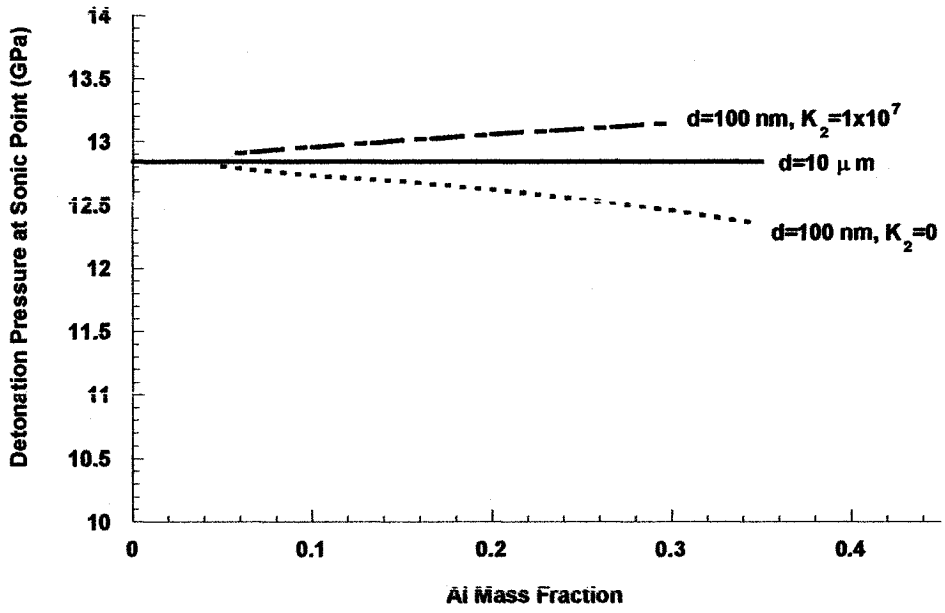

Figure 4.23 Detonation pressure at sonic point for aluminized nitromethane with heat transfer only

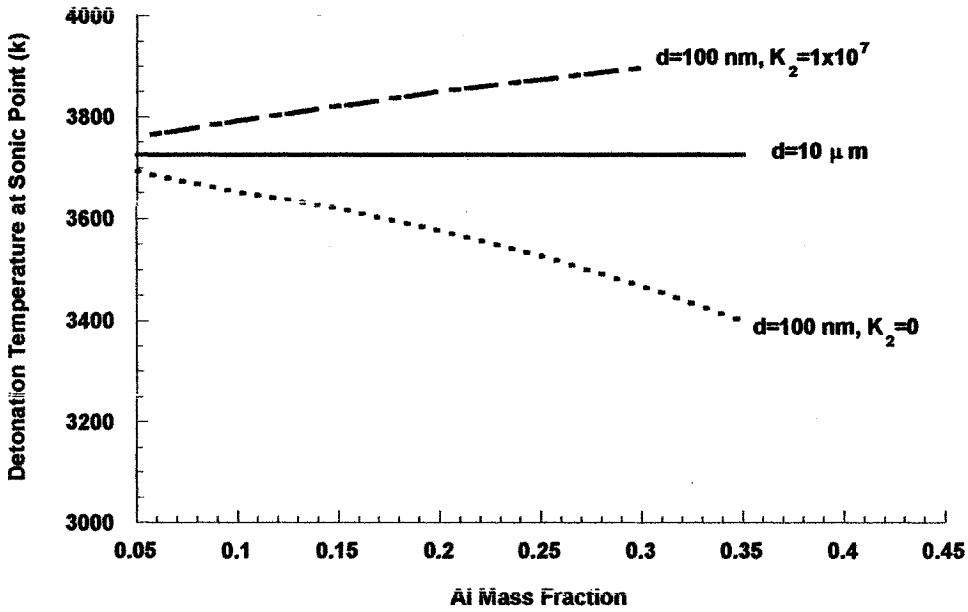

Figure 4.24 Detonation temperature at sonic point of aluminized nitromethane with heat transfer only

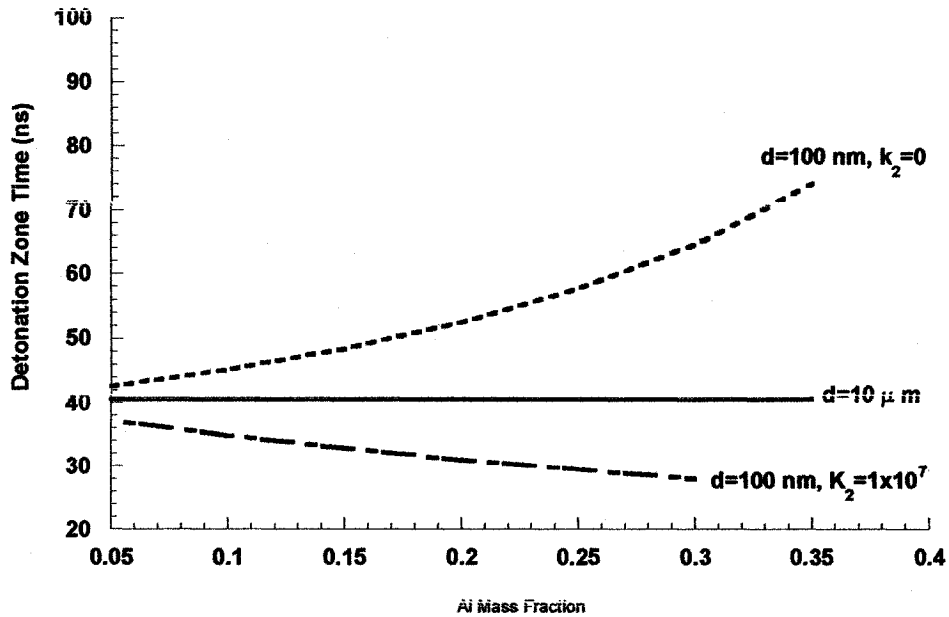

Figure 4.25 Detonation zone time of aluminized nitromethane with heat transfer only

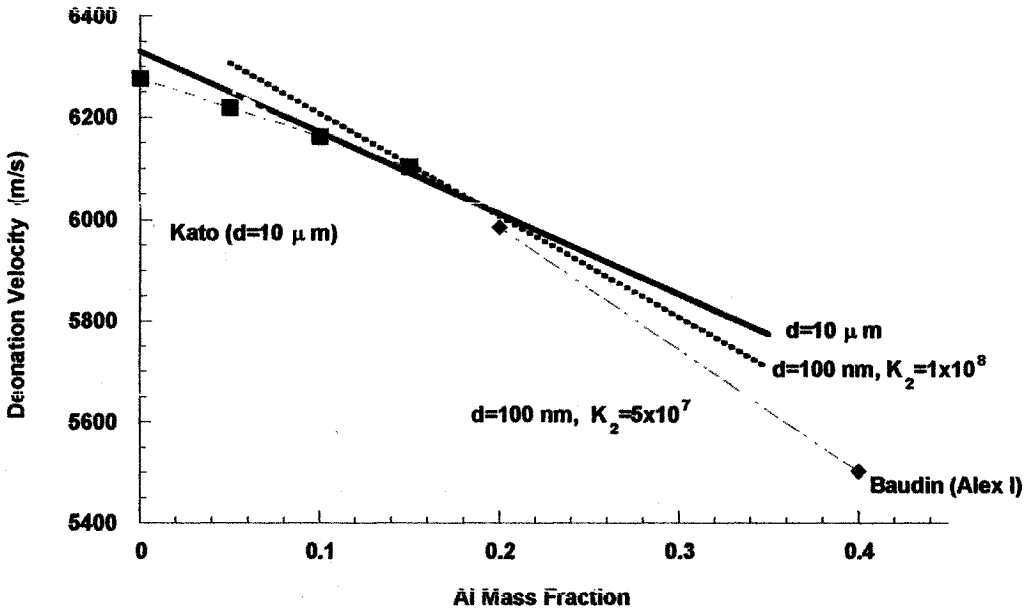

Figure 4.26 Detonation velocity of aluminized nitromethane with hot-spot reaction rate law

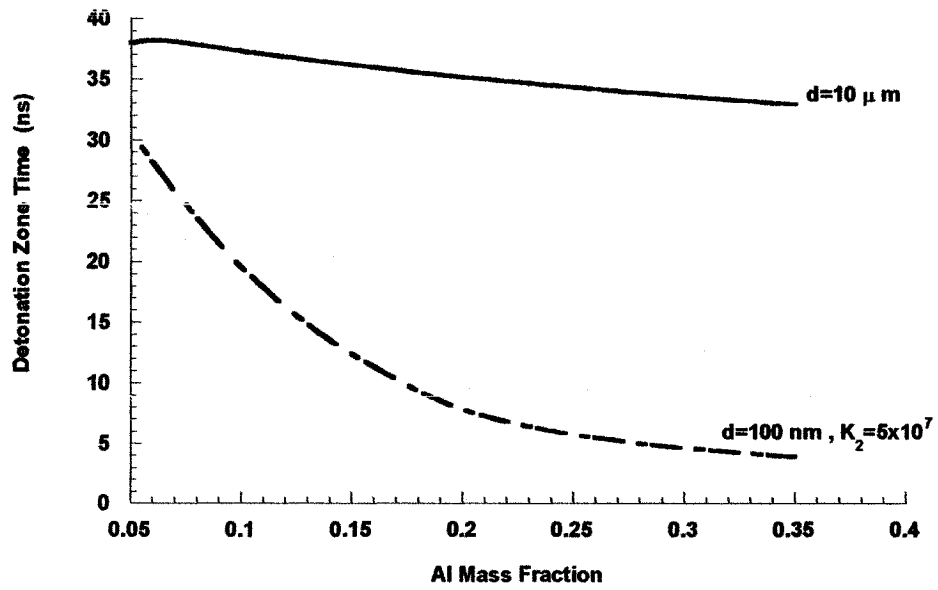

Figure 4.27 Detonation zone time of aluminized nitromethane with hot-spot reaction rate law

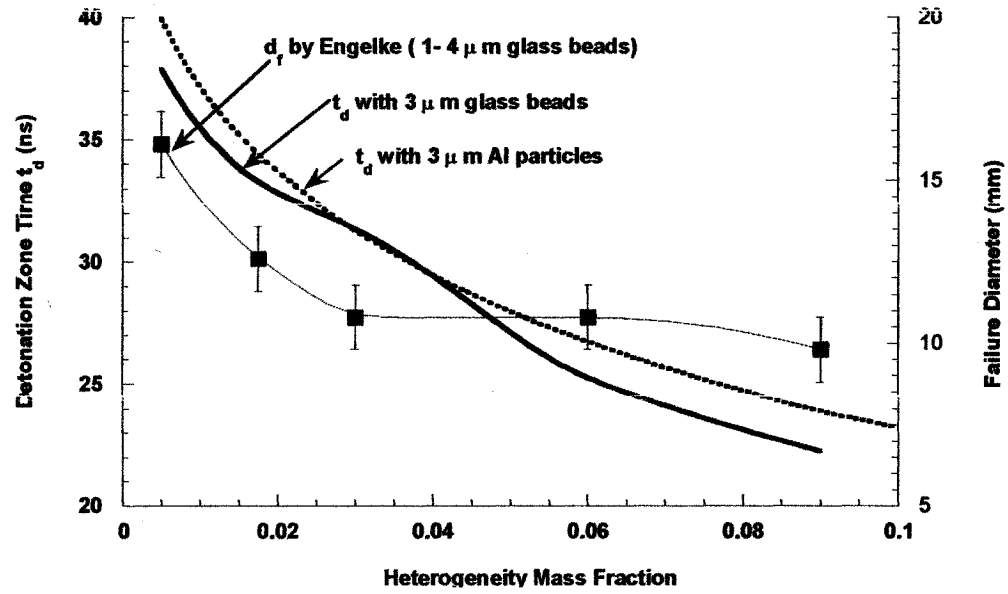

Figure 4.28 The calculated detonation zone time and the measured failure diameter vs. concentration of heterogeneities

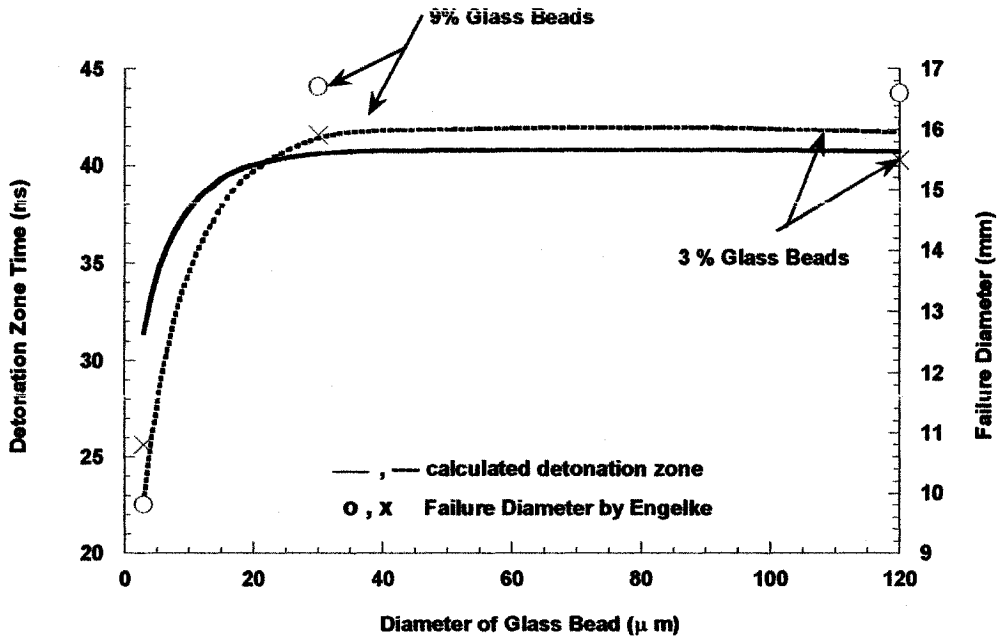

Figure 4.29 The calculated detonation zone time and the measured failure diameter vs. diameter of glass beads in NM/glass beads explosive

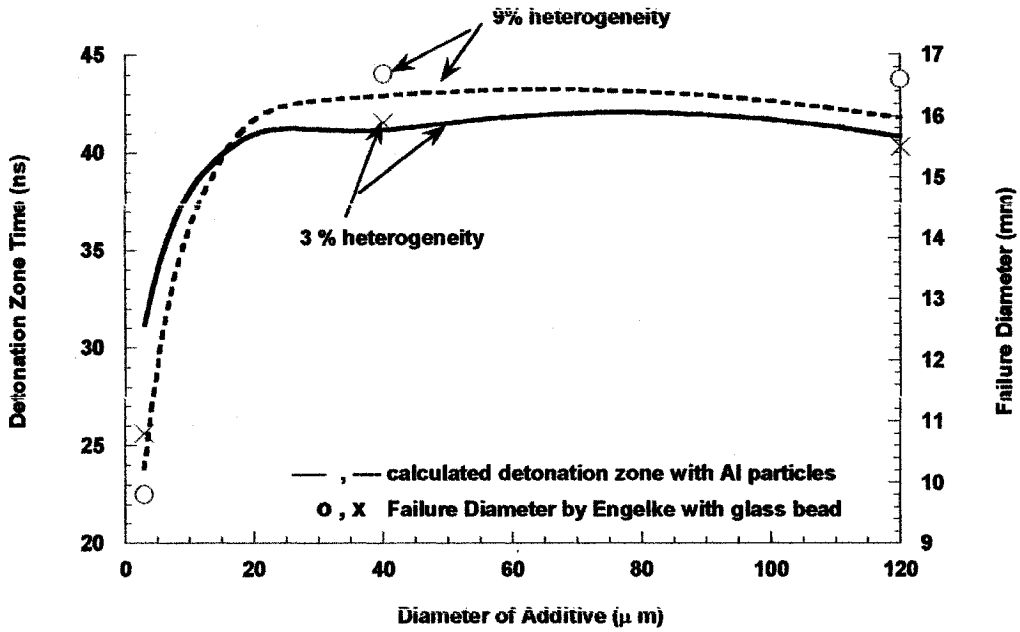

Figure 4.30 The calculated detonation zone time in NM/Al and the measured failure diameter in NM/glass beads

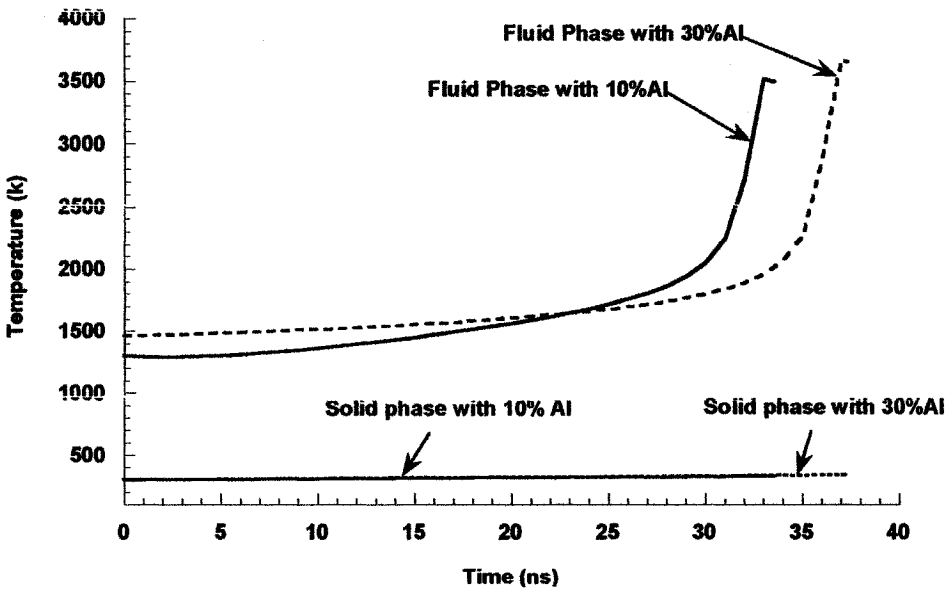

Figure 4.31 Temperature profile for both phases with hot-spot reaction rate law (d =10 μm)

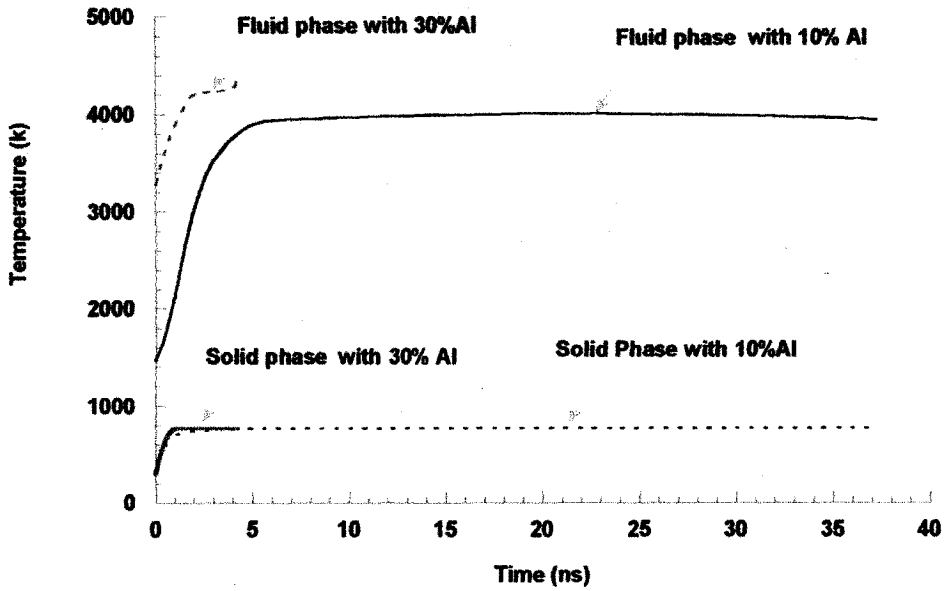

Figure 4.32 Temperature profile for both phases with hot-spot reaction rate law (d=100 nm, k_2 =5×10^7)

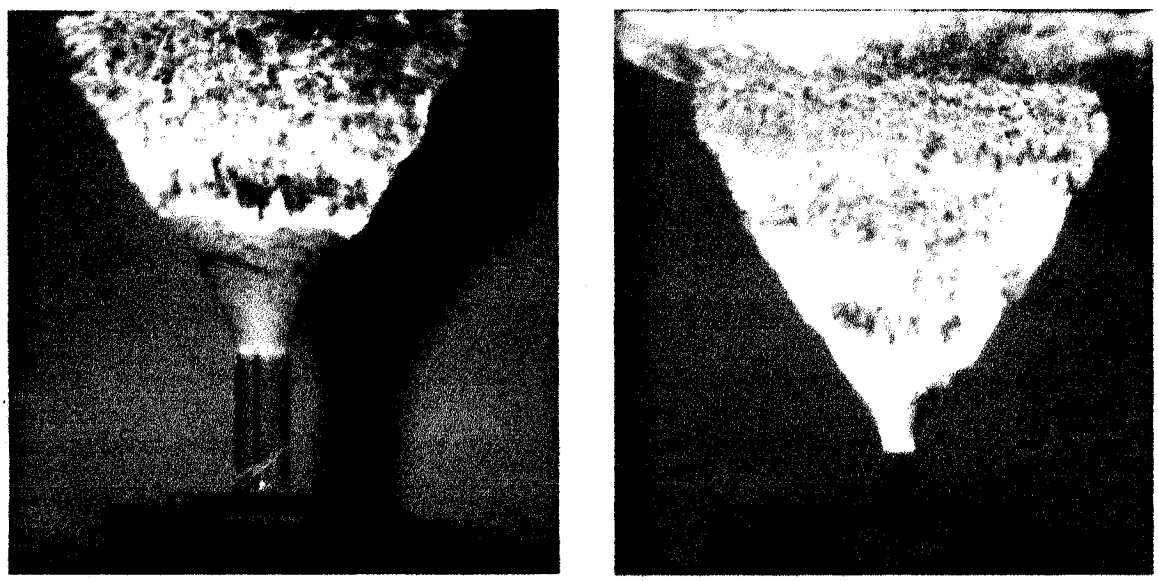

NM detonation NM/Alex detonation

Figure 4.33 Frames from high-speed records (Courtesy Haskins, P., 2002)

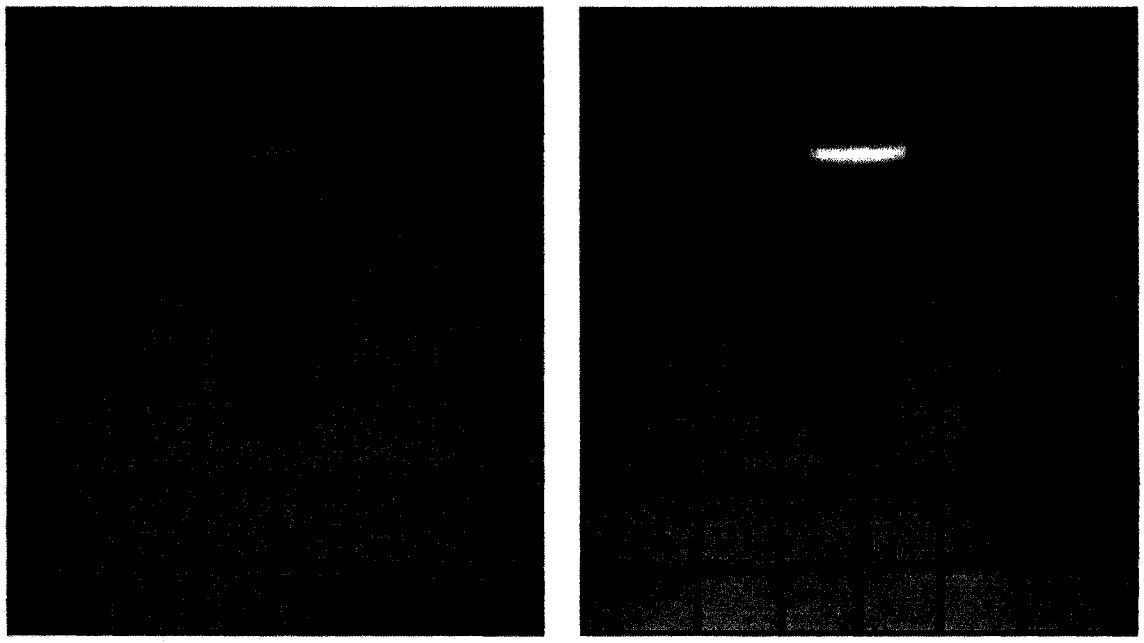

Δt =18 μs

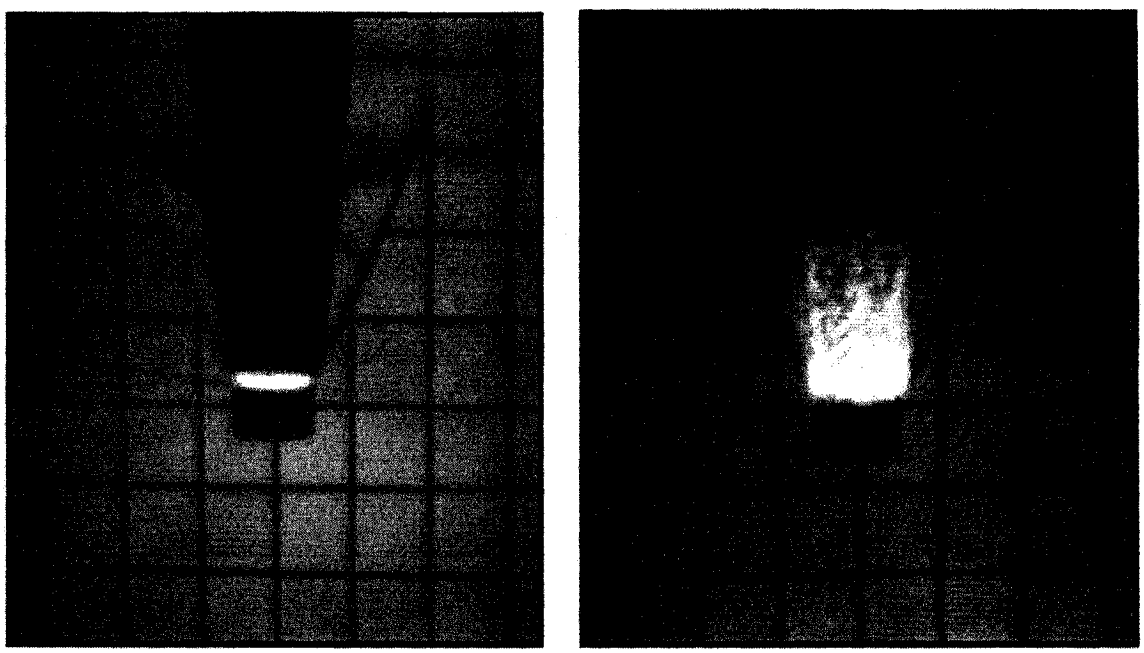

Δt =37 μs

"Regular" Tritonal Alex Tritonal

Figure 4.34 Aquarium test in Tritonal explosive (Courtesy Dorsett, H., 2001)

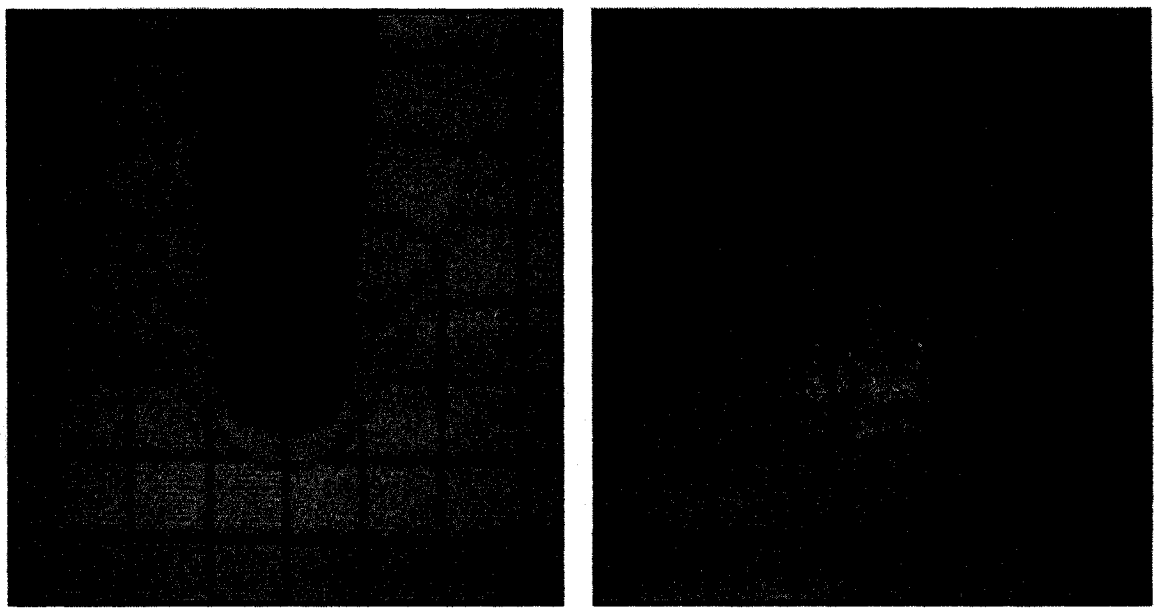

$\Delta t = 50$ μs

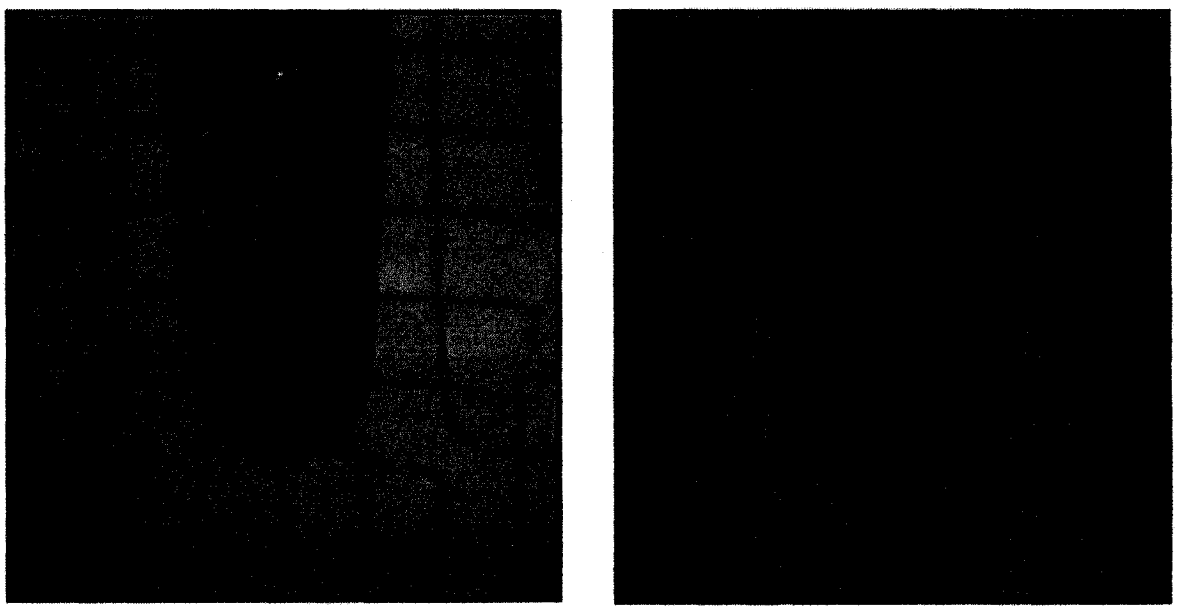

$\Delta t = 82$ μs

"Regular" Tritonal Alex Tritonal

Figure 4.35 Aquarium test in Tritonal explosive (Courtesy Dorsett, H., 2001)

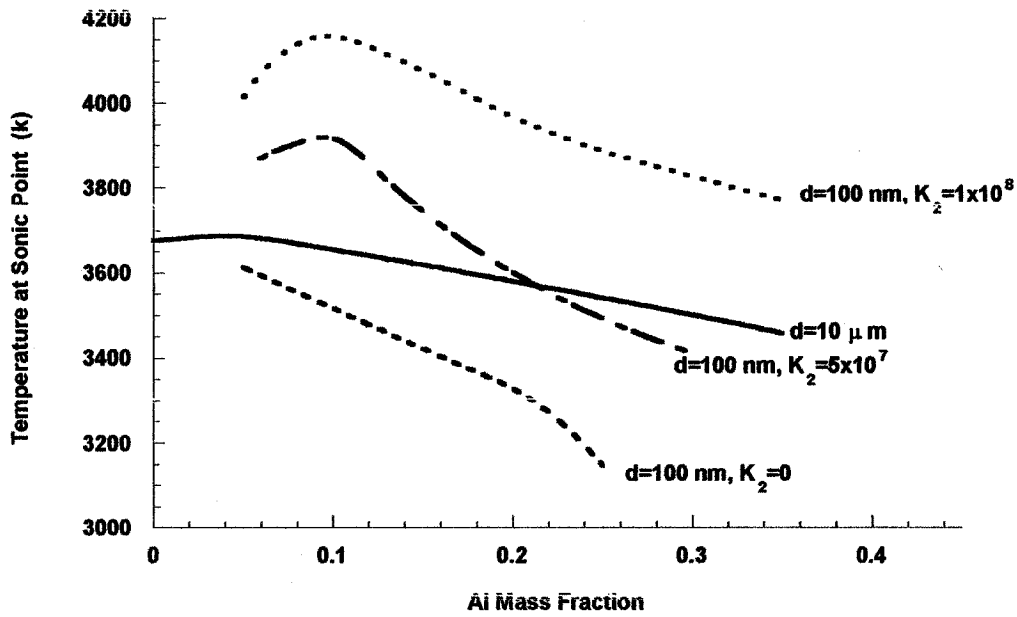

Figure 4.36 Detonation temperature at sonic point for aluminized nitromethane with hot-spot reaction rate law

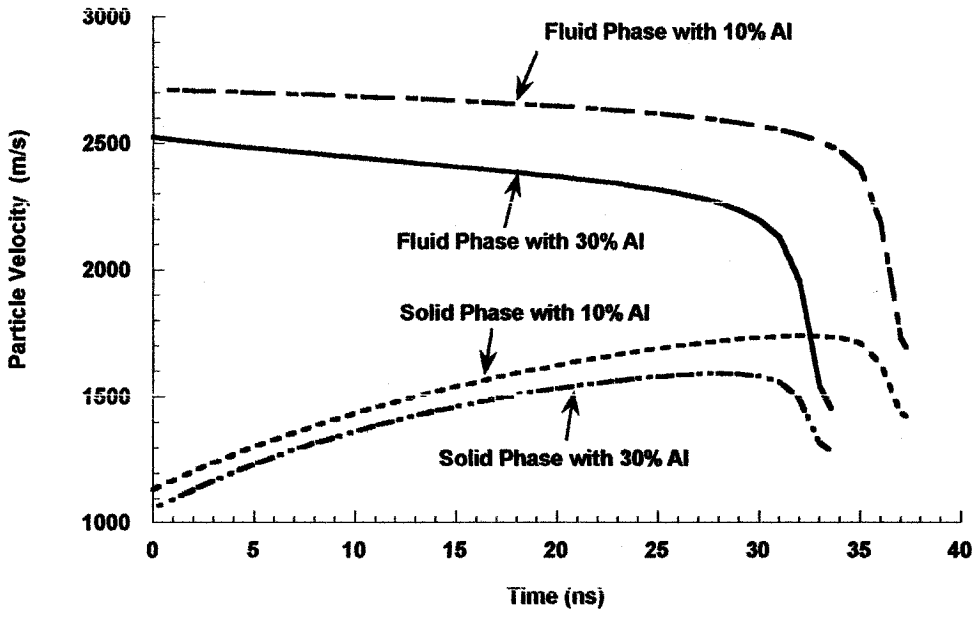

Figure 4.37 Particle velocity profile of both phases with hot-spot reaction rate law (d =10 μm)

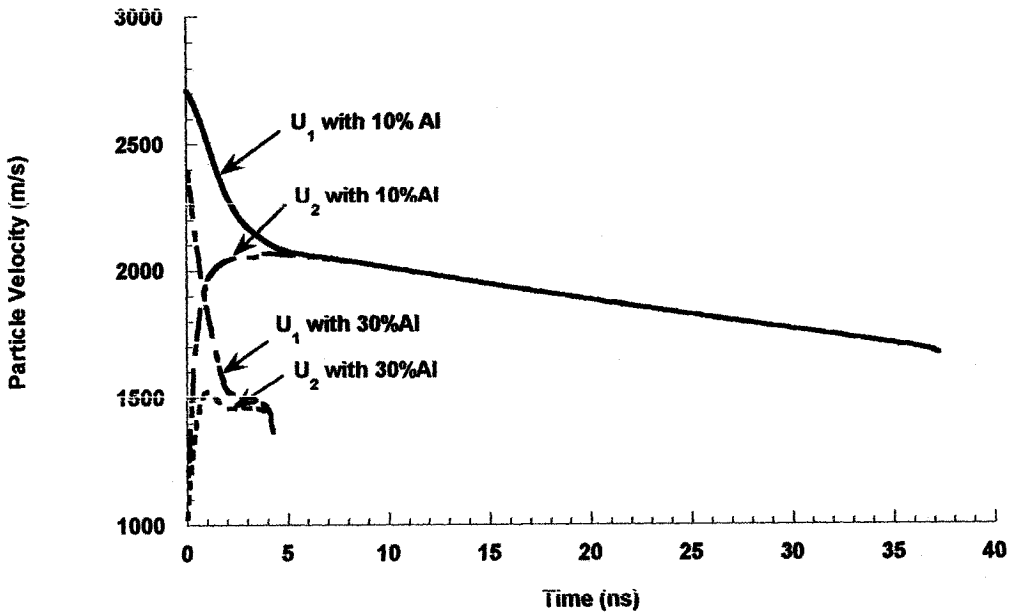

Figure 4.38 Particle velocity profile of both phases with hot spot reaction rate law (d = 100 nm)

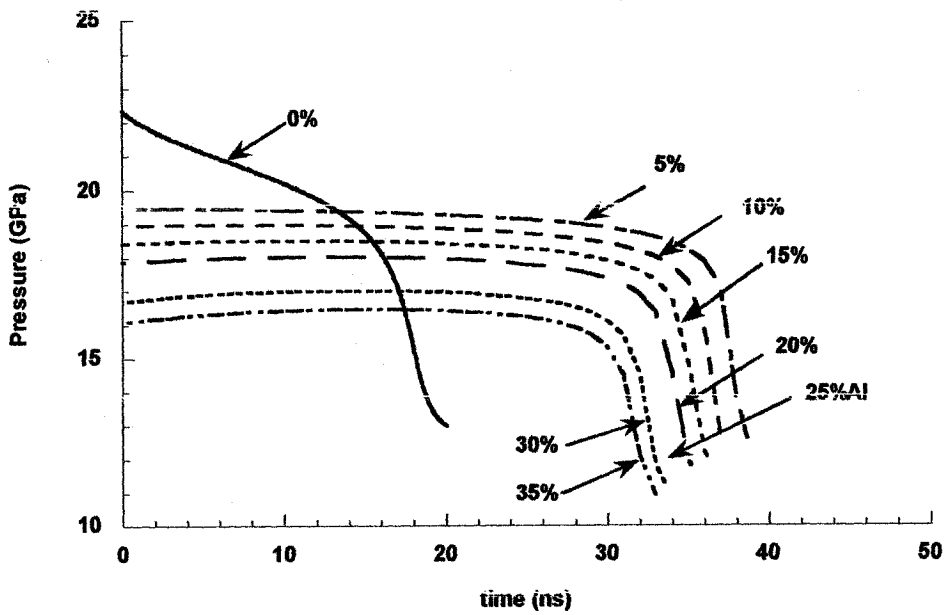

Figure 4.39 Pressure profile of aluminized nitromethane in detonation zone with hot-spot reaction rate law (d =10 μm)